

University of Montana

ScholarWorks at University of Montana

Graduate Student Theses, Dissertations, &
Professional Papers

Graduate School

1983

The Proterozoic Greyson-Spokane transition sequence: A stratigraphic and gravity study west-central Montana

Susan L. Bloomfield
The University of Montana

Follow this and additional works at: <https://scholarworks.umt.edu/etd>

Let us know how access to this document benefits you.

Recommended Citation

Bloomfield, Susan L., "The Proterozoic Greyson-Spokane transition sequence: A stratigraphic and gravity study west-central Montana" (1983). *Graduate Student Theses, Dissertations, & Professional Papers*. 4676.

<https://scholarworks.umt.edu/etd/4676>

This Thesis is brought to you for free and open access by the Graduate School at ScholarWorks at University of Montana. It has been accepted for inclusion in Graduate Student Theses, Dissertations, & Professional Papers by an authorized administrator of ScholarWorks at University of Montana. For more information, please contact scholarworks@mso.umt.edu.

COPYRIGHT ACT OF 1976

THIS IS AN UNPUBLISHED MANUSCRIPT IN WHICH COPYRIGHT SUBSISTS. ANY FURTHER REPRINTING OF ITS CONTENTS MUST BE APPROVED BY THE AUTHOR.

MANSFIELD LIBRARY
UNIVERSITY OF MONTANA
DATE: 1983

THE PROTEROZOIC GREYSON-SPOKANE TRANSITION SEQUENCE:
A STRATIGRAPHIC AND GRAVITY STUDY,
WEST-CENTRAL MONTANA

by

Susan L. Bloomfield

B.S., University of Delaware, 1980

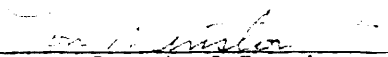
Presented in partial fulfillment of the
requirements for the degree of

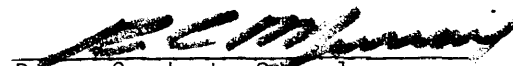
Master of Science

UNIVERSITY OF MONTANA

1983

Approved by:


Chairman, Board of Examiners


Dean, Graduate School


Date

UMI Number: EP40140

All rights reserved

INFORMATION TO ALL USERS

The quality of this reproduction is dependent upon the quality of the copy submitted.

In the unlikely event that the author did not send a complete manuscript and there are missing pages, these will be noted. Also, if material had to be removed, a note will indicate the deletion.



UMI EP40140

Published by ProQuest LLC (2014). Copyright in the Dissertation held by the Author.

Microform Edition © ProQuest LLC.

All rights reserved. This work is protected against unauthorized copying under Title 17, United States Code



ProQuest LLC.
789 East Eisenhower Parkway
P.O. Box 1346
Ann Arbor, MI 48106 - 1346

ABSTRACT

Bloomfield, Susan L., M.S., Spring, 1983

Geology

The Proterozoic Greyson-Spokane Transition Sequence: A
Stratigraphic and Gravity Study, West-Central Montana

Director: Don Winston



Four stratigraphic sections through the Greyson-Spokane transition sequence were measured at Trout Creek and Beaver Creek, east of the Eldorado thrust and at Wolf Creek and the Spokane Hills, west of the thrust. The transition sequence consists of four sediment types: 1) wavy couplet, 2) fine sand, 3) microlaminated couplet, and 4) coarse sand sediment types.

The four sediment types combine into three lithofacies: A, B, and C. Lithofacies A consists of the microlaminated couplet interbedded with the fine sand sediment type and represents a subtidal environment. Lithofacies B consists of the wavy couplet sediment type interbedded with fine sand beds and planar cross-bedded coarse sand beds. This lithofacies indicates an intertidal environment. Lithofacies C contains upper intertidal deposits represented by the horizontally-laminated coarse sand sediment type.

The repetitive succession of Lithofacies A, B, and C reveals an overall marine regression including four regressive-transgressive cycles. The four cycles define the transition sequence and correlate well across the four measured sections.

While the measure sections straddle the Eldorado thrust, they also straddle a proposed east-west trending Proterozoic fault zone (the Greenhorn line, Winston and others, 1982 ms.). The thickness of the transition sequence increases slightly south of the Greenhorn line possibly reflecting a higher subsidence rate. The data do not strongly suggest a fault zone. However, gravity data support evidence for changes in a tectonic style of thrusting around the Greenhorn line. Uplifted crystalline basement possibly acted as a buttress north of line causing thrusts to ramp steeply. South of the line, where no buttressing existed, the thrusts were able to ride at a low angle possibly into a down-dropped block.

Dedicated to Jan and Bill Bloomfield
for undying support and love.

ACKNOWLEDGEMENTS

I would like to sincerely thank Dr.s Don Winston, Steven Sheriff, and Charles Bryan for their guidance, encouragement, and critical review of my thesis. Funding was provided through a MONTS grant courtesy of Don Winston. Special thanks also go to Dr. David Fountain for providing gravity data and additional funding. My mother and sister, Jennifer, lasted through my entire field season and were outstanding field assistants. Thanks also go to Shirley Pettersen for typing the final draft of this thesis. I would also like to thank Chris McDonald, Jeff Mauk, Paul Kuhn, Bob Burnham, Cindy Livingston, and the Green Death for their support and friendship over the last two years. Finally, special thanks go to Rick Moore for constant support and inspiration.

TABLE OF CONTENTS

	Page
ABSTRACT	ii
ACKNOWLEDGEMENTS	iii
LIST OF FIGURES	vi
CHAPTER	
I. INTRODUCTION	1
Previous Work	1
Present Study	5
Structural Setting	5
II. SEDIMENT TYPES: DESCRIPTION AND INTERPRETATION	10
Wavy Couplet Sediment Type	10
Fine Sand Sediment Type	14
Microlaminated Couplet Sediment Type	16
Coarse Sand Sediment Type	19
Horizontally-laminated Subtype	19
Planar Cross-bedded Subtype	21
III. CORRELATION AND STRATIGRAPHIC SYNTHESIS	23
Lithofacies A	23
Lithofacies B	24
Lithofacies C	24
Correlation	24
Stratigraphic Synthesis	26

CHAPTER	Page
IV. GRAVITY ANALYSIS	30
V. CONCLUSION	40
REFERENCES CITED	43
APPENDICES	
A. Exact locations of measured sections	49
B. Measured Sections	51
C. Gravity Data	95
D. Gravity Program	104

LIST OF FIGURES

FIGURE	Page
1. Map of the Belt Basin	2
2. Map of proposed Proterozoic fault zones and crustal blocks	3
3. Map showing locations of measured sections plus orientation of Greenhorn and Townsend lines	4
4. Index to geologic maps used in compilation. .	6
5. Map showing location of measured sections and Eldorado thrust fault	8
6. Field photograph of wavy couplets sediment type	11
7. Hand specimen photograph of mudchips in wavy couplet sediment type.	13
8. Field photograph of fine sand sediment type .	15
9. Field photograph of microlaminated couplet sediment type	17
10. Field photograph of molar-tooth in microlaminated sediment type	18
11. Field photograph of horizontally-laminated coarse sand sediment type	20
12. Field photograph of low-angle planar cross- bedded coarse sand sediment type	22
13. Schematic stratigraphic column showing four regressive-transgressive cycles	25
14. Correlation across four measured sections . .	27
15. Generalized geologic map of study area . . .	31
16. Bouguer gravity map of study area	33
17. Observed and calculated gravity anomalies . .	36
18. Map showing thrust relationship to Greenhorn line	39

CHAPTER I

INTRODUCTION

During Middle Proterozoic time, sediments of the Belt Supergroup were deposited in a basin presently located in parts of Washington, Idaho, Montana, and southern Canada (Fig. 1). Don Winston and others (1982 ms.) proposed that the Belt basin was composed of several fault-bound blocks. The Proterozoic fault-zones between the blocks are referred to as lines (Fig. 2). They base their hypothesis on: 1) stratigraphic thickness changes across the fault zones, 2) response in Cretaceous to Paleocene thrusting, and 3) response in Eocene to Recent extension. This study tests part of Winston's hypothesis by focusing on one critical area: the intersection of the Greenhorn and Townsend lines (Fig. 3). A stratigraphic and sedimentological study of the Proterozoic Greyson-Spokane transition across the Greenhorn and Townsend lines was conducted to see if growth faults were reflected in the stratigraphic sequence or sedimentary environment. In addition, I compiled structural data and available maps and analyzed published gravity data to search for evidence of the proposed Proterozoic growth faults.

Previous Work

Several workers have mapped and described the Greyson and Spokane formations near Helena, Montana (Mertie and others, 1951; Nelson, 1963; Robinson and others, 1969; Weinberg, 1970; Bregman, 1971; Shaffer, 1971;

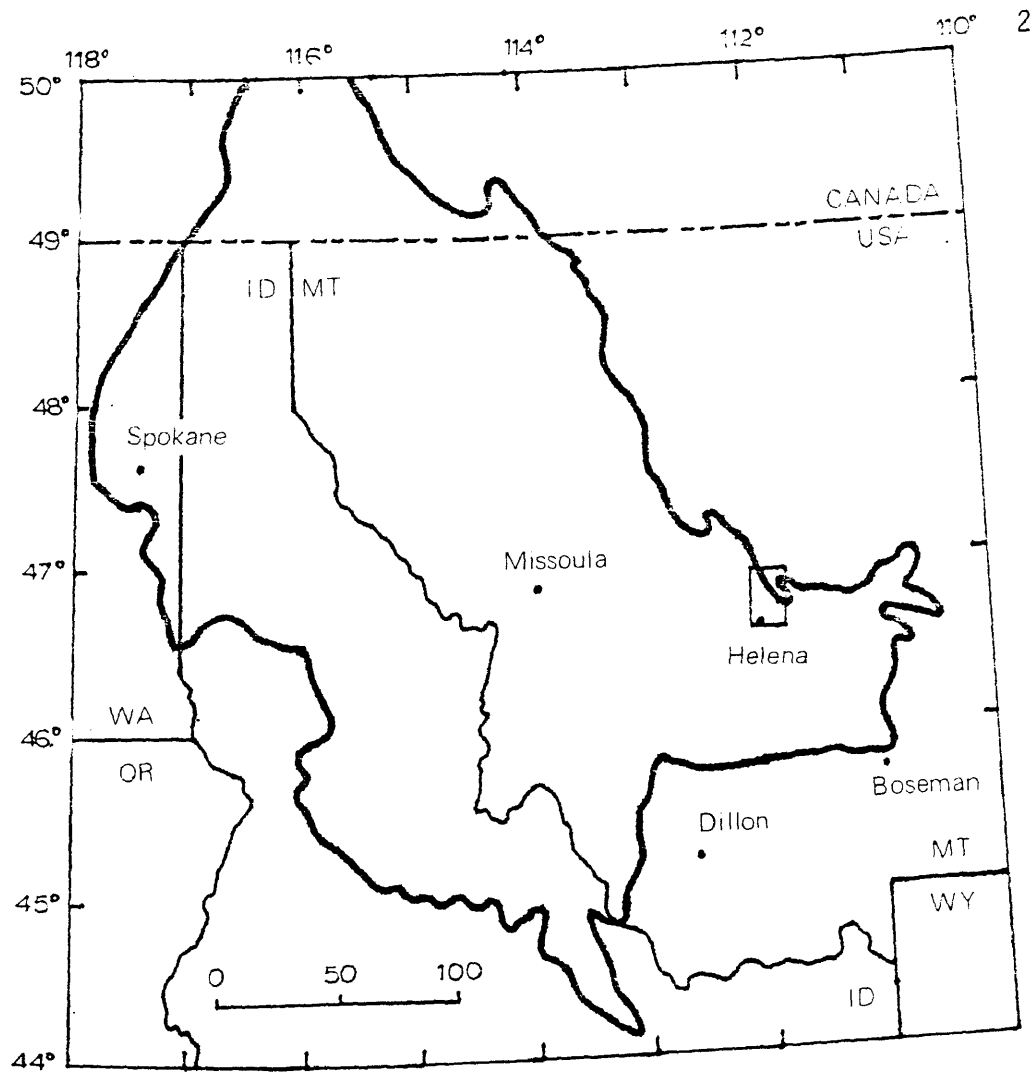


Figure 1. Map of Belt basin (after Harrison and others, 1974).

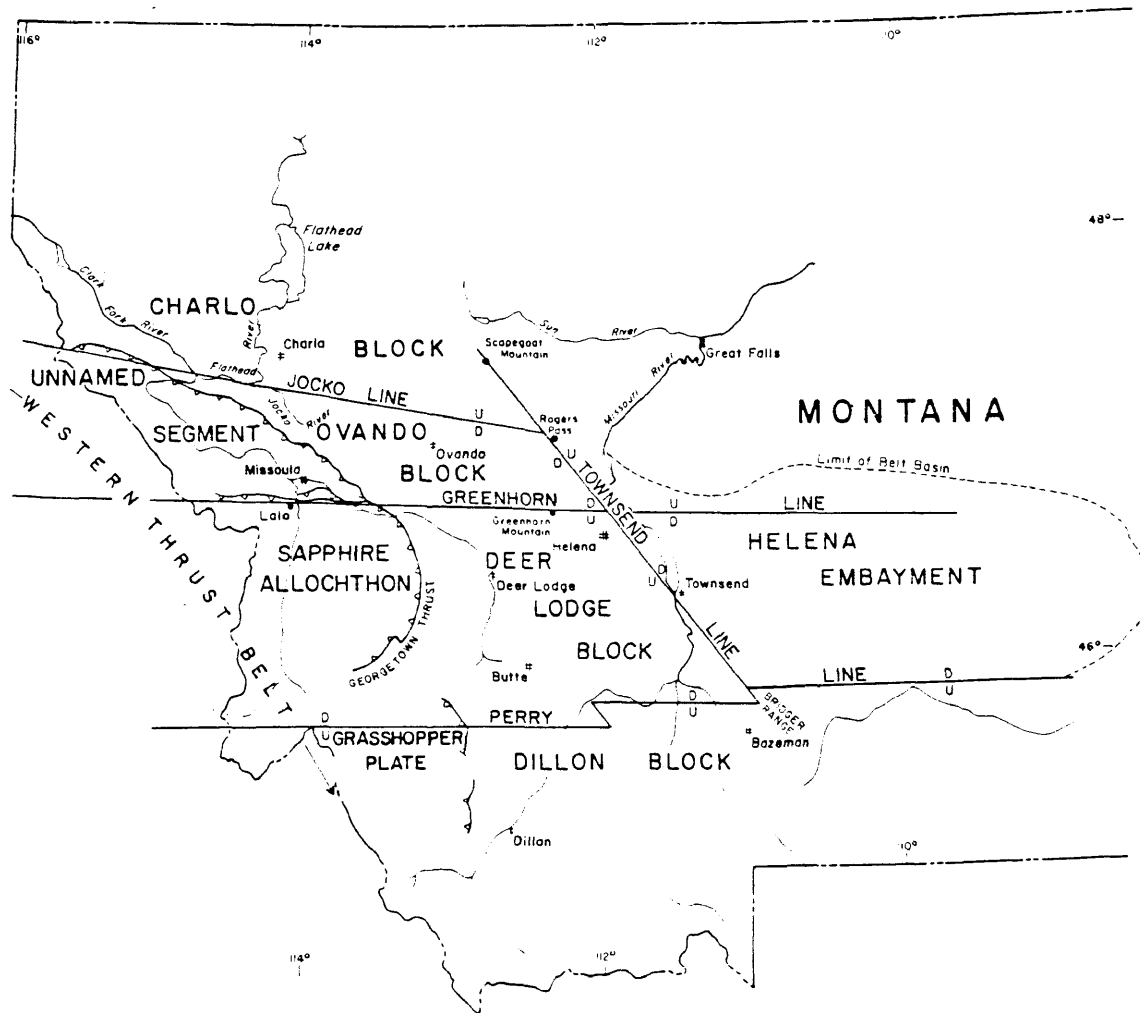


Figure 2. Map of proposed Proterozoic fault zones and crustal blocks in Montana (after Winston and others, 1982 MS).

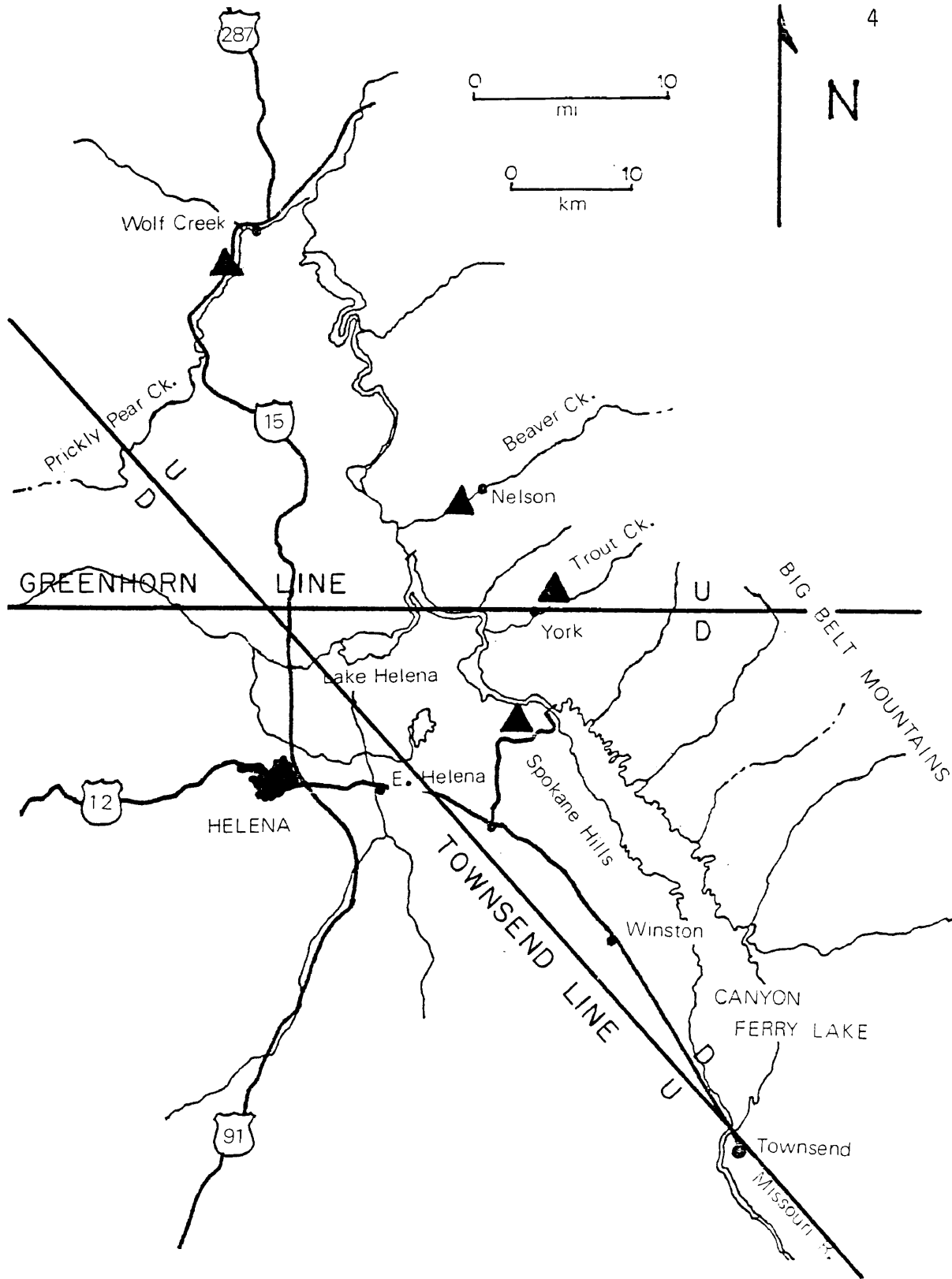


Figure 3. Map showing location of measured sections (black triangles) and orientation of Greenhorn and Townsend lines.

Durham, 1972; Schmidt, 1972; Whipple, 1980; see Fig. 4). Davis and others (1963) also conducted a gravity and aeromagnetic study of the East Helena and Canyon Ferry quadrangles. Structural studies concerned with Mesozoic and Cenozoic tectonics and their effect on the Belt terrane have also been conducted in this area (Bregman, 1976; Reynolds, 1978; Woodward, 1981).

Present Study

I measured stratigraphic sections through the Greyson-Spokane transition sequence at Trout Creek, Beaver Creek, Wolf Creek, and the Spokane Hills (Fig. 5). Exact locations are given in Appendix A. All sections were measured by Brunton compass and Jacob's staff from the brown and grey, sandy shale of the upper Greyson into red sandy silt and argillite of the lower Spokane. Data from a total of 595 meters of measured section include a graphic and written log of each section compiled at a scale of 1 inch to 5 feet (Appendix B).

The gravity data used in this study came from United States Department of Defense files and United States Geological Survey Open-file reports (Appendix C). A two dimensional modelling program provided a basis for interpreting the data (Appendix D).

Structural Setting

The locations of the four measured sections spatially bracket the Eldorado thrust, the easternmost major north-northwestern-trending thrust of the overthrust belt (Mudge, 1970). The Wolf Creek and Spokane Hills sections lie to the east of the Eldorado thrust, and the Trout

Figure 4. Index to geologic maps used in compilation of geologic map of study area. Numbers are keyed to references as follows: 1, Bregman (1971); 2, Durham (1972); 3, Davis and others (1963); 4, Knopf (1963); 5, Lyons (1944); 6, Mertie and others (1951); 7, Robinson and others (1969); 8, Shaffer (1971); 9, Weinberg (1970).

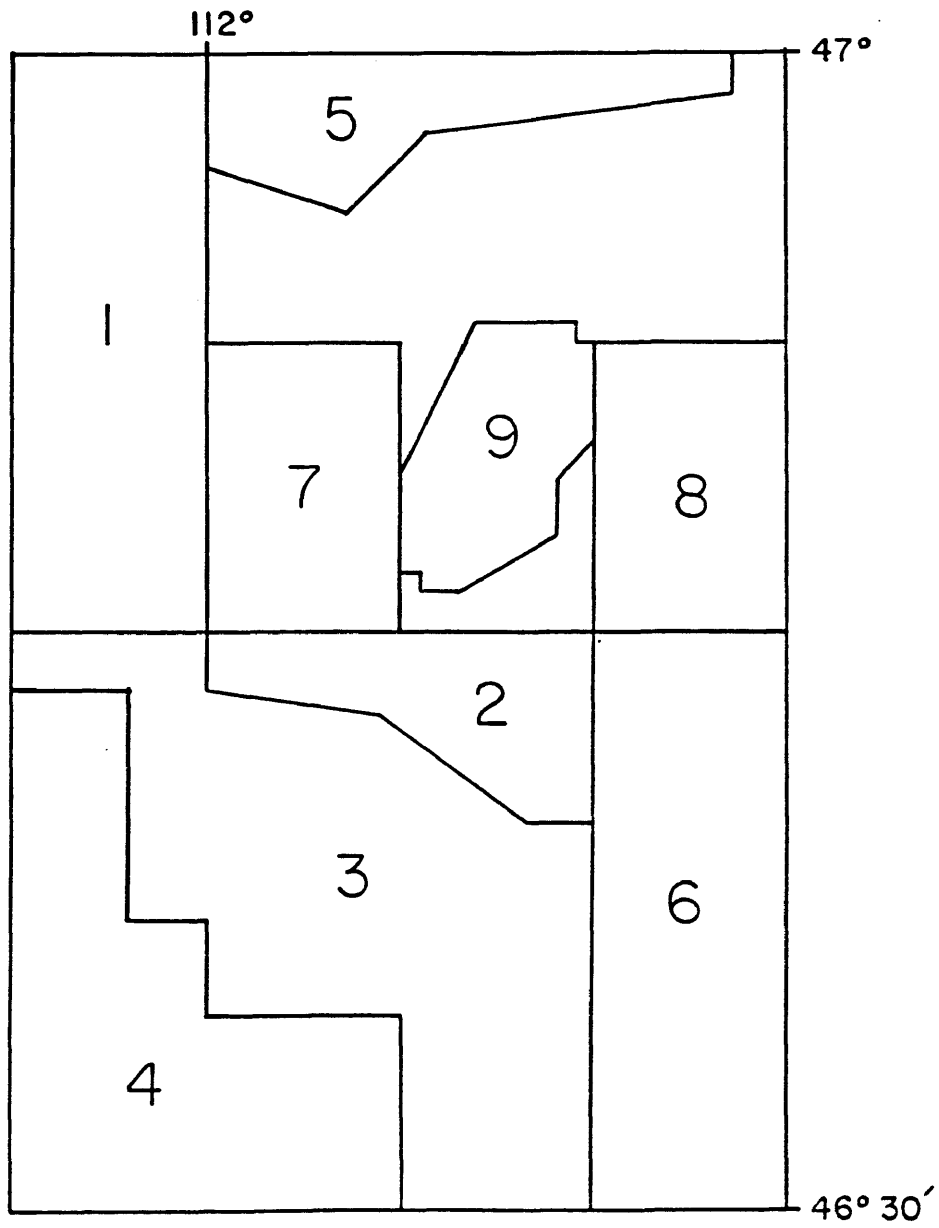


Figure 4

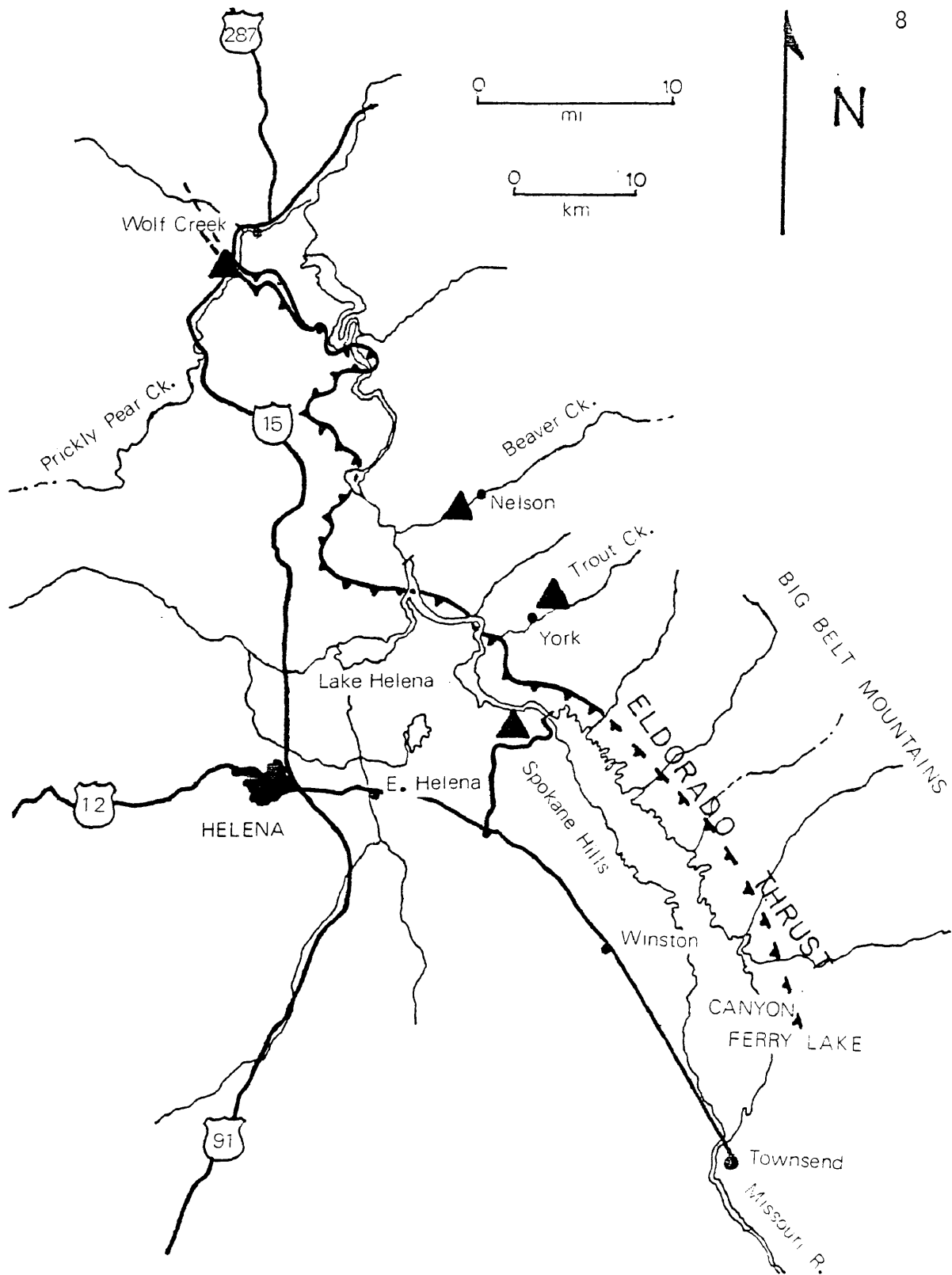


Figure 5. Map showing locations of measured sections (black triangles) in relation to Eldorado thrust fault.

Creek and Beaver Creek sections lie to the west of the thrust (Fig. 5). Bregman (1971) calculated a minimum displacement of 16.9 kilometers for the Eldorado thrust based on stratigraphic thicknesses and the geometry of the thrust. Bregman (1976) also noted a change in the configuration of the thrust along the north edge of the Helena embayment. South of the Greenhorn line the Eldorado is a low-angle thrust, whereas north of the Greenhorn line the Eldorado has ramped steeply, possibly onto a Precambrian crystalline buttress (Bregman, 1976; Woodward, 1981; Winston, 1982 ms.). Reynolds (1978) recognized extensional strike slip faults and listric normal which curve westward as they approach the Greenhorn line from the south.

CHAPTER II

SEDIMENT TYPES: DESCRIPTION AND INTERPRETATION

Several lithologies occur in the Greyson-Spokane transition sequence. Although these lithologies reflect original sedimentation, diagenesis and metamorphic history, they are classified chiefly on the basis of original sedimentary characteristics because diagenesis and metamorphism are of secondary importance in constructing a paleoenvironmental model. Criteria such as composition, grain size, sorting, and primary sedimentary structures define the sediment types.

The Greyson-Spokane transition consists of four major sediment types. They are in order of decreasing abundance: 1) wavy couplets; 2) fine sand; 3) microlaminated couplets; and 4) coarse sand. Each sediment type is described individually and interpreted in terms of sedimentary processes and paleoenvironment.

Wavy Couplet Sediment Type

The wavy couplet sediment type consists of silty, very fine sand layers sharply overlain by mud layers (Fig. 6). Both sand and mud layers are continuous, forming wavy bedding as described by Reineck and Singh (1975). Sand layers 0.5 to 2.5 cm. thick show current and wave ripple cross-laminations. These layers thicken and thin with average wavelengths of 8 cm. and amplitudes of 2 cm.. Most ripples are symmetrical and sharp-crested but some are flat-topped or reworked into

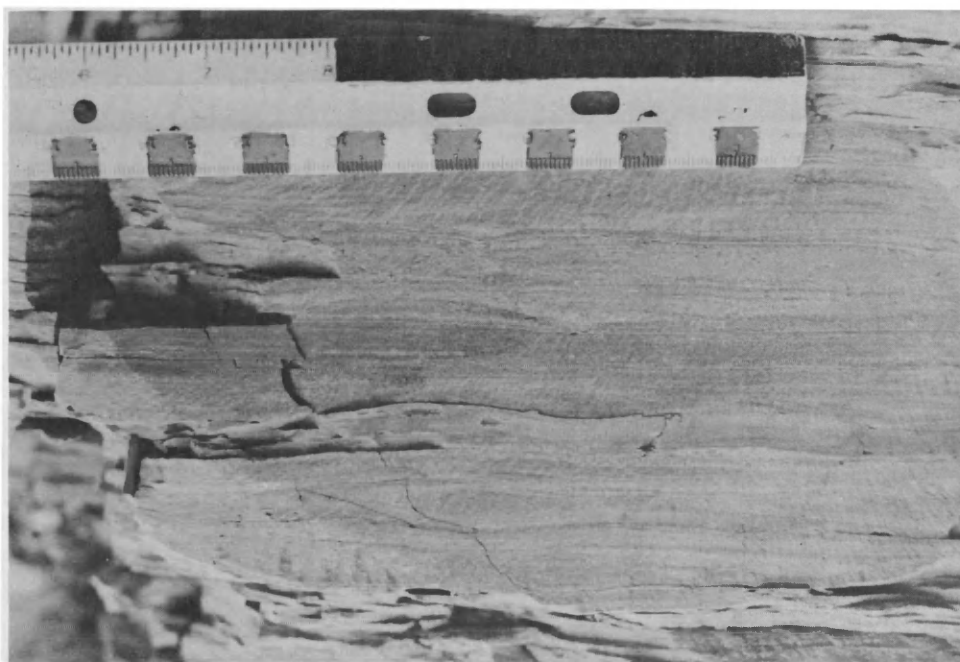


Figure 6. Wavy couplet sediment type.

interference patterns. Thin mud layers form drapes less than 1 cm. thick over the rippled sand layer beds. Together, a sand layer overlain by a mud layer constitutes a couplet which ranges from 0.5 to 3 cm. thick. Couplets cut by mudcracks commonly occur in this sediment type but in many parts of the section they are absent.

Interlamination of sand and clay forming wavy beds result from periods of traction-load transport and deposition from diurnal tidal currents alternating with periods of suspended-load deposition from standing water (Reineck and Singh, 1975). Because mud layers are preserved in wavy bedding, current velocities were probably low. Asymmetrical ripples in the sand layers result from tidal currents. During high water, symmetrical ripples formed by wave oscillation in shallow water and flat-topped ripples formed by receding water and subsequent exposure. Finally, clay settled from suspension in standing water onto these rippled beds. Shallow mudcracks indicate brief subaerial exposure. Mudchips were probably deposited by tidal currents in the sand layers (Fig. 7).

Many workers describe similar sedimentary packages from modern tidal environments (Reineck and Singh, 1975; Reineck, 1975; Sellwood, 1975) and others have interpreted similar Proterozoic sequences as intertidal deposits (Button and Vos, 1977; Bhattacharyya and others, 1980; Watchorn, 1980; Whipple, 1980).

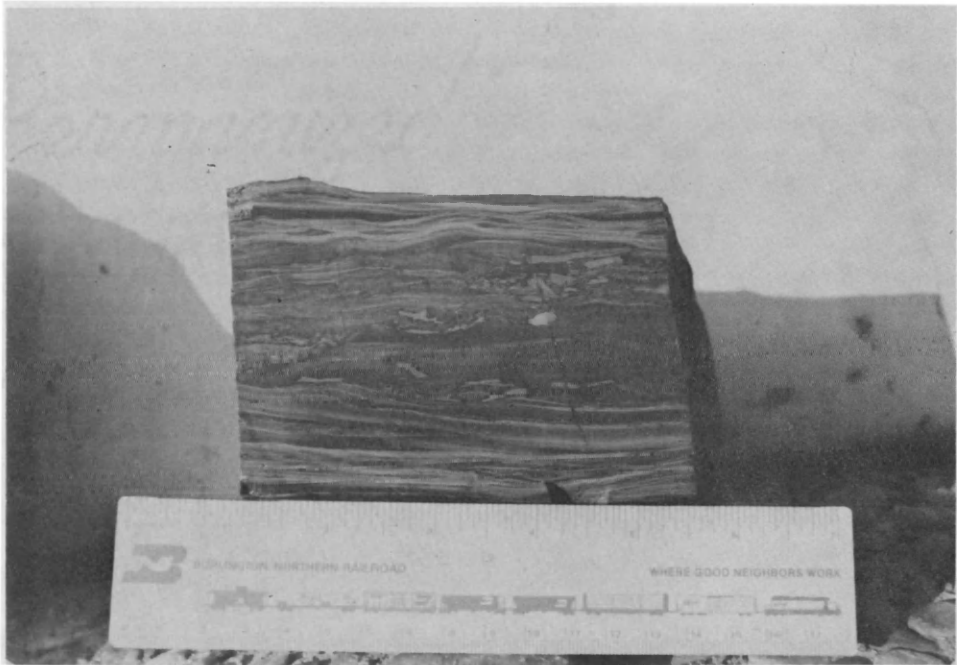


Figure 7. Mudchips in the wavy couplet sediment type.

Fine Sand Sediment Type

The fine sand sediment type consists of very fine-grained, well-sorted, quartzose sand beds which average 3 to 8 cm. in thickness. Locally they range up to 40 cm. thick. Where fine sand beds are less than 5 cm. thick, internal stratification is dominated by asymmetrical ripple cross-laminations. As in the wavy couplet sediment type, they mostly appear sharp-crested, but are locally flat-topped and reworked. Beds thicker than 5 cm. are horizontally-laminated at the base, changing to ripple cross-laminated near the top (Fig. 8). Fine sand beds capped by mud drapes are interstratified with the wavy couplet sediment type.

Horizontally-laminated sand beds form in the plane-bed phase of the upper flow regime by traction-load current sedimentation (Simons and others, 1965). Flat laminations have also been produced in a flume by migrating oscillation ripples (McBride and others, 1975). Several workers have interpreted horizontally-laminated and ripple-topped sand layers as subtidal to intertidal deposits. Button and Vos (1977) and Klein (1970) proposed shallow subtidal sand bodies or bars as a possible explanation for these types of sand beds. Some authors postulate a more landward environment, such as shoreface deposits or reworked tidal sand shoals (Bhattacharyya and others, 1980; Watchorn, 1980). Ripple-topped sand beds may also be evidence for late-stage emergence run-off in an intertidal flat (Watchorn, 1980). Fine sand beds probably formed in environments that ranged from subtidal to high intertidal. They are common throughout the section regardless of evidence for subaerial exposure in the surrounding wavy couplet sediment type.

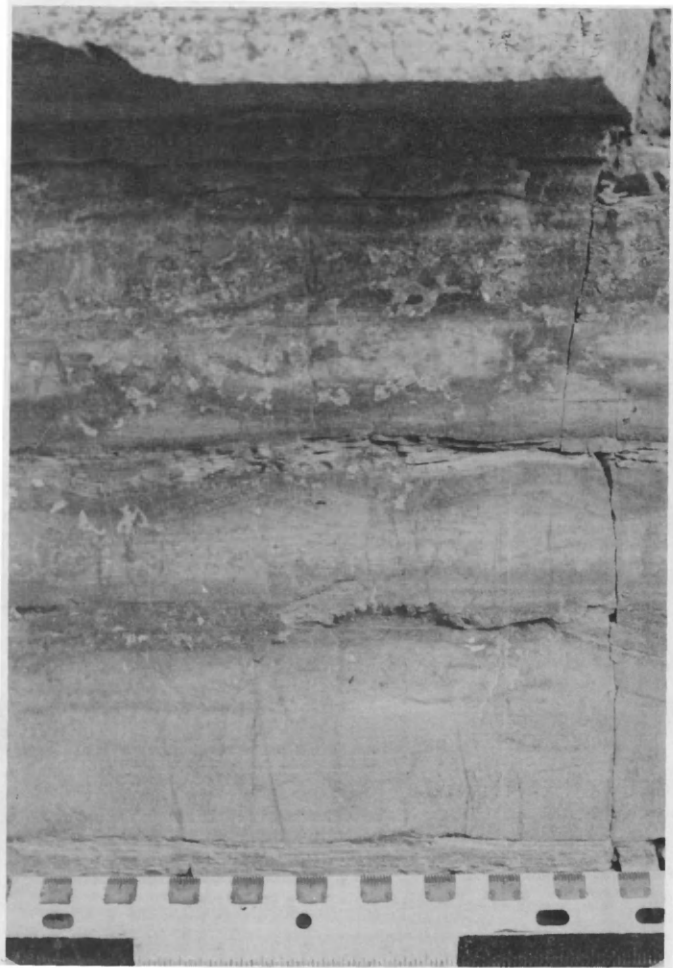


Figure 8. Fine sand bed horizontally-laminated at base, changing to current ripple cross-laminated near top.

The frequency and regularity of fine sand beds suggest that they represent fair weather processes. Whipple (1980) interprets fining-upward sequences that begin with similar fine sand beds as fluvial or sheetwash deposits in the Upper Middle Spokane. The fine sand beds of the Greyson-Spokane transition sequence probably represent fluvial or sheetwash deposits reworked by tides.

Microlaminated Couplet Sediment Type

The microlaminated couplet sediment type consists of millimeter-scale silt layers sharply overlain by mud layers of the same scale. Individual couplets are less than 5 mm. thick and are laterally continuous for several meters. Locally, silt layers pinch out or pass laterally into millimeter-scale foreset cross-laminations. Couplet thickness ranges from less than 1 to 5 mm. and composition ranges from terrigenous through carbonaceous or calcareous. Thinner, carbonaceous couplets are commonly dislocated as tabular sheets and form centimeter-scale soft sediment folds. Locally, sets of couplets are truncated by scour and fill structures (Fig. 9). These carbonaceous couplets commonly occur interstratified with dolomitic couplets, which are normally thicker and contain "molar-tooth" (Fig. 10; see O'Connor, 1972, for description of molar-tooth). Stromatolites and stromatofoms are interstratified with molar-tooth structures.

Silt layers overlain by clay layers reflect alternating current velocities, possibly from tidal currents. Variations in currents and subsequent reworking caused the laminations (Thompson, 1975). The



Figure 9. Soft-sediment deformation in carbonaceous microlaminated couplets.



Figure 10. Molar-tooth structures in calcareous microlaminated couplets.

carbon-rich couplets incorporate organic material which may represent very thin cohesive mats that required slightly higher current velocities to remove (Grotzinger, 1981). Stronger, possibly storm currents induced the soft-sediment folds and scour and fill structures in the carbonaceous couplets. Stromatolites have been recognized as both intertidal and supratidal indicators (Reineck and Singh, 1975; Button and Vos, 1977) and as subtidal indicators as well (Gebelein, 1969; Bhattacharyya and others, 1980). Stromatolites within the microlaminated couplet sediment type are probably a good indicator for the subtidal environment because they lack any evidence for subaerial exposure.

Coarse Sand Sediment Type

A. Horizontally-laminated Coarse Sand Subtype

The horizontally-laminated coarse sand subtype consists of individual, horizontally-laminated sand beds up to 80 cm. thick (Fig. 11). Grain size varies from less than 1.0 ϕ to 2.5 ϕ , with poor to good sorting. Grains probably from the coarse sand environment are scattered in the fine sand sediment type and in the sand layers of the wavy couplet sediment type. These beds are interstratified with the wavy couplet sediment type.

Horizontally-laminated beds of the coarse sand sediment type record deposition from the upper flow regime like those of the fine sand sediment type. However, this sediment subtype is less abundant and includes a wider range of grain size and sorting than the fine sand sediment type. Larger grain size and individual bed size indicate

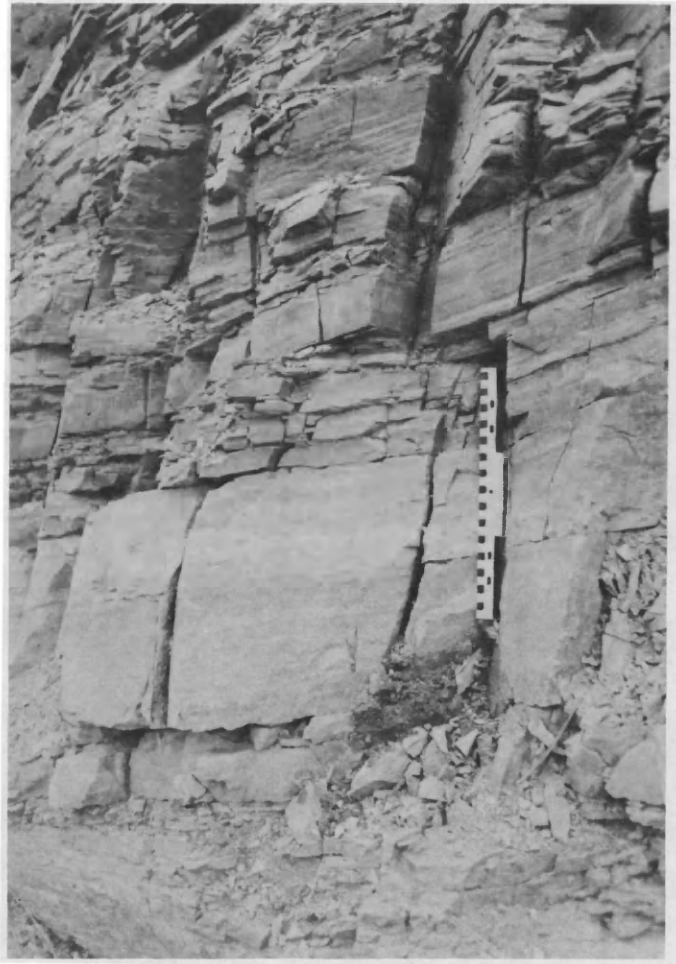


Figure 11. Horizontally-laminated coarse sand bed interbedded with the wavy couplet sediment type.

greater and more variable current velocities and perhaps a different source area, possibly reflecting transport by longshore currents (Winston, pers. comm.). Bhattacharyya and others (1980) interpreted poorly-sorted, horizontally-laminated sand beds as high intertidal storm deposits. Variations in bed size, grain size, and sorting plus association with subaerial sedimentary structures also support this hypothesis.

B. Planar Cross-bedded Coarse Sand Subtype

Planar cross-bedded sand beds form low angle tabular sets which range from 10 to 50 cm. thick (Fig. 12). Individual sets are continuous across several meters of outcrop but locally contain foreset laminations or are truncated by other low-angle cross-beds. This subtype is interbedded with the wavy couplet sediment type.

Low-angle planar cross-beds may represent upper flow regime processes in the marine foreshore. Slight deviations in beach slope between tidal cycles causes truncation of previously deposited layers and therefore produces low-angle cross-bedding that is typical of foreshore deposits (Clifton, 1969). Foresets within this subtype may represent micro-delta bar deposits formed by washover fans (Schwartz, 1982).

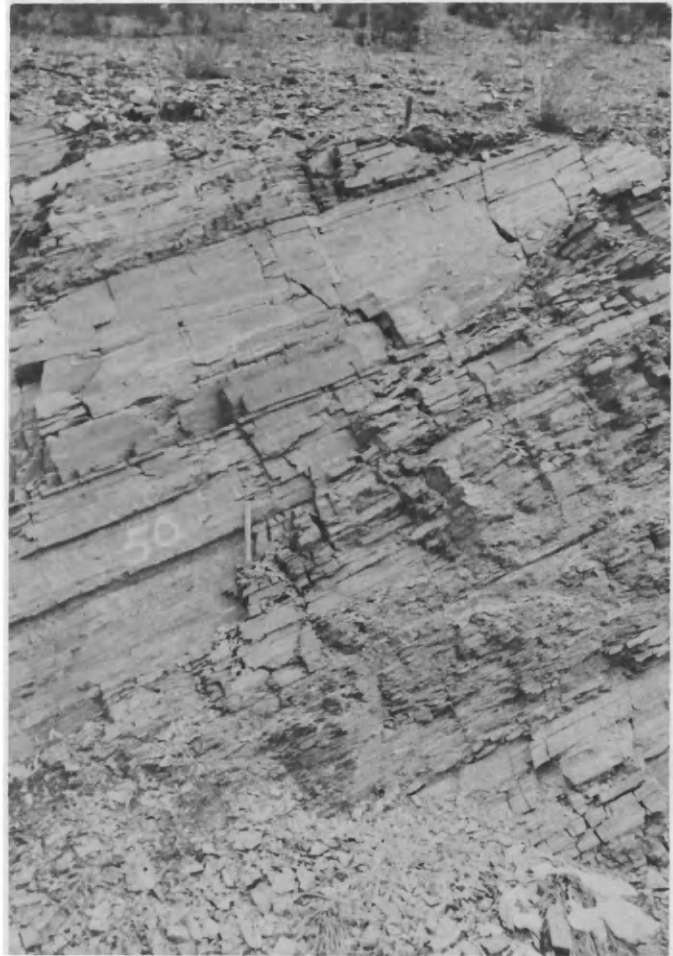


Figure 12. Low-angle planar cross-bedded coarse sand bed interbedded with the wavy couplet sediment type.

CHAPTER III

CORRELATION AND STRATIGRAPHIC SYNTHESIS

The last chapter discussed individual sediment types and proposed some depositional environments. The vertical succession of these sediment types in the Greyson-Spokane transition sequence defines three lithofacies labelled A, B, and C. This section 1) describes specific depositional environments for each of the lithofacies based on sediment type and stratigraphic juxtaposition, 2) correlates the measured sections, and 3) discusses conclusions based on the stratigraphy and sedimentation of the Greyson-Spokane transition sequence.

Lithofacies A

Lithofacies A consists primarily of the microlaminated couplet sediment type with occasional interstratified beds of the fine sand sediment type. Parallel lamination, absence of subaerial sedimentary structures, common dolomite, and stromatolites typify this lithofacies.

The structures within this lithofacies are characteristic of subtidal deposits. Carbonaceous microlaminated couplets probably formed by algal mats and stromatolites indicate deposition in the photic zone. Therefore, the subtidal environment of this part of the Helena embayment was probably shallow. The fine sand beds within this subfacies are generally thicker and less common than those interbedded with the wavy couplet sediment type. Subtidal fine sand beds were probably deposited and reworked by longshore currents (Whipple, 1980).

Lithofacies B

Lithofacies B consists primarily of interbedded wavy couplet and fine sand sediment types. The planar cross-bedded coarse sand subtype also occurs in this lithofacies. Mudcracks and mudchips commonly occur within the wavy couplets sediment type. Wavy bedding along with desiccation structures generally indicates an intertidal flat environment. Horizontally-laminated fine sand beds represent reworked, lower intertidal sand shoals. Planar cross-bedded coarse sand beds represent beach deposits also in a lower intertidal environment.

Lithofacies C

Lithofacies C consists of the horizontally-laminated coarse sand sediment subtype. This lithofacies occurs interstratified with the wavy couplet sediment type and is interpreted as an upper intertidal deposit. Whipple (1980) interpreted similar deposits in the Upper Spokane formation as beach berm deposits. Bhattacharyya and others (1980) interpreted horizontally-laminated coarse sand beds to be storm deposits which resulted from more intense wave action and turbulence.

Correlation

Each measured section has been subdivided into sequences of Lithofacies A, B and C. Correlation based on the succession of lithofacies reveals four marine regressive-transgressive cycles. Each cycle comprises an upward succession of Lithofacies ABCB (Fig. 13).

SCHEMATIC STRATIGRAPHIC COLUMN

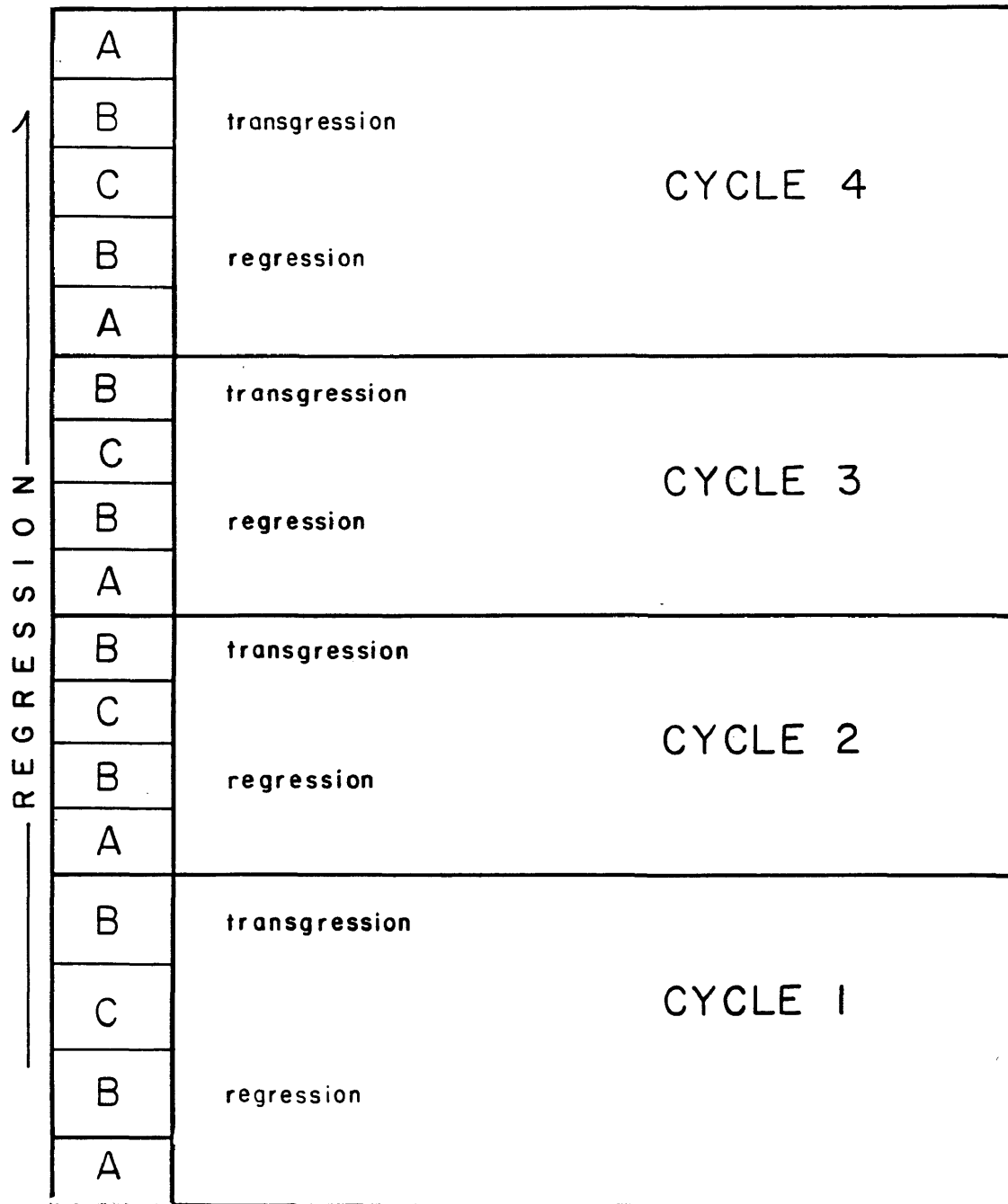


Figure 13. Schematic stratigraphic column showing four regressive-transgressive cycles.

The four cycles form the transition sequence and each cycle correlates well throughout all four measured sections (Fig. 14). Sections at Wolf Creek, Trout Creek, and Beaver Creek are approximately 100 meters thick while the Spokane Hills section is 220 meters thick.

Stratigraphic Synthesis

The Greyson-Spokane transition sequence represents a regressive sequence in a tide-dominated environment. However, it does not fit the "classic" tidal sequence because: 1) it lacks tidal channel deposits, and 2) lack of documented bimodal-bipolar current directions.

Several workers have interpreted Precambrian sequences (Klein, 1970a; Siedlecka, 1978) and Paleozoic sequences (Barnes and Klein, 1975; Walker and Harms, 1975) which lack evidence for tidal channels as tidal deposits. Several conditions might explain the absence of tidal channels. In a predominantly fine-grained system, a large volume of silt and clay that overwhelms sand may diminish development of beaches and shoals. Therefore, unrestricted tidal currents move over the flats in broad, uniform flow with little tendency to form channels. Lack of vegetation in the Proterozoic and the subsequent lack of a cohesive framework binding the surface of the tidal flat also enabled tidal currents to flow uniformly over the flat.

Sedimentary structures and bed configuration in the Greyson-Spokane transition sequence suggest an environment with low hydraulic energy. Extensive lateral continuity of individual beds suggest a broad, flat, featureless tidal flat and shelf. Nearshore wave intensity

CORRELATION OF REGRESSIVE TRANSGRESSIVE CYCLES

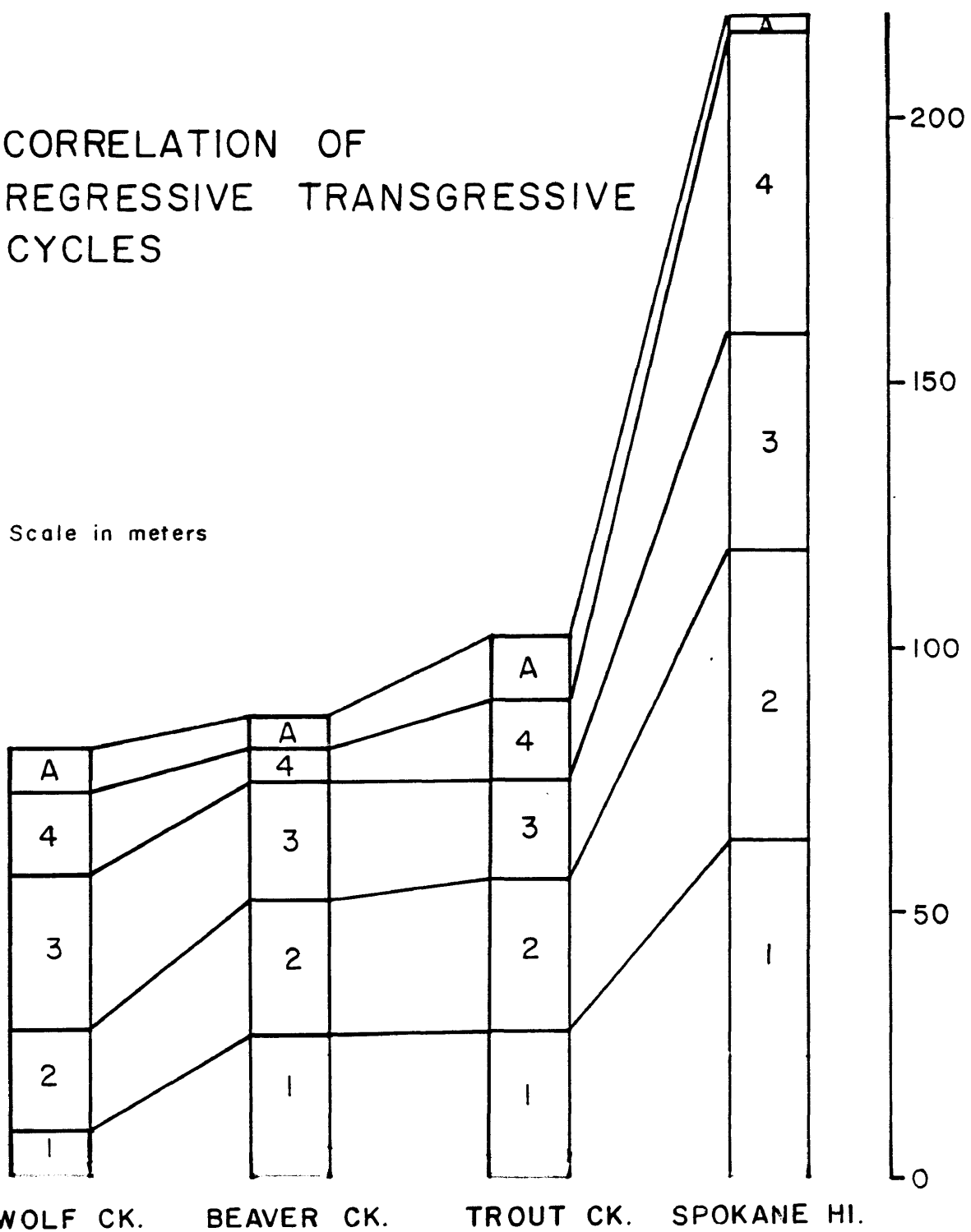


Figure 14. Correlation across four measured sections based on succession of lithofacies A, B, C, and D.

was probably generated by local winds rather than the wind fetch across the entire Belt sea. Because of the very large, shallow shelf, waves generated further out in deeper water "felt bottom" and lost energy as they travelled to shore. Additional evidence for low energy includes: 1) suspension-deposited silt and clay in the subtidal and intertidal zones rather than cross-bedded sands of more turbulent systems, and 2) preserved clay in wavy bedding rather than flaser bedding in the current-formed deposits.

Only apparent current directions were observed at the measured sections, therefore bimodal-bipolar current directions could not be documented. Although bimodal-bipolar current directions provide strong evidence for tidal currents, not all tidal deposits are bipolar. Time-velocity asymmetry produces unimodal crossbed directions in some tidal regimes (Klein, 1971; Watchorn, 1980). Therefore, even though tidal channels and bimodal-bipolar current directions are not documented in the Greyson-Spokane transition zone, a tidal flat interpretation is still possible.

Very fine sand, silt, and clay dominate the Greyson-Spokane transition zone. In the upper middle Spokane Formation, Whipple (1980) interprets horizontally-laminated subfeldspathic arenites as delta sheetwash and braided alluvial deposits surrounded by tidal flat deposits. The fluvial sediment input certainly affected sedimentation in the Spokane Formation. However, fine sand beds in the Greyson-Spokane transition sequence never occur in sets and never appear to be channel deposits. They probably represent totally reworked

sediments of a tidal environment whereas higher in the Spokane, they may represent primary fluvial deposits. The coarse sand size in the beach and storm deposits may indicate a different source with transport by longshore currents.

CHAPTER IV

GRAVITY ANALYSIS

The purpose of a gravity analysis of the study area was to look for more evidence for the proposed Proterozoic fault zones. Ideally, blocks of crystalline basement vertically offset near the fault zones would cause lateral changes in density and produce gentle, low frequency gravity trends. High frequency anomalies result from shallower sources. This study examines regional trends, anomalous residual features, and discusses interpretation of these features with respect to the proposed fault zones.

Gravity data were obtained from the U.S. Department of Defense. I hand-contoured Bouguer anomaly values at 5 milligal intervals over the study area and used a computer program to model a gravity profile over the area. Density contrasts are based on values published by Davis and others (1963) and Harrison and others (1980).

A generalized geologic map and Bouguer gravity map are shown in Figures 15 and 16. Major structural features include: 1) the Eldorado and related thrusts (York, Trout Creek, and Wolf Creek thrusts), 2) the exposed Paleozoic rocks north and east of the Scout Camp thrust, 3) the Helena and Townsend Valleys, and 4) the Boulder batholith and other Cretaceous intrusives.

The limited availability of gravity data beyond the study area made it difficult to discern a regional trend. Ballard (1980)

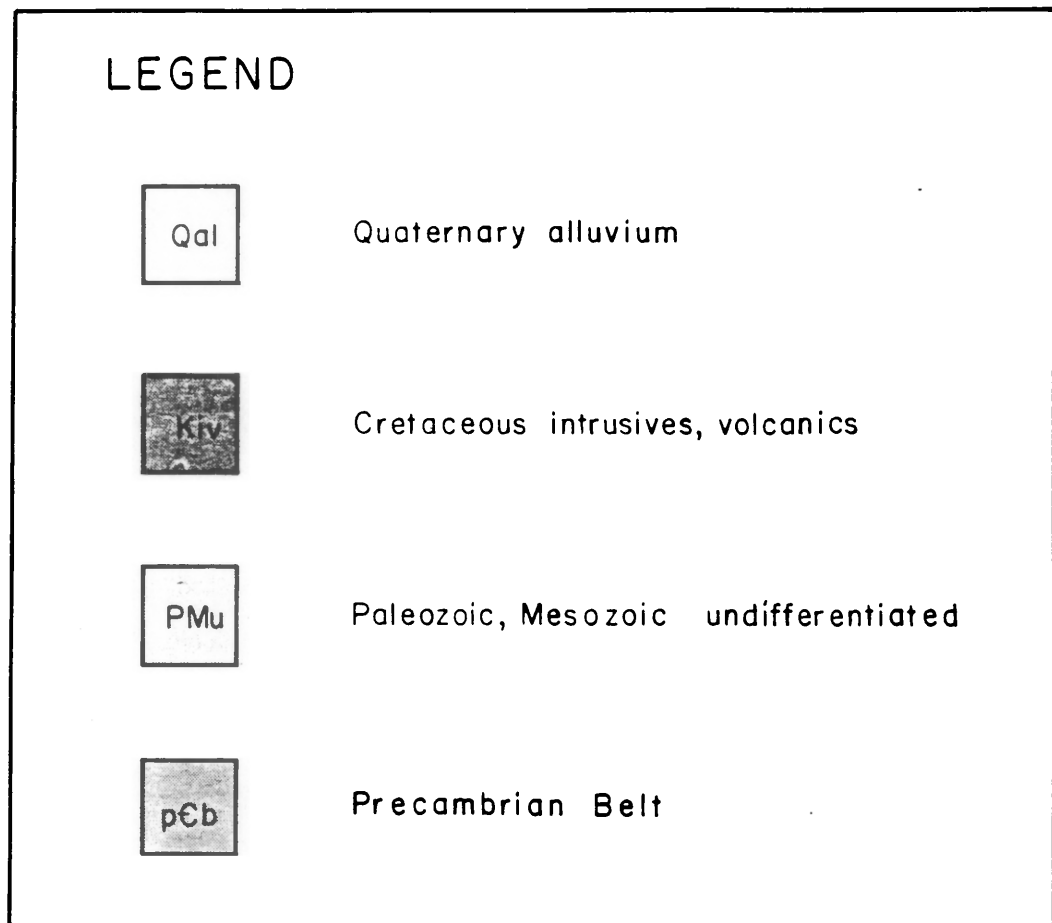


Figure 15. Generalized geologic map of the study area. See figure 4 for compilation index.

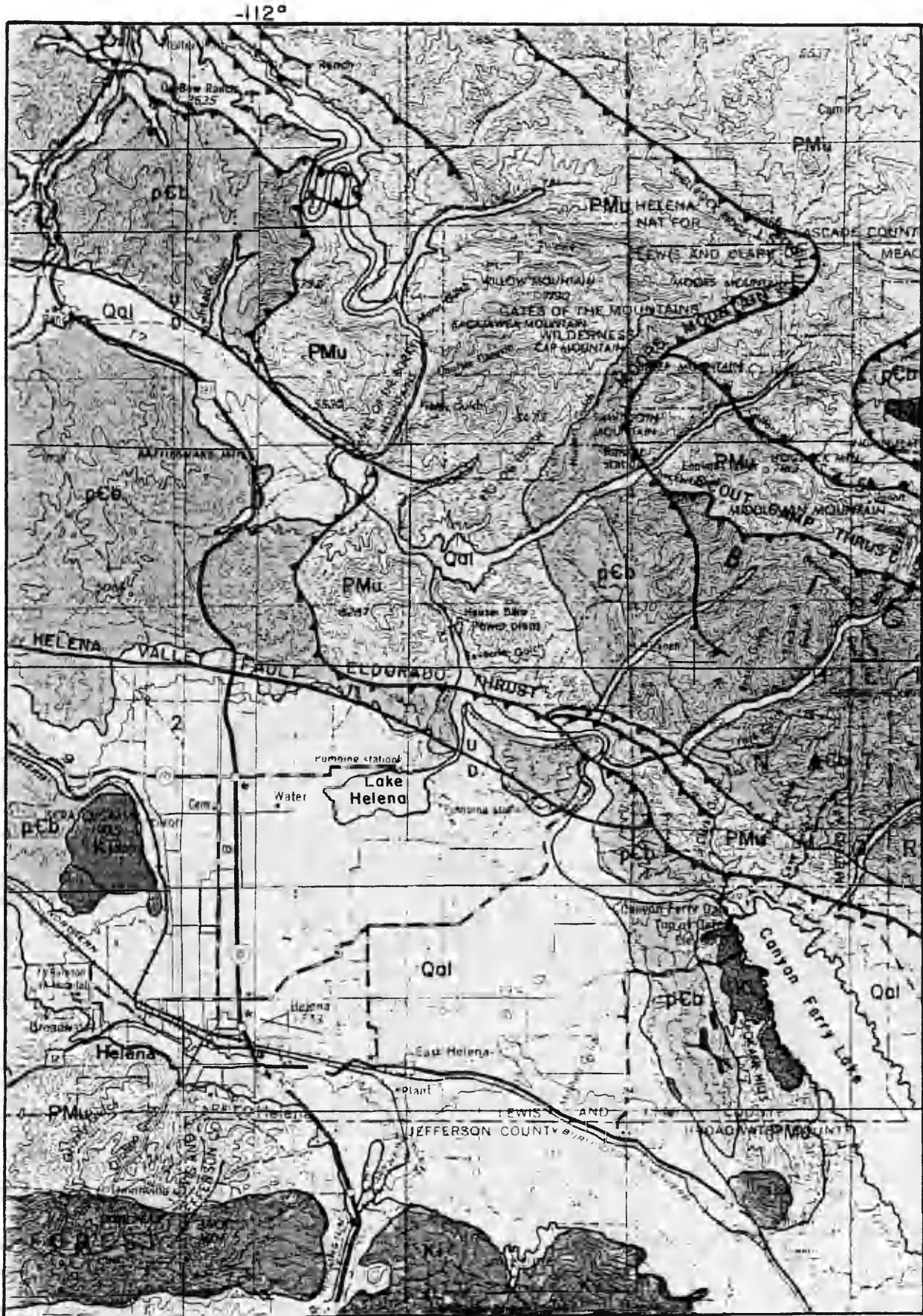


Figure 15.

Figure 16. Bouguer gravity map of the study area. Contours at 5 mgal. Cross-section in figure 17 from A to A'.

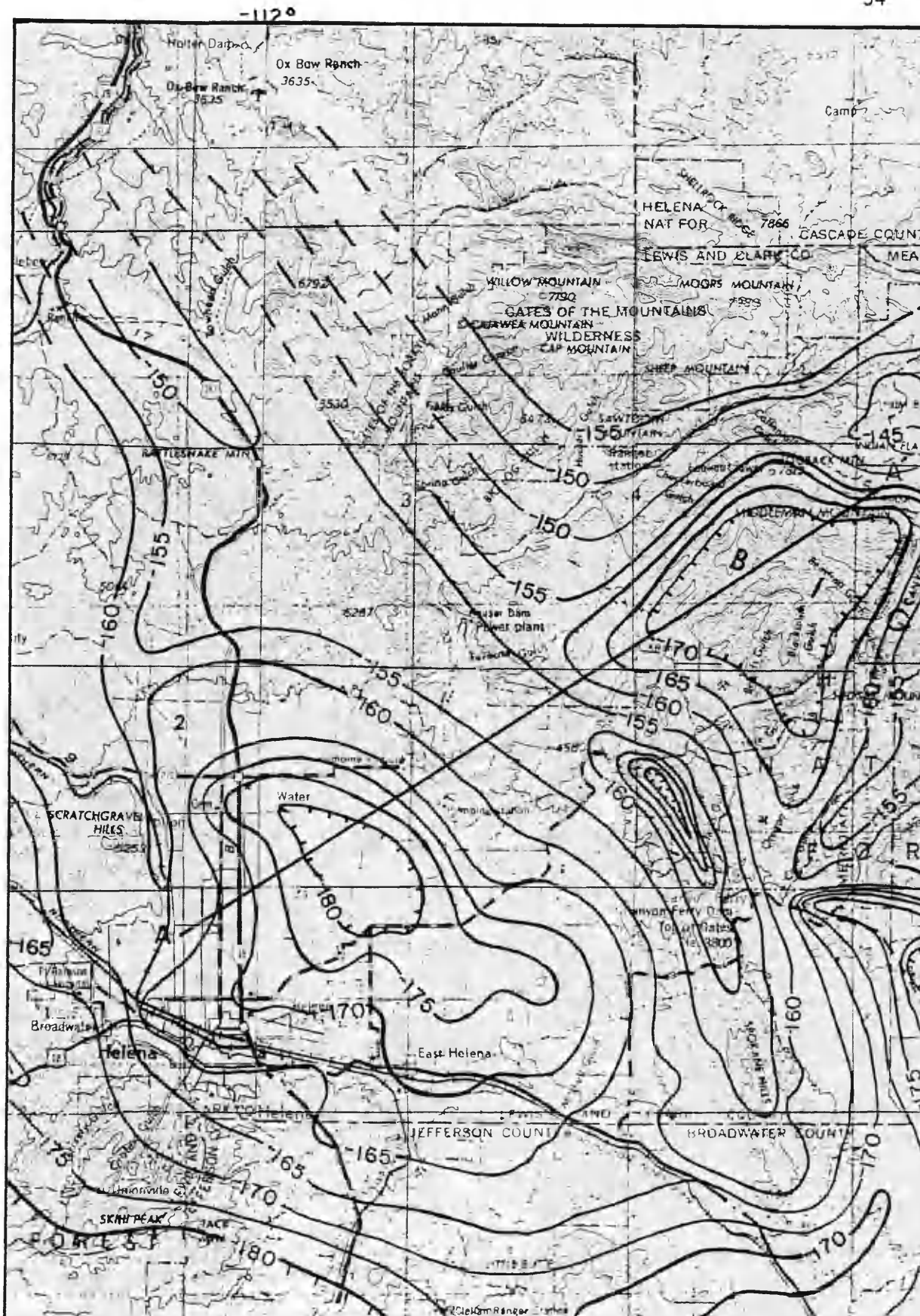


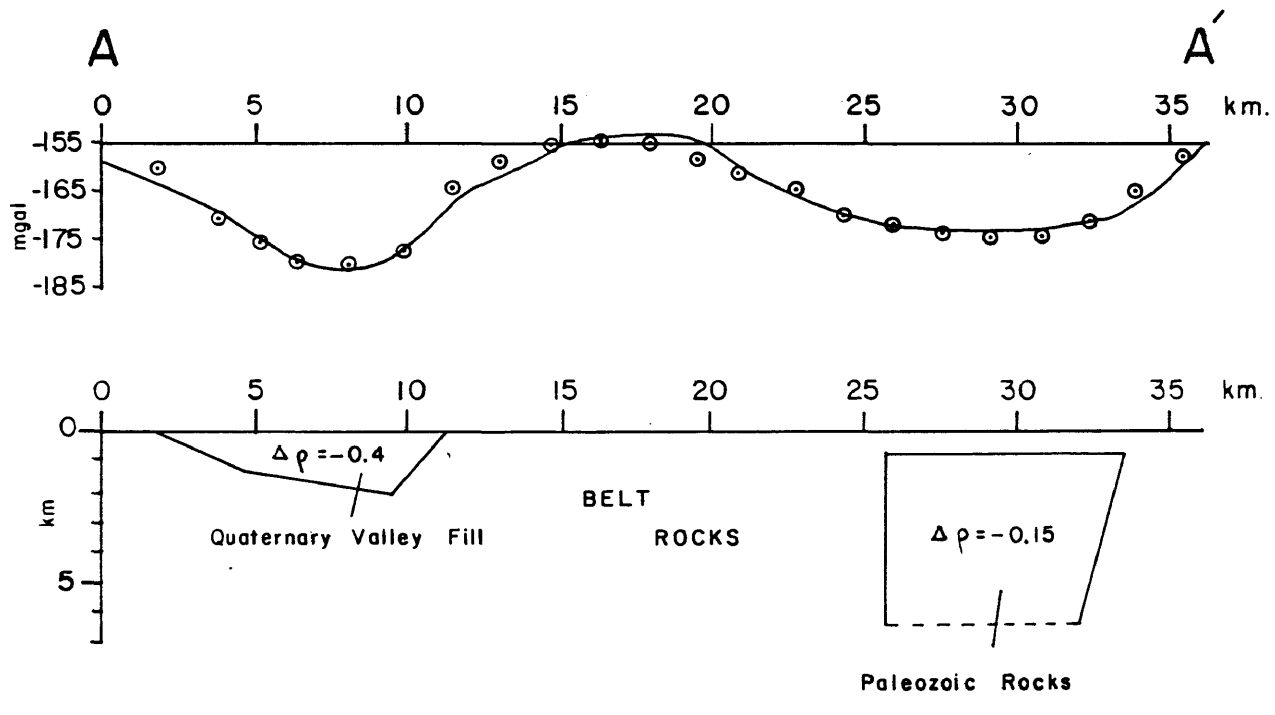
Figure 16

determined the regional trend near Helena to be a southwest-dipping plane which varies no more than 5 milligals through the study area. Therefore, regional gravity was ignored because of its negligible effect over the study area.

The higher frequency anomalies are well correlated with local geology. The Eldorado and related thrusts are reflected by a relatively high ridge which follows the thrust's north-northwesterly trend. Gravity lows with amplitudes of 20 to 25 milligals coincide with the Helena and Townsend Valleys and their low density fill (about 2.4 g/cm³). The Boulder batholith and satellite quartz monzonite intrusives also show up as gravity lows because of their negative density contrast with Belt rocks. Belt rocks generally coincide with higher gravity readings than the Paleozoic rocks so that the gravity low situated just south and west of the Scout Camp thrust and east of the Eldorado thrust requires further explanation.

Figure 17 shows the observed gravity and calculated anomalies from A to A' on Figure 16, a subsurface structure map and assumed density contrasts. In the cross-section, the gravity low over the Helena Valley is best modelled using a -0.4 g/cm³ density contrast with surrounding Belt rocks. Using this model, basin fill approximates 2000 meters thick, in good agreement with values of 1800 meters obtained by Davis and others (1963). The gravity high to the east of Helena Valley may be explained by Belt rocks ramped over Belt rocks. Belt rocks also crop out immediately east of the York and associated thrusts, although the gravity is anomalously low. Further to the

GRAVITY PROFILE ACROSS A - A'



DENSITY VALUES

Quaternary rocks	2.40
Paleozoic rocks	2.65
Belt rocks	2.80

Observed gravity	—
Calculated gravity	⊙ ⊙

Figure 17. Observed and calculated gravity anomalies from A to A' with model and densities used given below.

east, Paleozoic rocks are exposed along the Scout Camp thrust, and generally cover the northeastern corner of the study area. The anomalous gravity low over the Belt rocks south of the Scout Camp thrust may best be explained by Belt rocks thrust over Paleozoic rocks. A gravity model which places a lower density slab beneath Belt rocks in between the Eldorado and Scout Camp thrusts adequately accounts for the observed gravity low. As shown in Figure 17, the low density slab is flat-lying and near the surface.

The high frequency gravity data of this study are well explained by near surface geology, such as basin fill, intrusive stocks, and major thrust faults. Crystalline basement can not be delineated because the maximum anomaly expected over the uplifted basement block would be 10 to 12 milligals (using $+0.1 \text{ g/cm}^3$ density contrast at 2400 meters depth). Near surface structures produce anomalies with amplitudes of 20 to 25 milligals which might mask lower amplitude anomalies. However, it is reasonable to discuss the possible control of near surface structures by deeper structures. Several workers note changes in tectonic style around the area marked by the intersection of Winston's (1982 ms.) Greenhorn and Townsend lines.

Major thrusts within the Helena embayment steepen and curve westward as they approach the Greenhorn line (Reynolds, 1978) and pass into left-lateral strike slip faults north of the line (Birkholtz, 1967; Bregman, 1976; Woodward, 1981; Fig. 18). The Eldorado thrust also shifts westward north of the Greenhorn line. Bregman (1971, 1976) noticed that the thrust changed from high-angle imbricate slices north

of the Helena embayment to a single, low-angle slab near the Greenhorn line. He concluded that the imbricate thrusts north of the line resulted from buttressing by the crystalline basement. South of the line, where no similar buttressing exists, the thrust was able to ride at a low angle into the Helena embayment (Fig. 18). The most significant finding of this gravity study supports the hypothesis of low-angle, single sheet thrusting in the Helena embayment. Presumably, Belt rocks moved over nearly flat-lying Paleozoic rocks as a single sheet without the buttressing effect from a crystalline basement block.

The gravity part of this study did not prompt any new conclusions about crustal or near surface structure. Also in part, because of limited data outside the study area, there are no indications of "deep" basement offsets in the data. However, they do suggest a change in the tectonic style of the eastern thrust belt near Helena, which might represent a change in deeper crustal configuration.

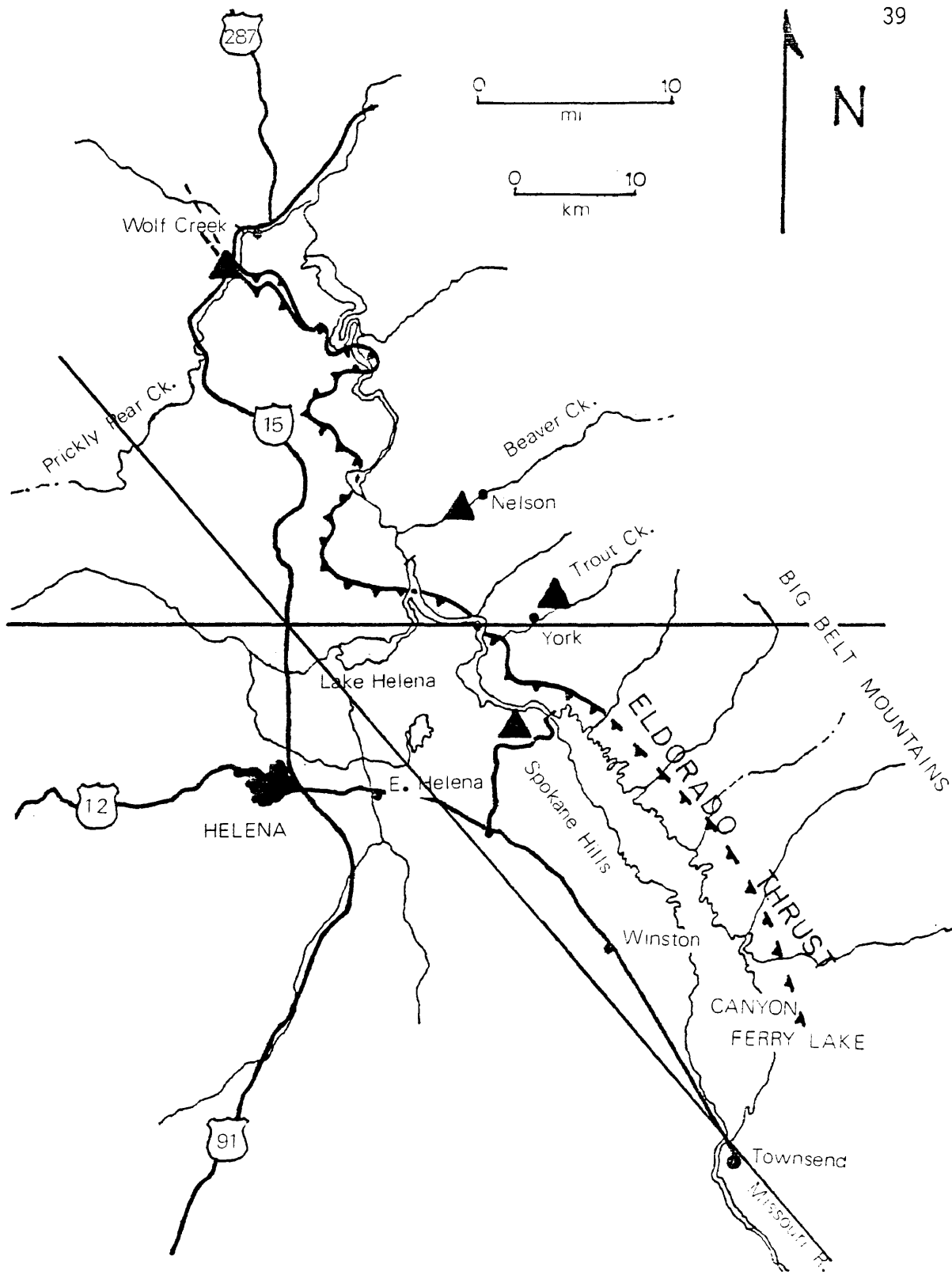


Figure 18. Map showing change in orientation of the Eldorado thrust near the Greenhorn line of Winston and others (1982 MS).

CHAPTER V

CONCLUSIONS

The stratigraphy and sedimentary structures of the Greyson-Spokane transition sequence reflect sedimentation in the intertidal to subtidal zone of a shallow, flat shelf. Rocks in the transition sequence record an overall marine regression including four regressive-transgressive cycles. The four cycles define the transition sequence and are well correlated across the four measured sections. The occurrence of both horizontally-laminated fine sand beds and horizontally-laminated coarse sand beds suggests two source areas. Sheetwash and fluvial deposits which occur in the Upper Middle Spokane Formation (Whipple, 1980) probably represent the source for the abundant fine sand fraction. Variation in sediment input from this source may explain changes in the proportion of fine sand to silt and clay size material throughout the Greyson-Spokane transition sequence. Coarse sand, possibly reflecting a different source, may have been brought in by longshore currents.

Gravity data in the area encompassing the measured sections generally reflect near surface geology and structure. An anomalous gravity low over Belt rocks on the upper plate of the Scout Camp thrust may be modelled by placing a thin slab of Belt rocks over a nearly horizontal block of lower density, Paleozoic rocks. These results suggest that the Scout Camp thrust is a low-angle, single

sheet thrust, and agree with Bregman's (1971, 1976) conclusions about the Eldorado thrust to the west.

Evidence for Proterozoic fault zones from the data in this thesis is similar to data used by Winston and others (1982 ms.). Their primary evidence consists of stratigraphic thickness changes and differential thrusting response across their proposed lines. North of the Greenhorn line and east of the Townsend line, the Greyson-Spokane transition sequence is approximately 100 meters thick. South of the Greenhorn line, in the Helena embayment, the sequence is 220 meters thick. Since the measured sections are located on two different thrust plates, only sections on the same plate may be correlated with known distance between them. Some reconstruction is necessary to compare sections across the Eldorado thrust. Several estimates of shortening from the Idaho-Wyoming and Canadian thrust belts fall very close to 50 percent (Royce and others, 1975). The Trout Creek (120 meters) and Spokane Hills (240 meters) sections lie on opposite sides of the Eldorado thrust approximately 10 kilometers apart. Using the 50 percent shortening value, the minimum distance between two sections which straddle the Greenhorn line increases to 20 kilometers. This displacement value agrees fairly well with Bregman's (1971) estimate of 16.9 kilometers. A slight thickness change south of the Greenhorn line may suggest a higher rate of subsidence however, evidence for faulting seems weak.

An additional conclusion drawn from this study is the suggestion for a mappable contact between the Greyson and Spokane Formation.

Previous workers used the first appearance of red color in the rocks for the contact (Mertie and others, 1951; Durham, 1972). The lowest red beds vary in stratigraphic level from section to section in the transition sequence. A change in primary sedimentary features rather than secondary diagenetic features would be more clearly definable and consistent. For this reason, I propose that the contact be drawn at the top of the last calcareous microlaminated couplet sequence. This would reduce the confusion caused by the irregular diagenetic red and green coloration of the rocks in the Greyson-Spokane transition sequence.

REFERENCES CITED

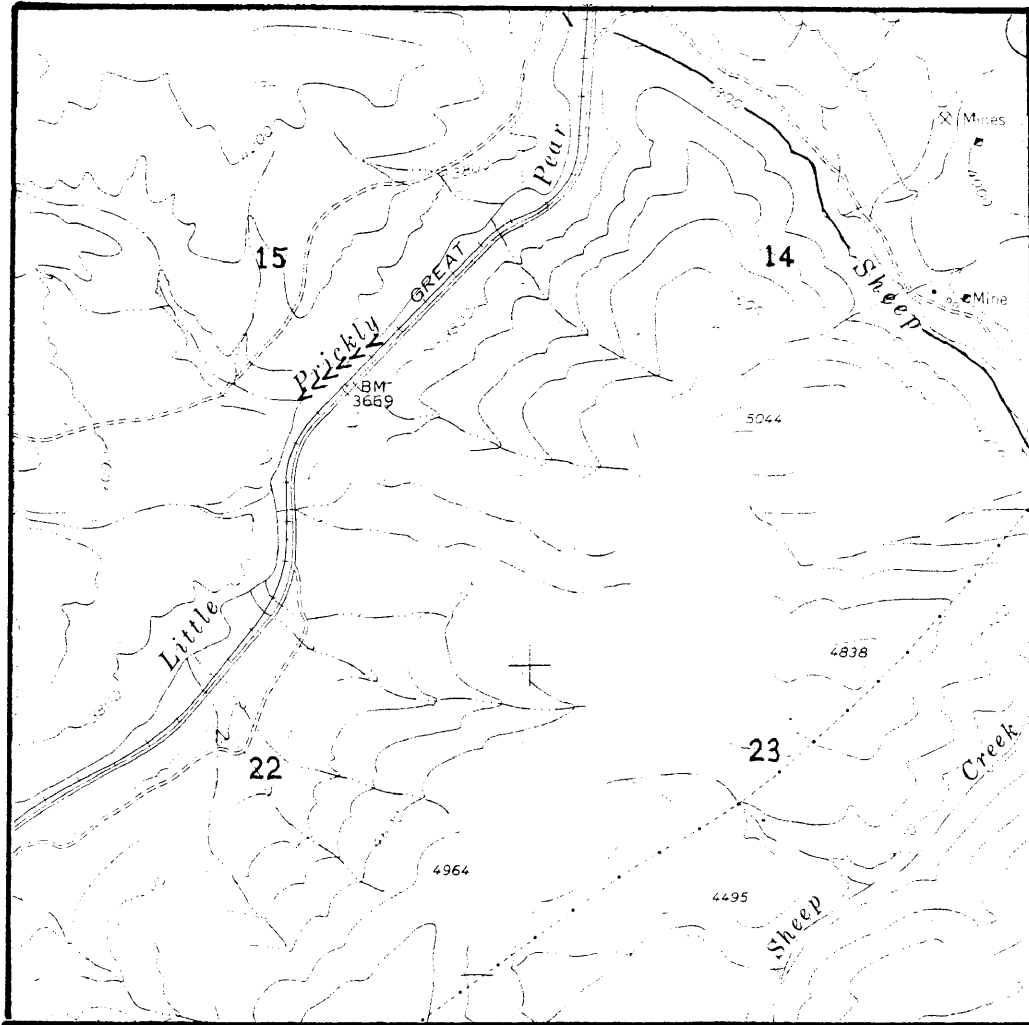
- Ballard, J.H., 1980, Seismic and gravity investigation of the crust and upper mantle in southwestern Montana, M.S. thesis, Univ. of Montana, 98 p.
- Barnes, J.J., and Klein, G. deV., 1975, Tidal deposits in the Zabriskie Quartzite (Cambrian), eastern California and Western Nevada: in Ginsberg, R.N., ed., Tidal Deposits, Springer-Verlag, Berlin, p. 5-12.
- Bhattacharyya, A., Sarkar, S., and Chanda, S.K., 1980, Storm deposits in the Late Proterozoic Lower Bhandar Sandstone of Vindhyan Supergroup around Maihar, Satna District, Madhya Pradesh, India: Jour. Sed. Pet., v. 50(4), p. 1327-1335.
- Birkholtz, D.O., 1967, Geology of the Camas Creek Area, Meagher County, Montana, M.A. thesis, Montana College Mineral Sci. Tech., Butte, Montana, 68 p.
- Bregman, M.L., 1971, Structural geology of the Sheep Creek and Rattlesnake Mountain quadrangles, Lewis and Clark County, Montana: Ph.D. thesis, Univ. of New Mexico, Albuquerque, N.M., 99 p.
- _____, 1976, Change in tectonic style along the Montana thrust belt: Geology, v. 4, p. 775-778.
- Clifton, H.E., 1969, Beach lamination: Nature and Origin: Marine Geol. v. 7, p. 553-559.
- Davis, W.E., Kinoshita, W.T., and Smedes, H.W., 1963, Bouguer gravity, aeromagnetic, and generalized geologic map of East Helena and Canyon Ferry quadrangles and part of the Diamond City quadrangle, Lewis and Clark, Broadwater, and Jefferson Counties, Montana: U.S. Geol. Surv. Map GP-444.
- Durham, J.A., 1972, Structural geology of the northern part of the East Helena quadrangle, Lewis and Clark County, Montana: M.S. thesis, Univ. New Mexico, Albuquerque, 71 p.
- Gebelein, C.D., 1969, Distribution, morphology, and accretion rate of recent subtidal algal stromatolites, Bermuda: Jour. Sed. Pet. v. 39, p. 49-69.
- Grotzinger, J.P., 1981, The stratigraphy and sedimentation of the Wallace Formation, northwestern Montana and northern Idaho: M.S. thesis, Univ. of Montana, 153 p.

- Harrison, J.E., Kleinkopf, M.D., and Wells, J.D., 1980, Phanerozoic thrusting in Proterozoic Belt rocks, northwestern United States: *Geology*, v. 8, p. 407-411.
- Harrison, J.E., Griggs, A.B., and Wells, J.D., 1974, Tectonic features of the Precambrian Belt basin and their influence on post-Belt structures: *U.S. Geol. Surv. Prof. Paper 866*, 15 p.
- Klein, G.deV., 1970, Tidal origin of a Precambrian quartzite - The lower fine-grained quartzite (Middle Dalradian) of Islay, Scotland: *Jour. Sed. Pet.* v. 40(3), p. 973-985.
- _____, 1970b, Depositional and dispersal dynamics of intertidal sand bars: *Jour. Sed. Pet.* v. 40(4), p. 1095-1127.
- Knopf, A., 1963, Geology of the northern part of the Boulder batholith and adjacent area, Montana: *U.S. Geol. Surv. Misc. Inv. Map I-381*.
- Lyons, J.B., 1944, Igneous rocks of the northern Big Belt Range, Montana: *Geol. Soc. Amer. Bull.* v. 55, p. 445-472.
- McBride, E.F., Shepard, R.G., Crawley, R.A., 1975, Origin of parallel, near horizontal laminae by migration of bedforms in a small flume: *Jour. Sed. Pet.* v. 45, p. 132-139.
- Mertie, J.B., Jr., Fisher, R.P., and Hobbs, S.W., 1951, Geology of the Canyon Ferry quad, Montana: *U.S. Geol. Surv. Bull.* 972, 97 p.
- Mudge, M.R., 1970, Origin of the disturbed belt in northwestern Montana: *Geol. Soc. Amer. Bull.*, v. 81, p. 377-392.
- O'Connor, M.P., 1972, Classification and environmental interpretation of the cryptalgal organosedimentary "Molar-tooth" structure from the Late Precambrian Belt-Purcell Supergroup: *Jour. Geol.* v. 80, p. 592-610.
- Reineck, H.E., 1975, German North Sea tidal flats: *in* Ginsberg, R.N., ed., *Tidal Deposits*, Springer-Verlag: Berlin, p. 5-12.
- Reynolds, M.W., 1978, Thrust faults near the Lewis and Clark line in Montana: *U.S. Geol. Surv. Prof. paper 1100*, p. 68-69.
- Robinson, G.D., McCallum, M.E., and Hays, W.H., 1969, Upper Holter Lake Quadrangle, Lewis and Clark County, Montana: *U.S. Geol. Surv. Geol. Quad. Map GQ-840*.
- Royce, Jr., F., Warner, M.A., and Reese, D.L., 1975, Thrust belt structural geometry and related stratigraphic problems, Wyoming-Idaho-Northern Utah: *Rocky Mt. Assoc. Geol. 1975 Symp.*, p. 41-54.

- Schmidt, R.G., 1972, Geologic map of the Wolf Creek Quadrangle, Lewis and Clark, County, Montana: U.S. Geol. Surv. Quad. Map GQ-974.
- Shaffer, W.L., 1971, Geology of the Hogback Mountain area, northern Big Belt mountains, Montana: M.S. thesis, Univ. New Mexico, Albuquerque, 66 p.
- Schwartz, R.K., 1982, Bedform and stratification characteristics of some modern small-scale washover sand bodies: *Sedimentology* v. 29, p. 835-849.
- Sellwood, B.W., 1975, Lower Jurassic tidal-flat deposits, Bornholm, Denmark: *in* Ginsberg, R.N., ed., *Tidal Deposits*, Springer-Verlag, Berlin, p. 93-101.
- Siedlecka, A., 1978, Late Precambrian tidal-flat deposits and algal stromatolites in the Batsfjord formation, east Finnmark, North Norway: *Sed. Geol.* v. 21, p. 277-310.
- Talwani, M., Worzel, J.L., and Landisman, N., 1959, Rapid gravity computations for two-dimensional bodies with applications to the Mendicino fracture zone: *Jour. Geophys. Res.* v. 64, p. 49-59.
- Thompson, R.W., 1975, Tidal-flat sediments of the Colorado River delta northwestern Gulf of California: *in* Ginsberg, R.N., ed., *Tidal Deposits*, Springer-Verlag, Berlin, p. 57-65.
- Walker, R.G., and Harms, J.C., 1975, Shorelines of weak tidal activity: Upper Devonian Catskill formation, Central Pennsylvania: *in* Ginsberg, R.N., ed., *Tidal Deposits*, Springer-Verlag, Berlin, p. 103-108.
- Watchorn, M.B., 1980, Fluvial and tidal sedimentation in the 300 Ma Mozaan Basin, South Africa: *Precambrian Res.* v. 13, p. 27-42.
- Weinberg, D.M., 1970, Structural geology of the Beaver Creek area, Big Belt Mountains, Montana: M.S. thesis, Univ. New Mexico, Albuquerque, 49 p.
- Whipple, J.W., 1980, Depositional environment of the middle Proterozoic Spokane Formation-Empire Formation transition zone, west-central Montana: U.S. Geol. Surv. Open-file report 80-1232, 103 p.
- Winston, D., Jacob, P., Baldwin, D.O., and Reid, J.P., 1982, Proterozoic block faulting in the Belt basin, Montana and Idaho, Its effect on Rocky Mountain thrusting and Basin and Range extension: unpub. man.
- Woodward, L.A., 1981, Tectonic framework of disturbed belt of west-central Montana: *Amer. Assoc. Petrol. Geol. Bull.* v. 65, p. 291-302.

Appendix A

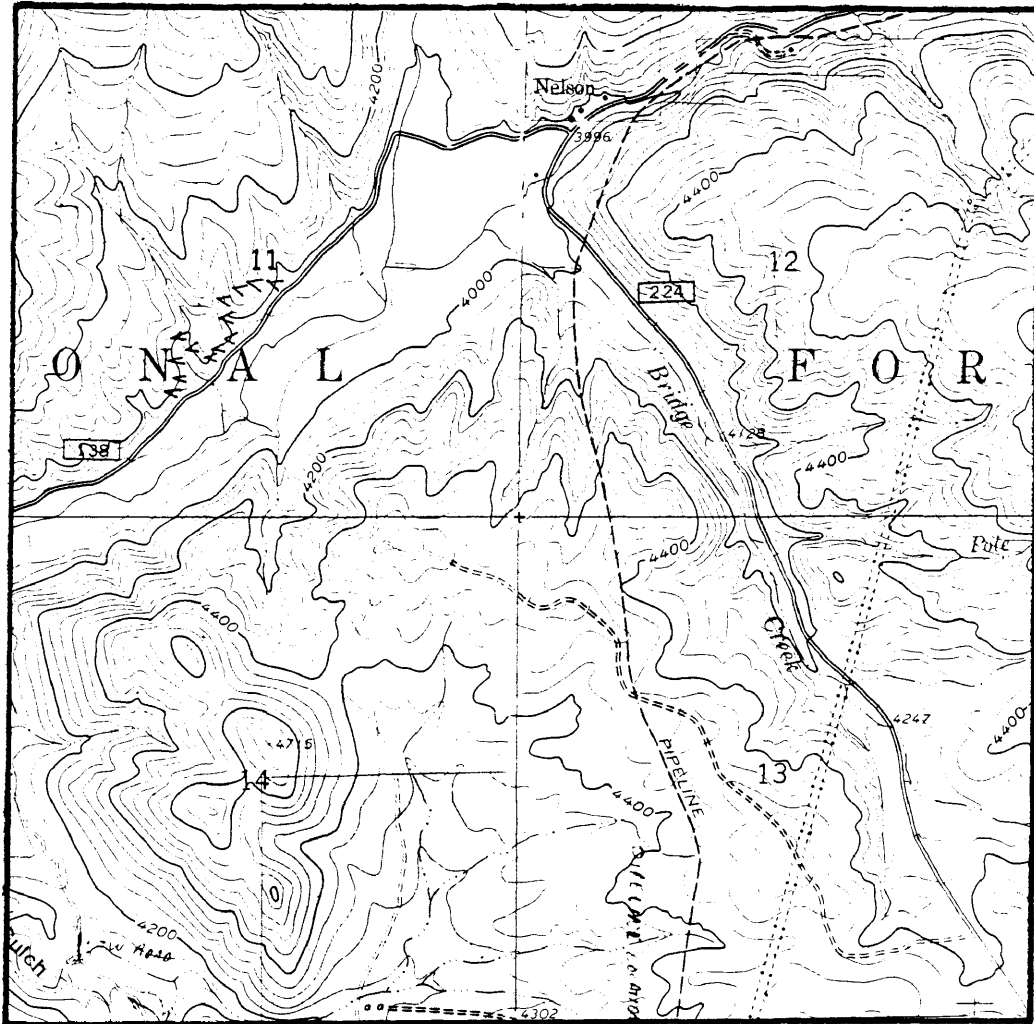
Exact locations of measured sections



WOLF CREEK SECTION

Located in Section 15, T.14 N., R.4 W.

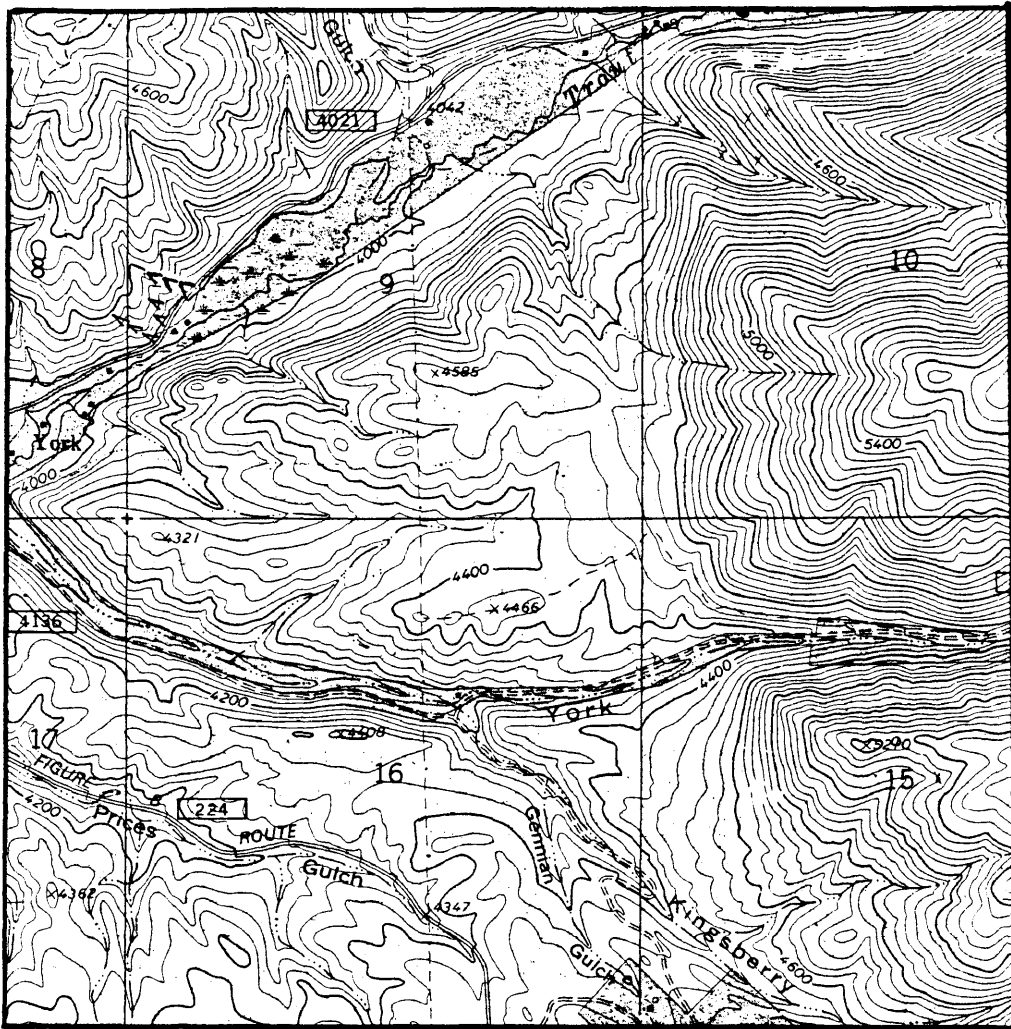
(2.8 miles south on I-15 from Wolf Creek, Montana)



BEAVER CREEK SECTION

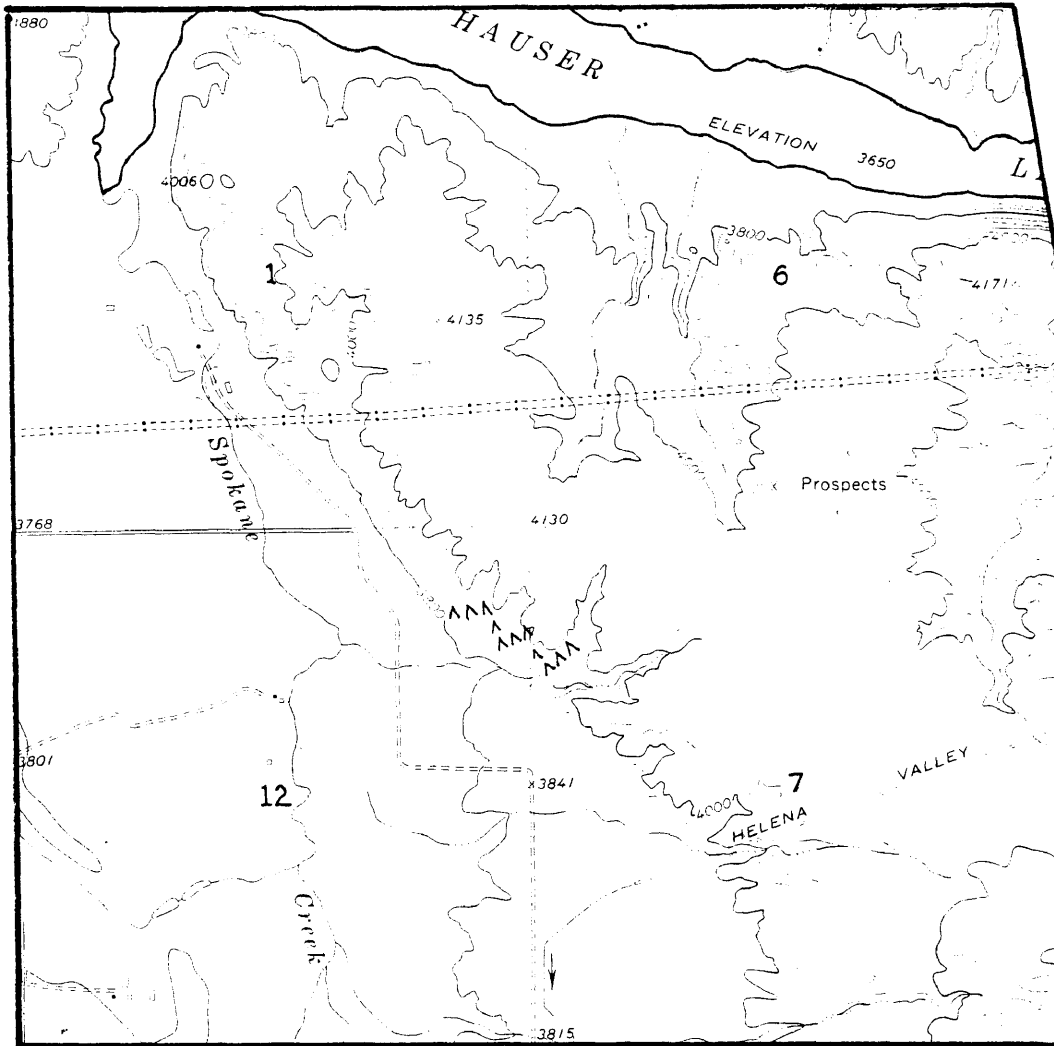
Located in Section 11, T.12 N., R.2 W.

(1.3 miles east from Nelson, Montana)



TROUT CREEK SECTION

Located in Section 9, T.11 N., R.2 W.

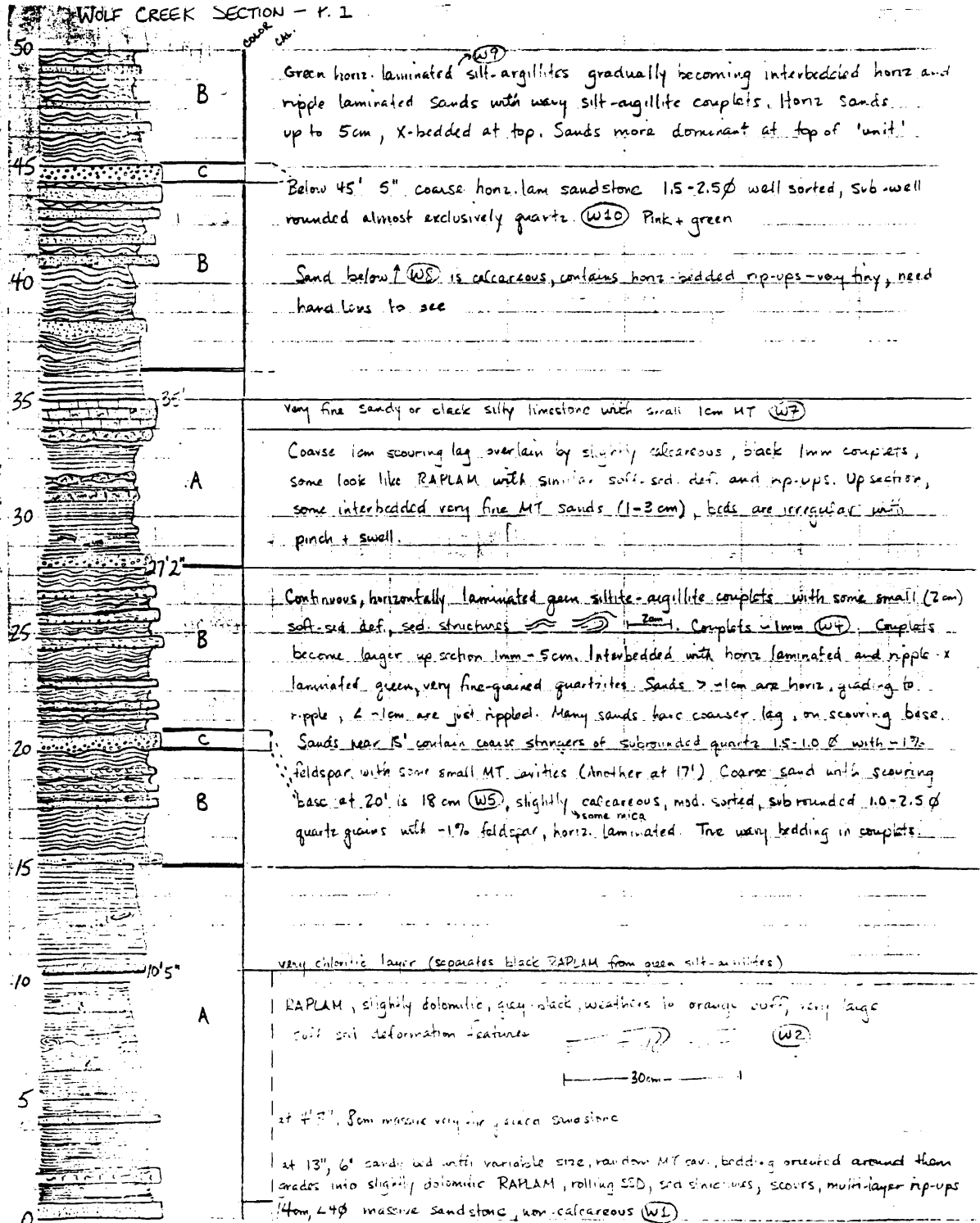


SPOKANE HILLS SECTION

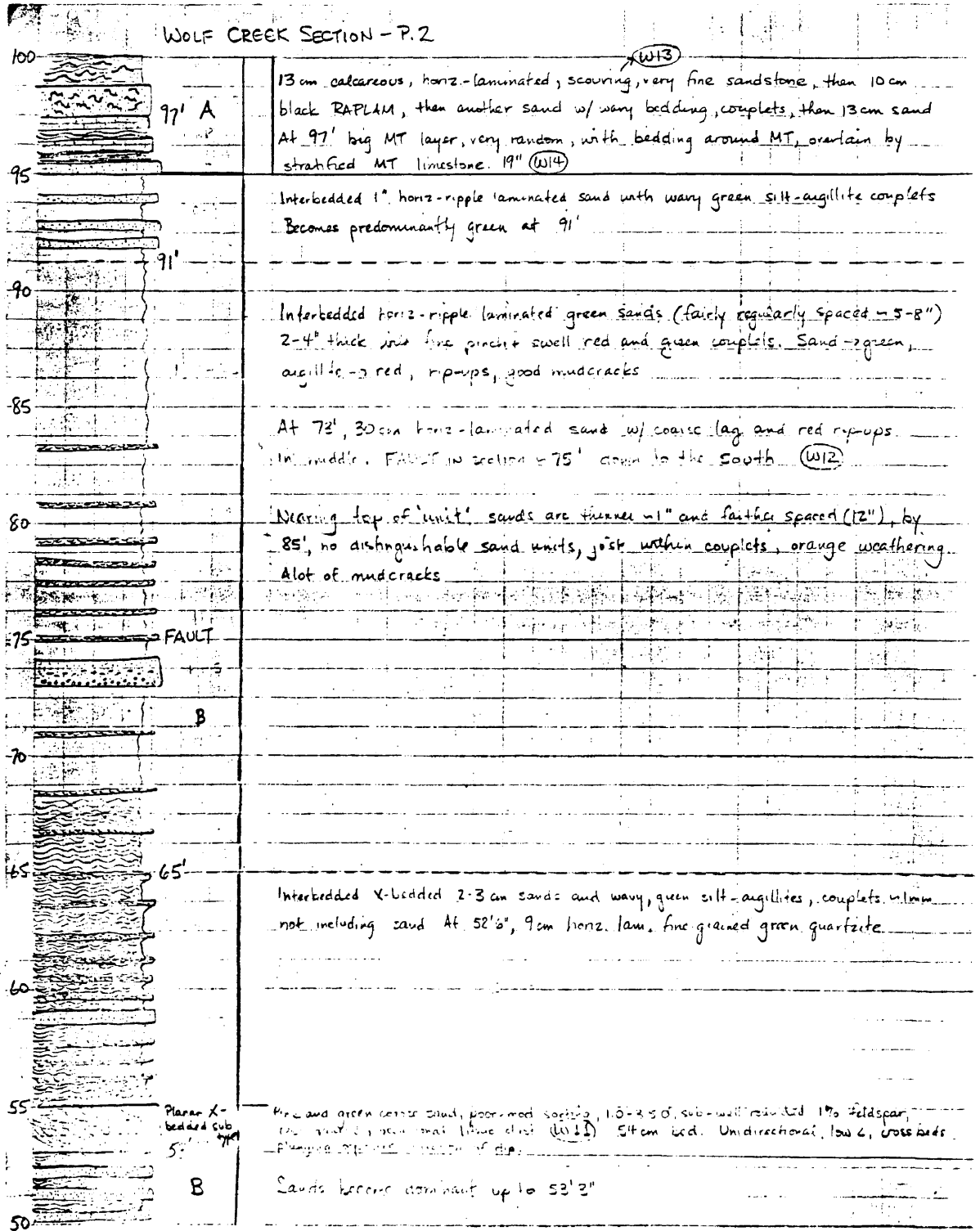
Located in Section 12, T. 10 N., R.2 W.

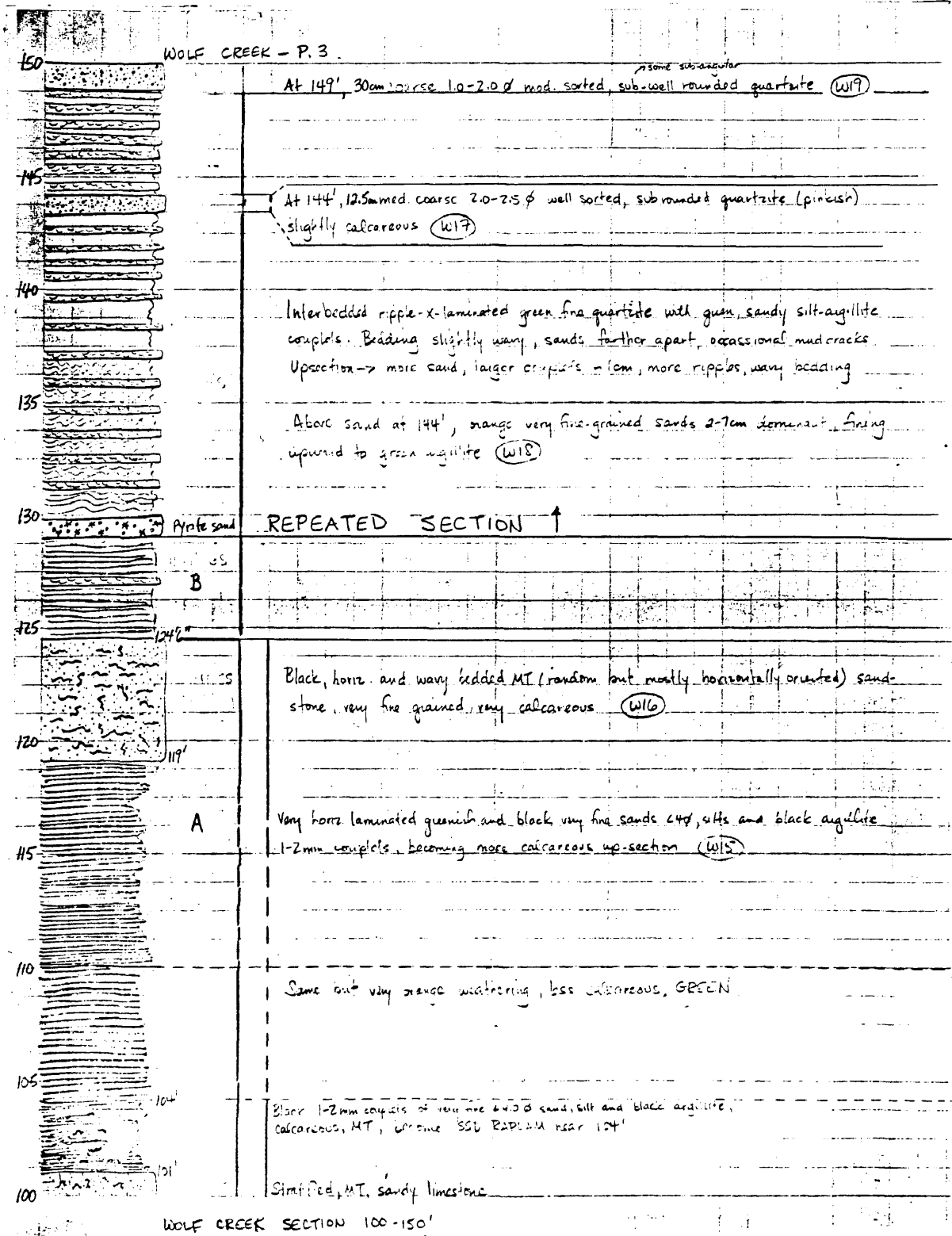
(on Curly McMaster's property)

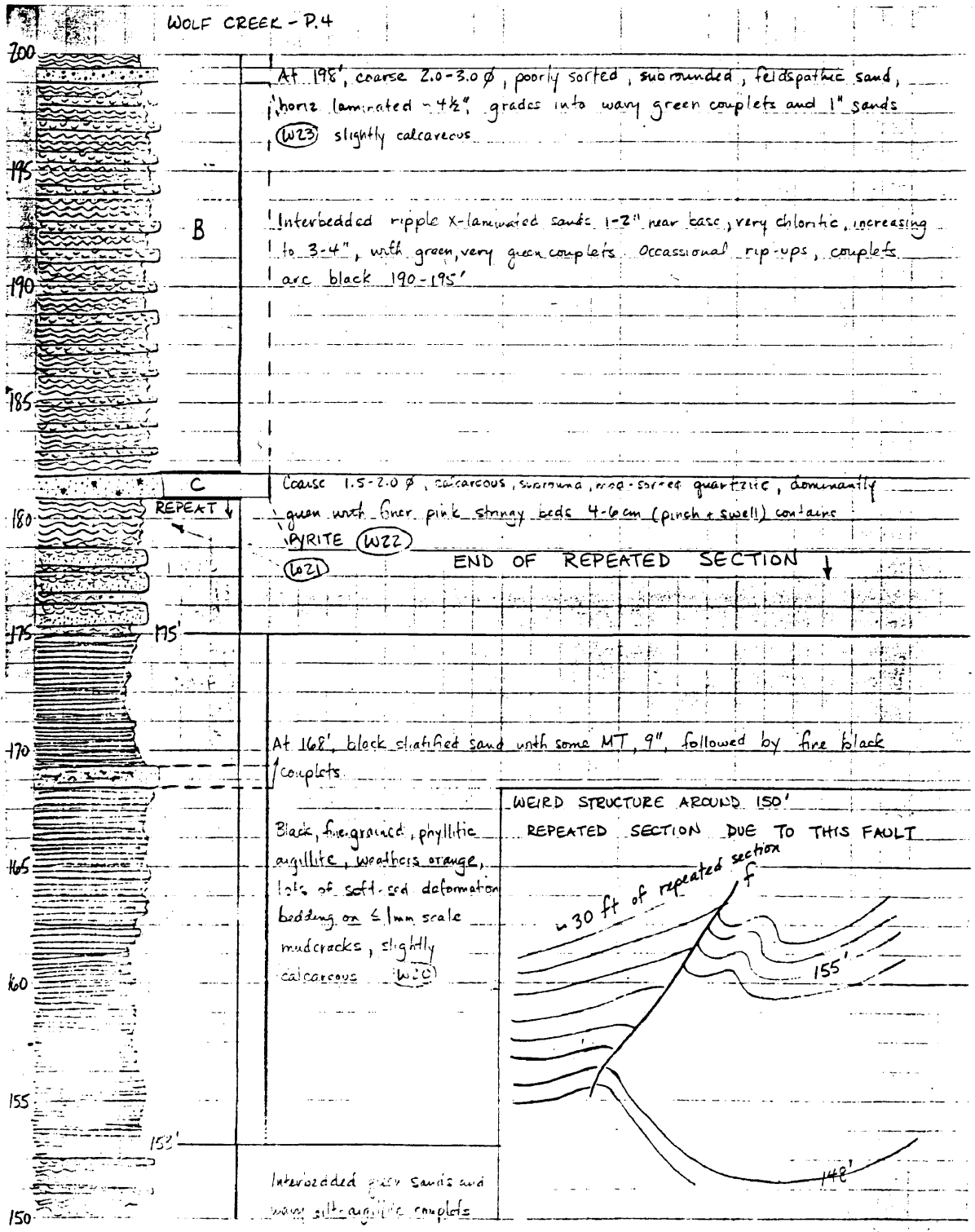
Appendix B
Measured Sections

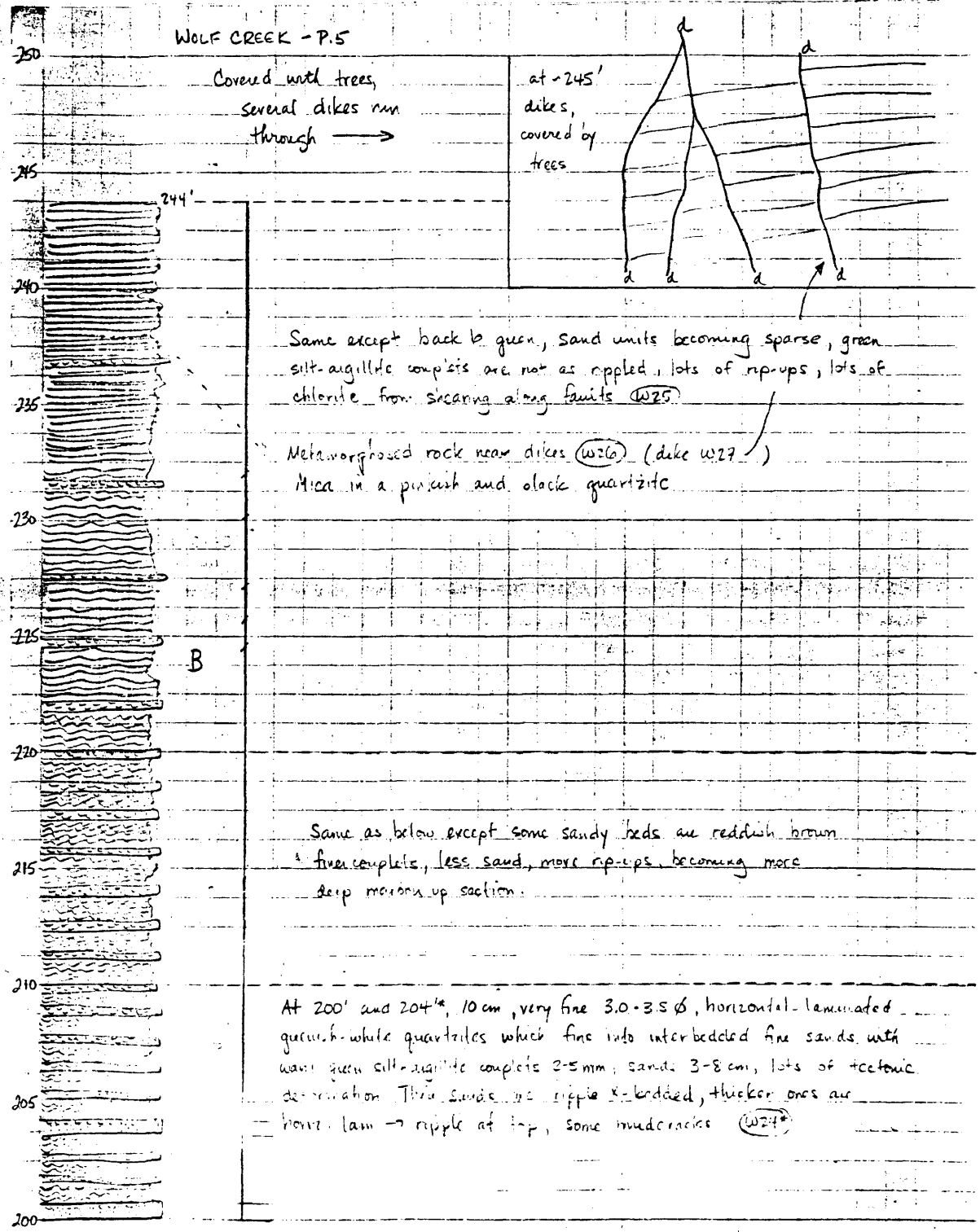


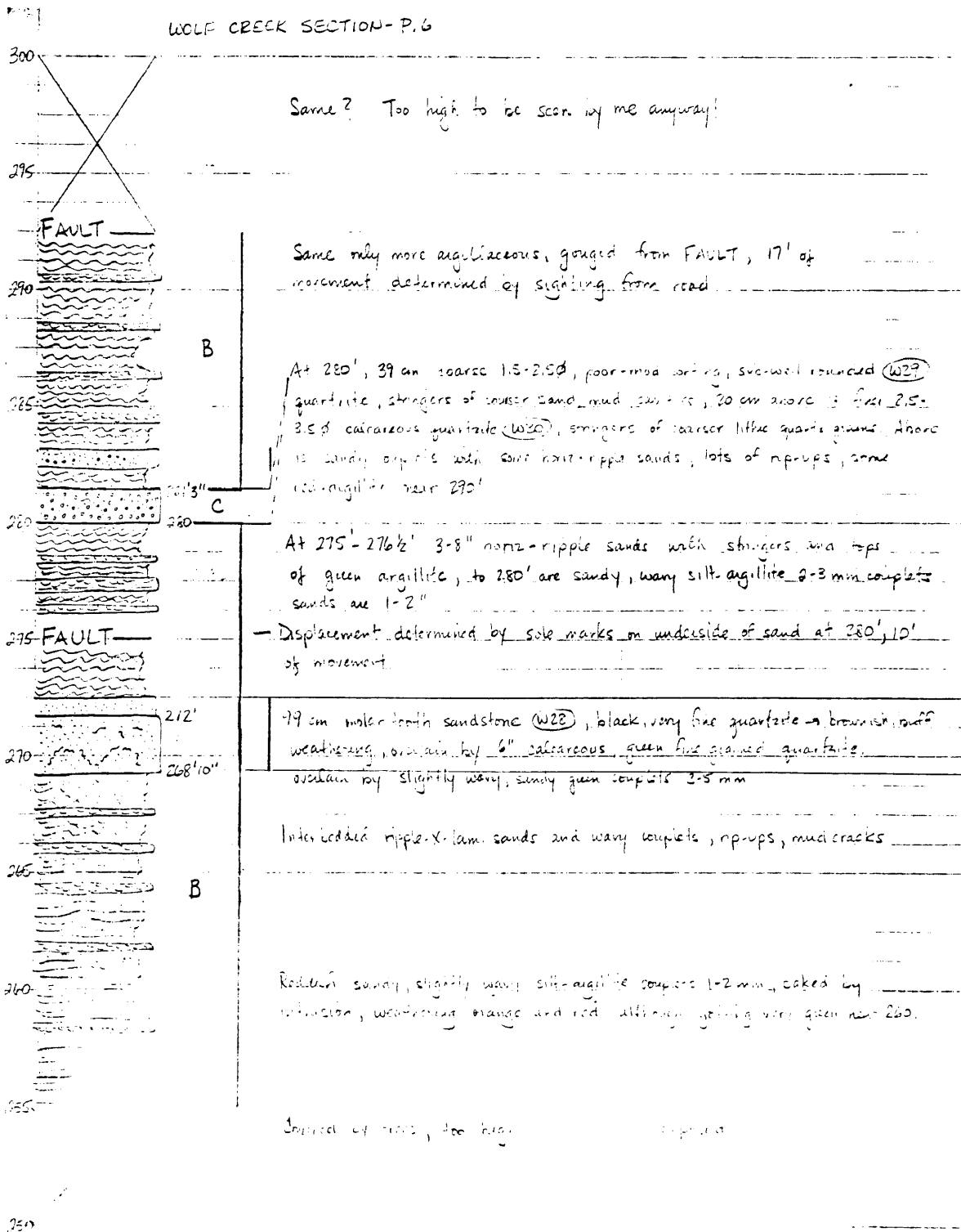
WOLF CREEK SECTION 430 ft.



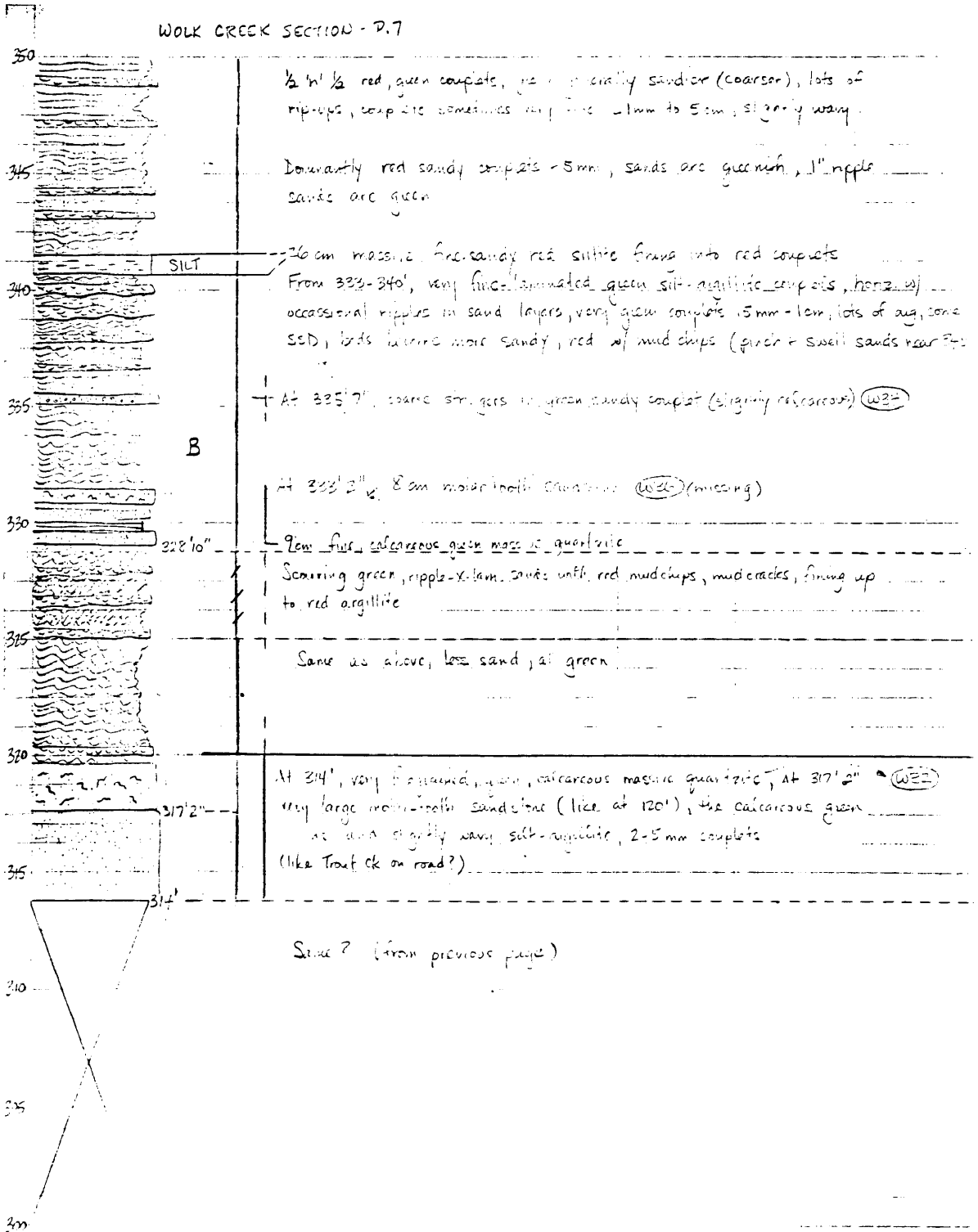


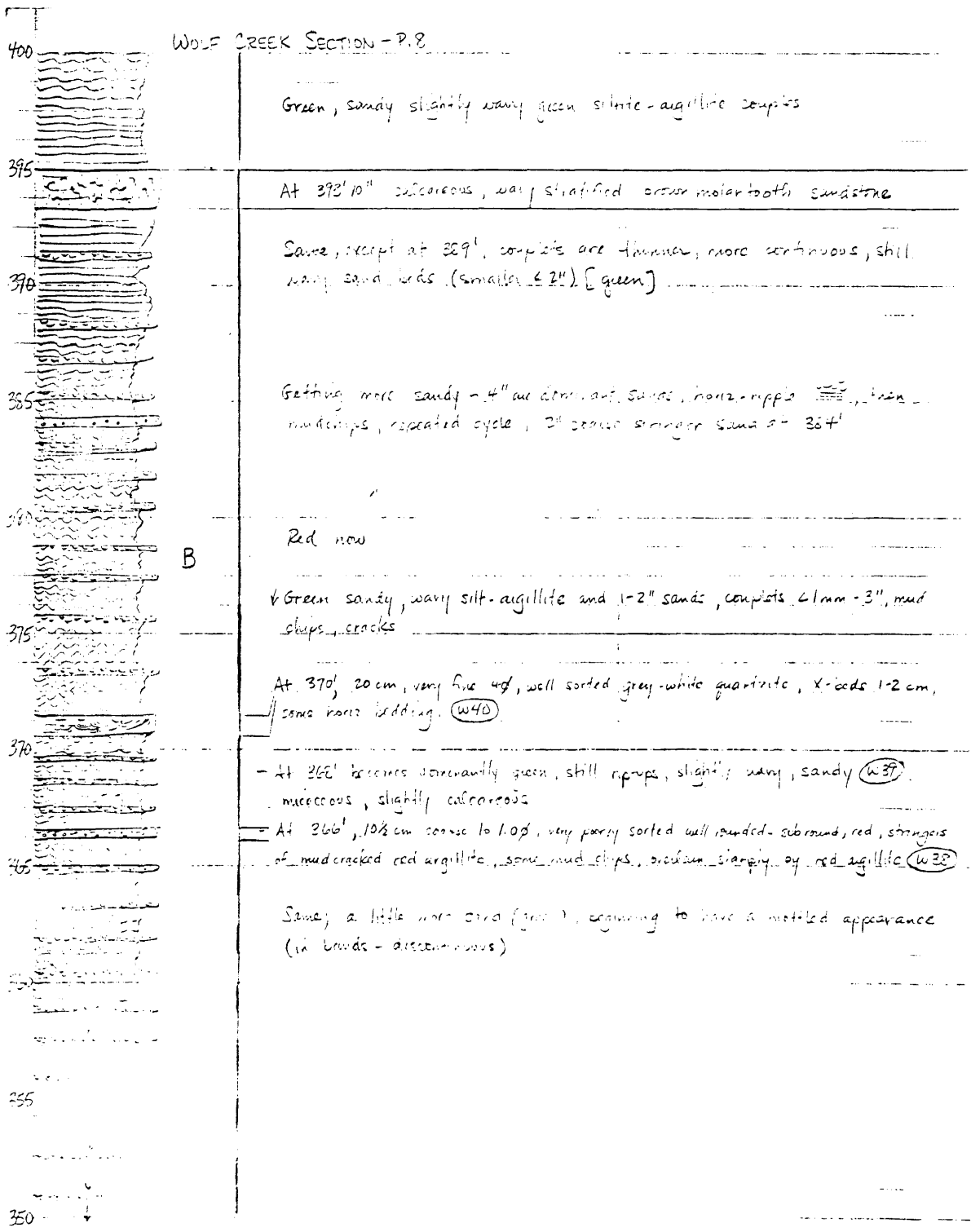




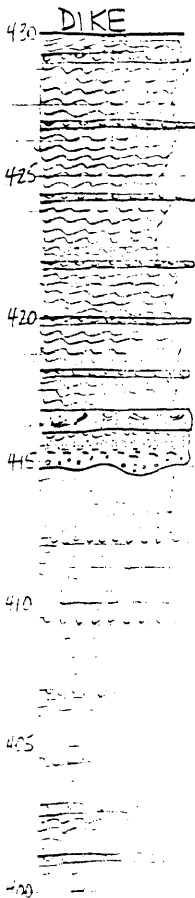


WOLK CREEK SECTION - P.7





WOLF CREEK SECTION - P. 9 (END)



Dike - end of section

Red and green wavy bedded sand and siltite-agillite, rip-ups, X-bedding, sands 1-3"

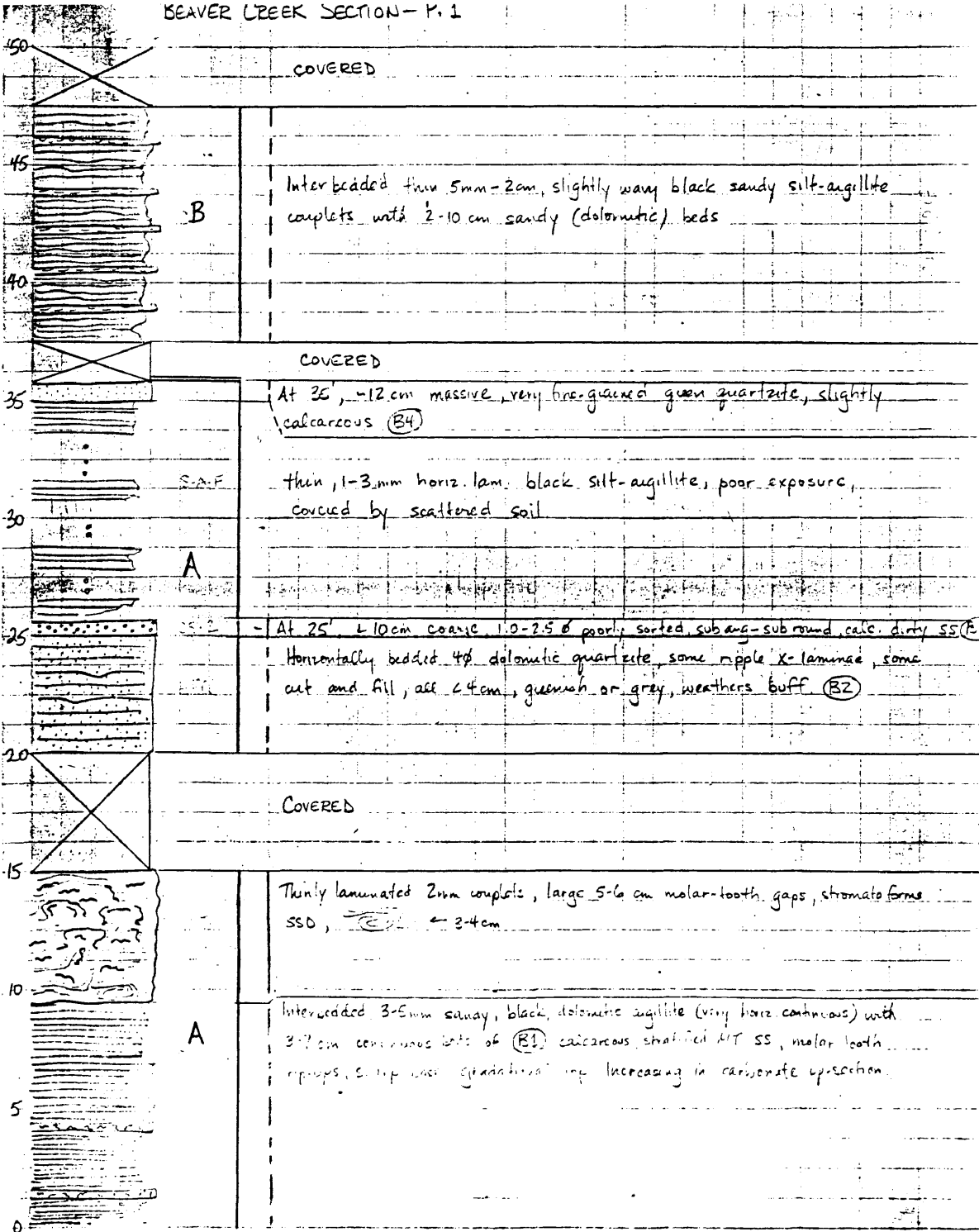
At 416', 13 cm calcareous, waste, 20-30% (fine) quartzite with 3" trough X-bedding, some horse bedding (W41)

B

At 415', coarse stringer sand is overlain and deeply scored by matrix... similar to containing large rip-ups, folded over (red) thin green, turning into green X-bedded sand 8-15"

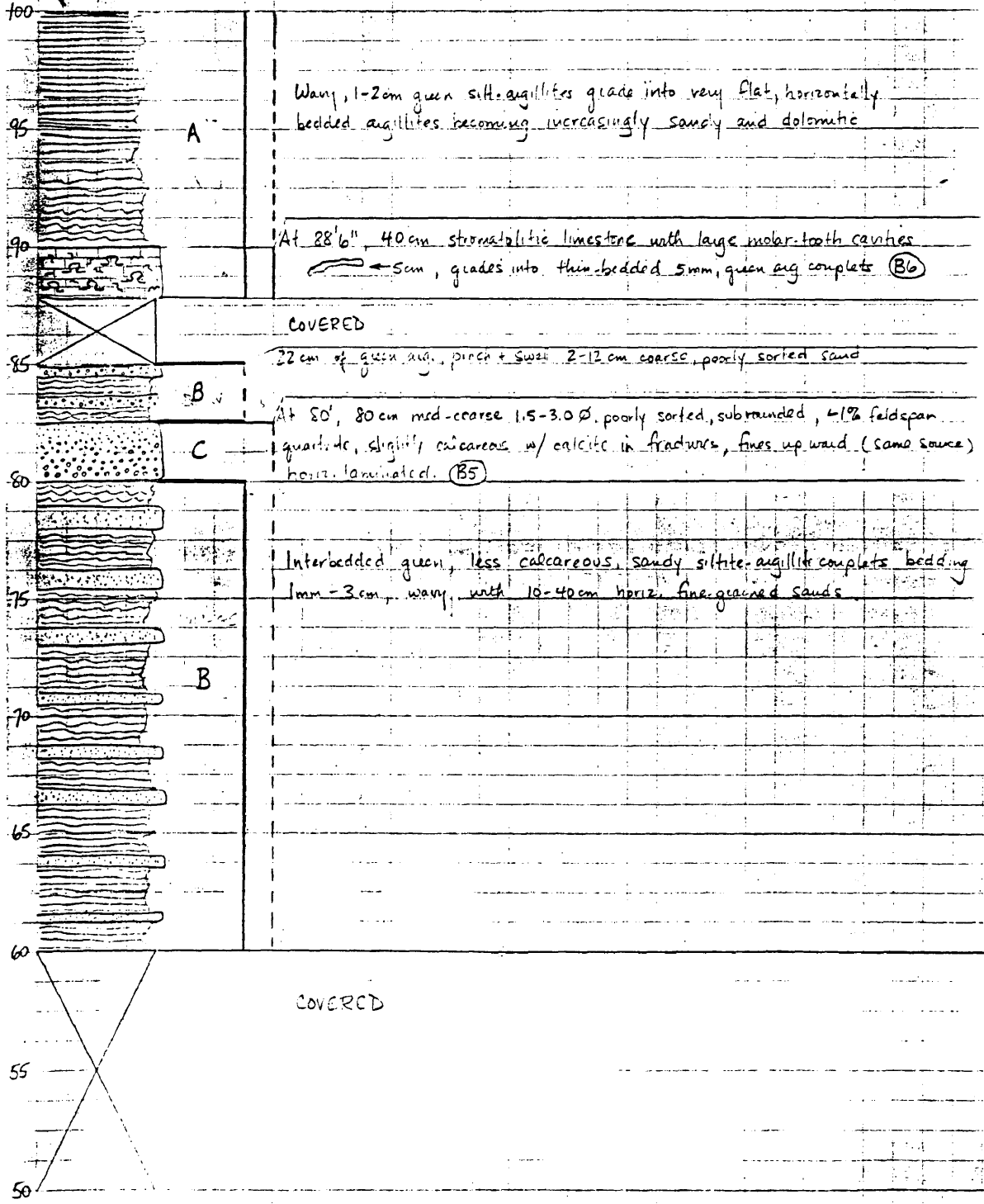
Green, sandy slightly wavy silt-agillite composite becoming red, mottled look because of green sand beds, sands thin to 1", still mud-cracks, rip-ups. Becomes more siltite to 415'

BEAVER CREEK SECTION - P. 1

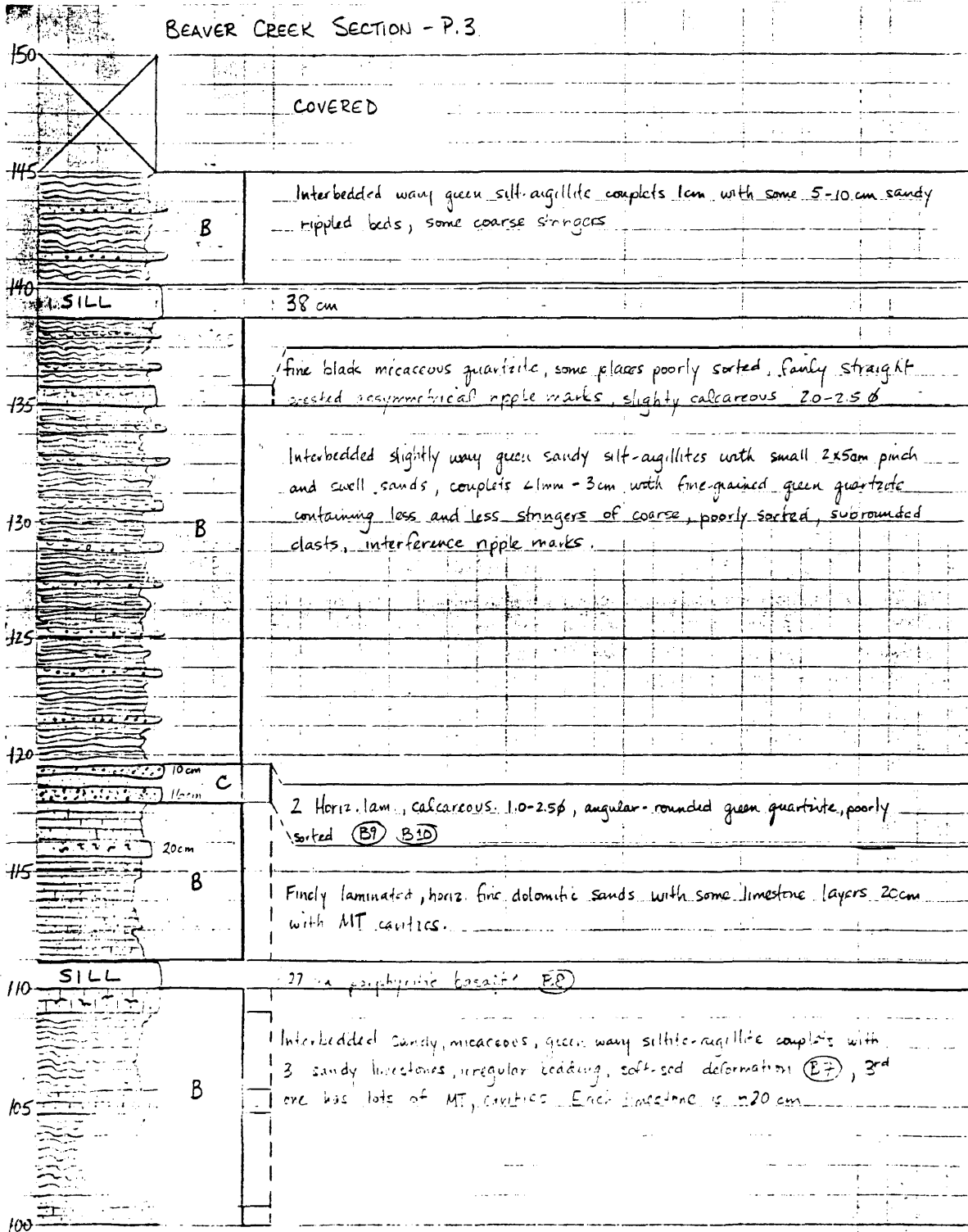


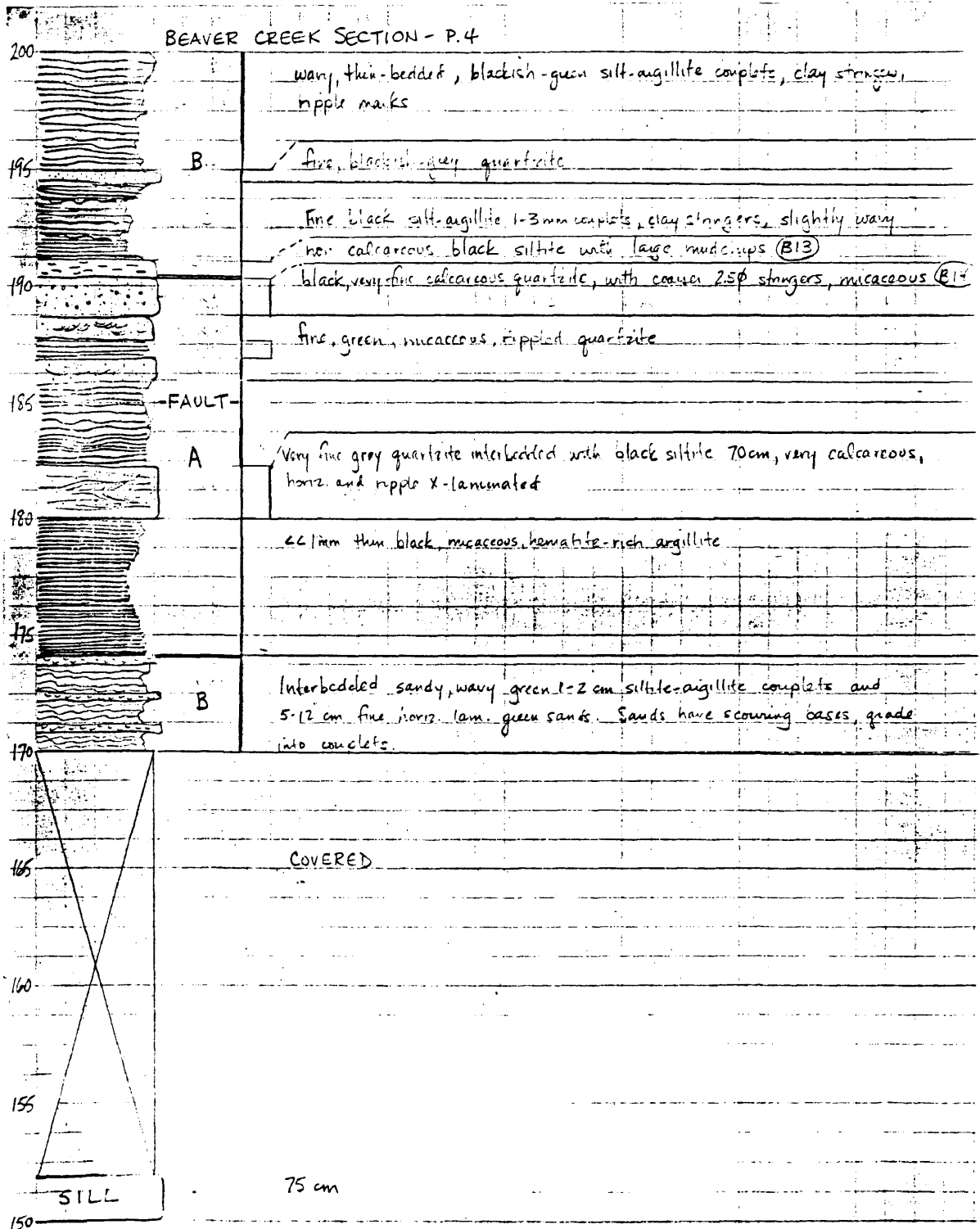
U.C.

BEAVER CREEK SECTION - P.2

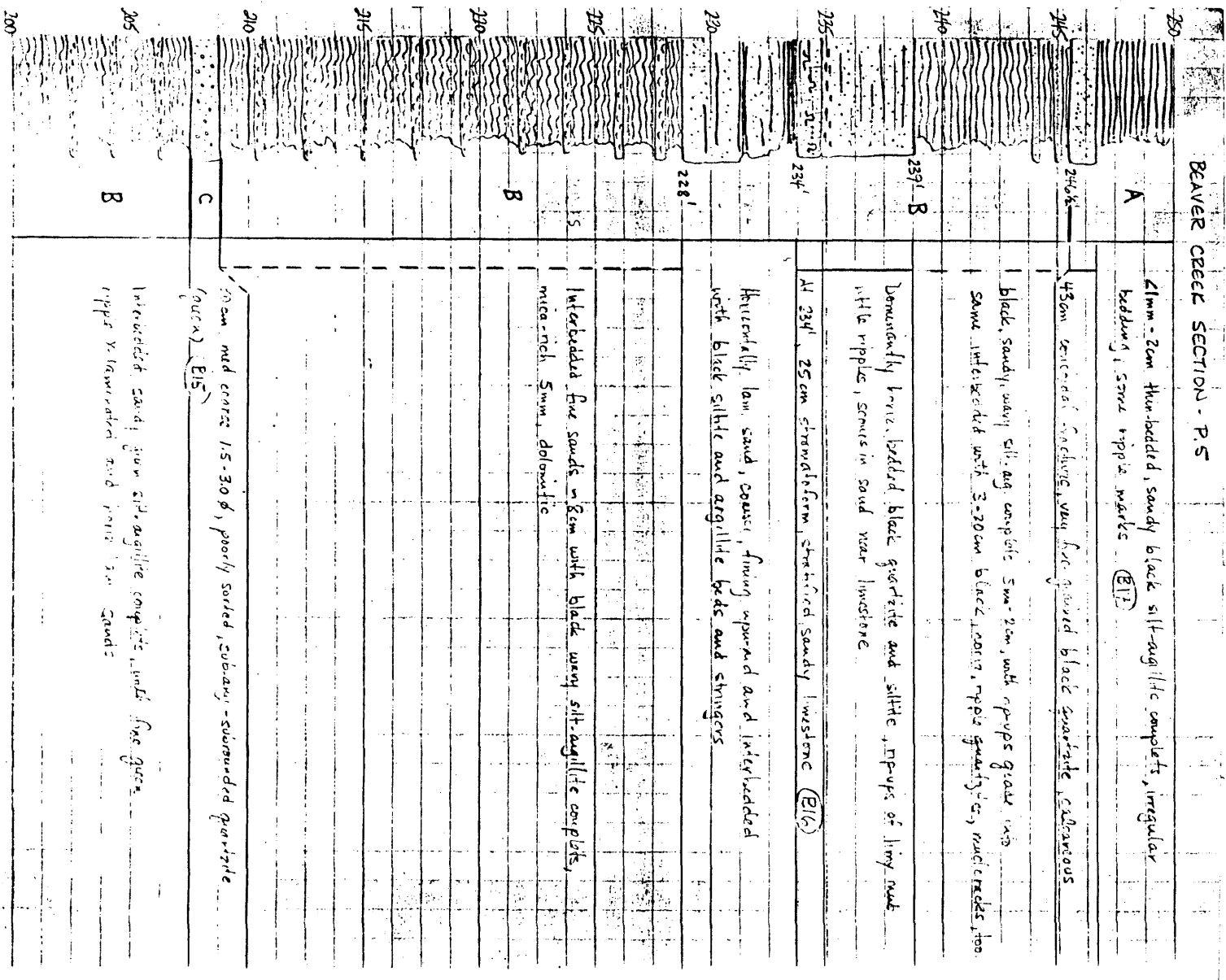


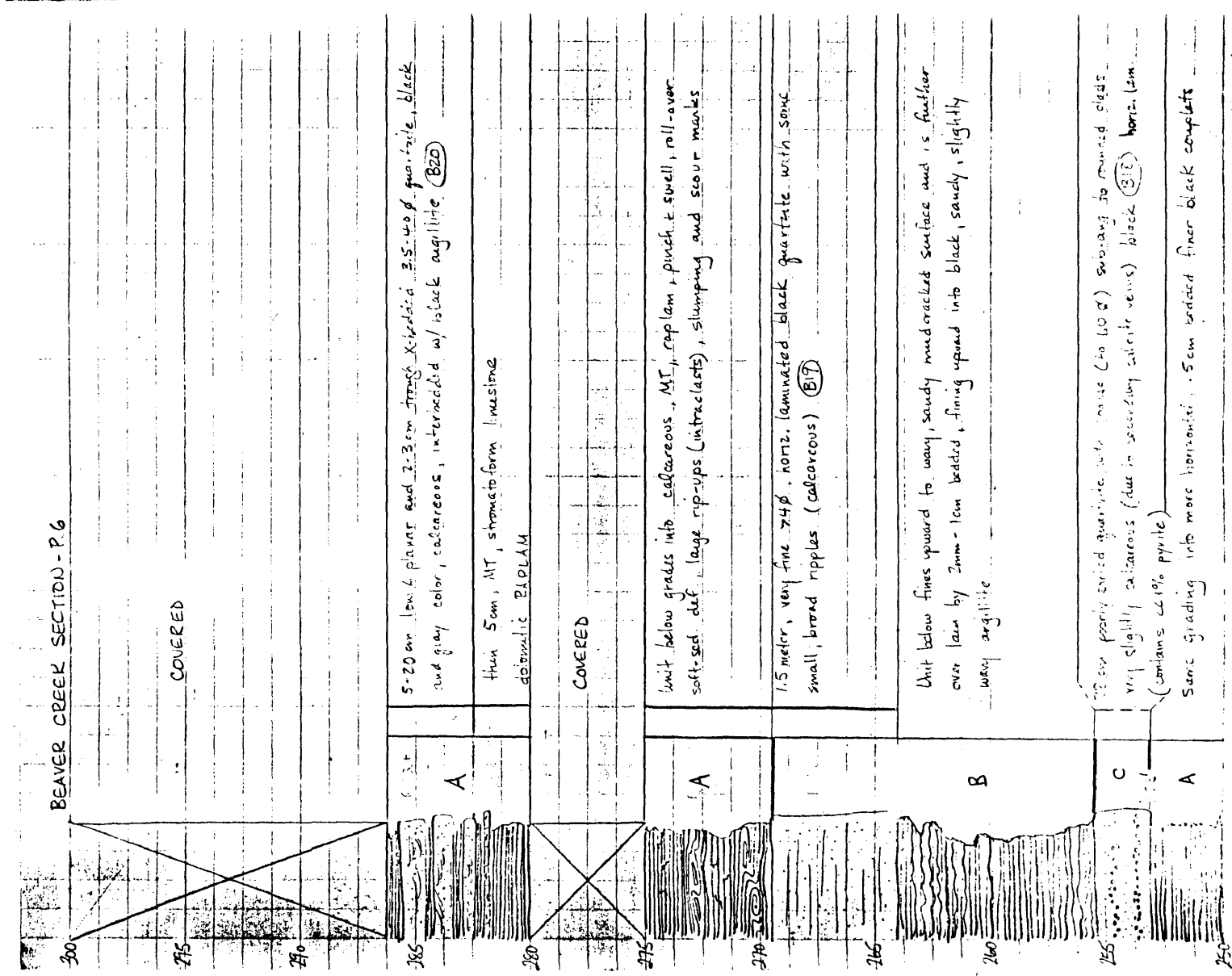
BEAVER CREEK SECTION - P. 3

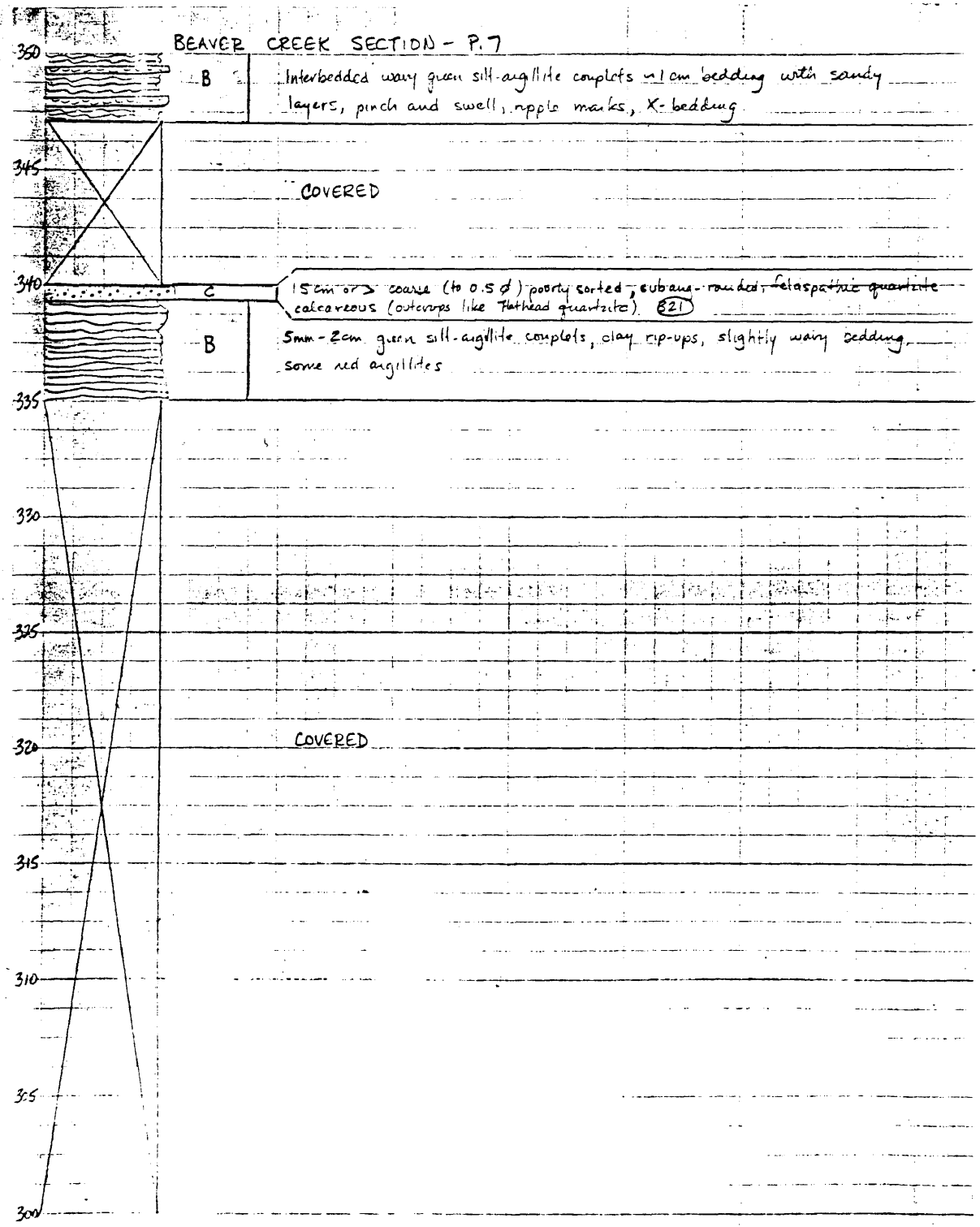




BEAVER CREEK SECTION - P. 5





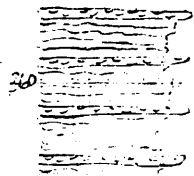


BEAVER CREEK SECTION - P. 8 (LAST PAGE)

370

RED INCREASES

365



B

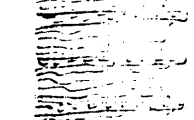
Interbedded 2-5 cm horiz but mainly ripple sands fining upward to argillite, couplets 7-12 cm total. argillites → red, sands black. weather reddish green. lots of mudcracks

360

SILL

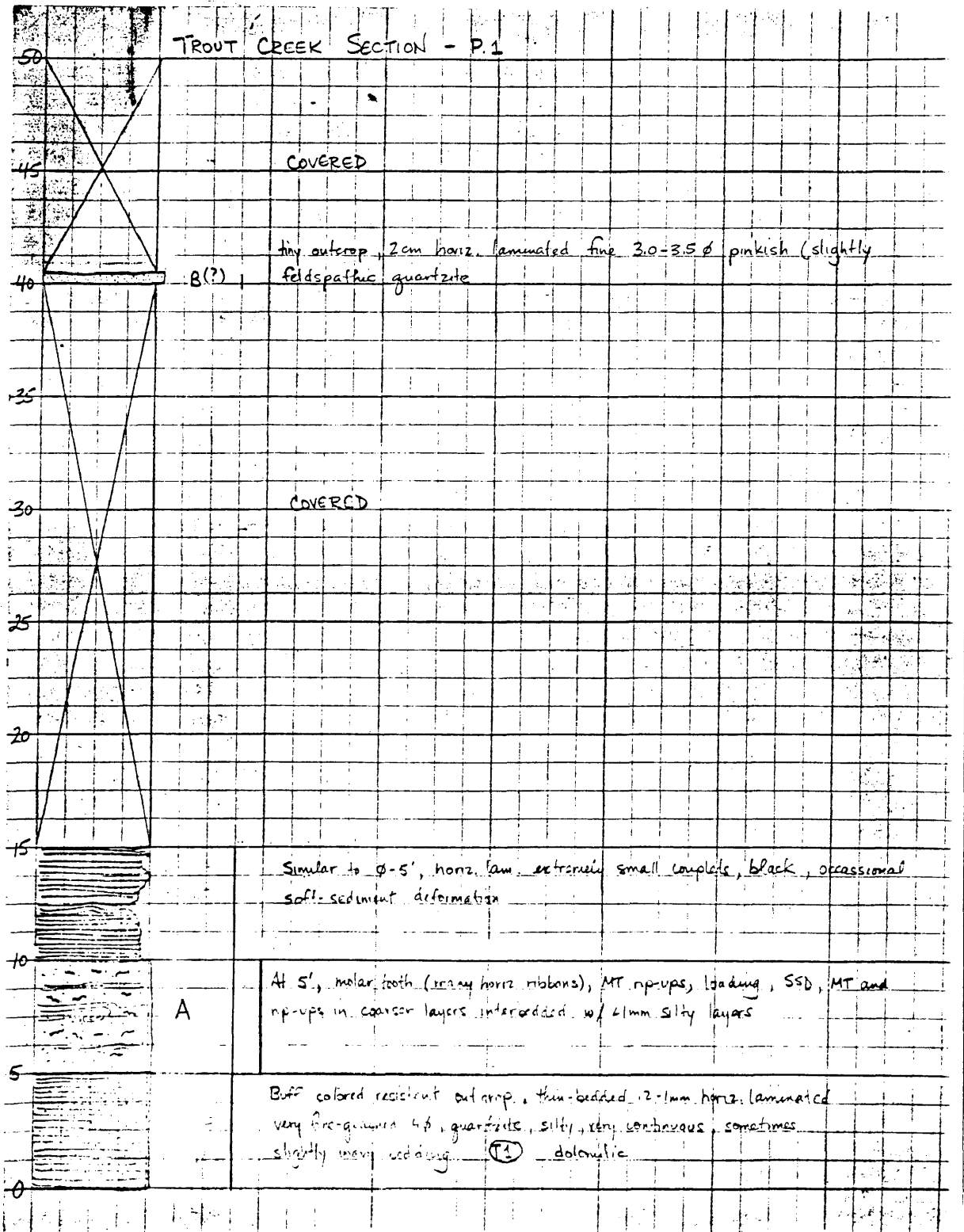
~40 cm (B22)

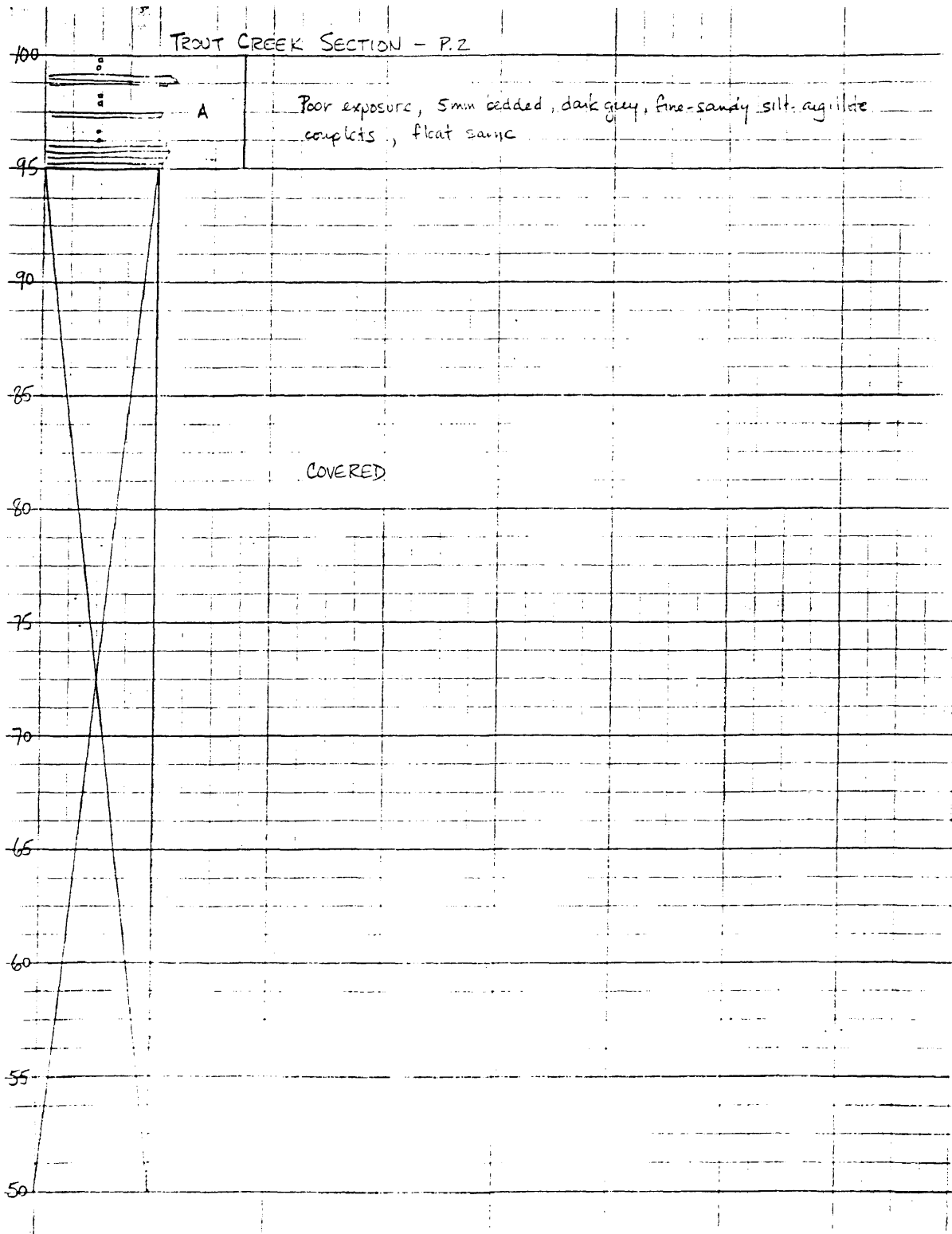
350

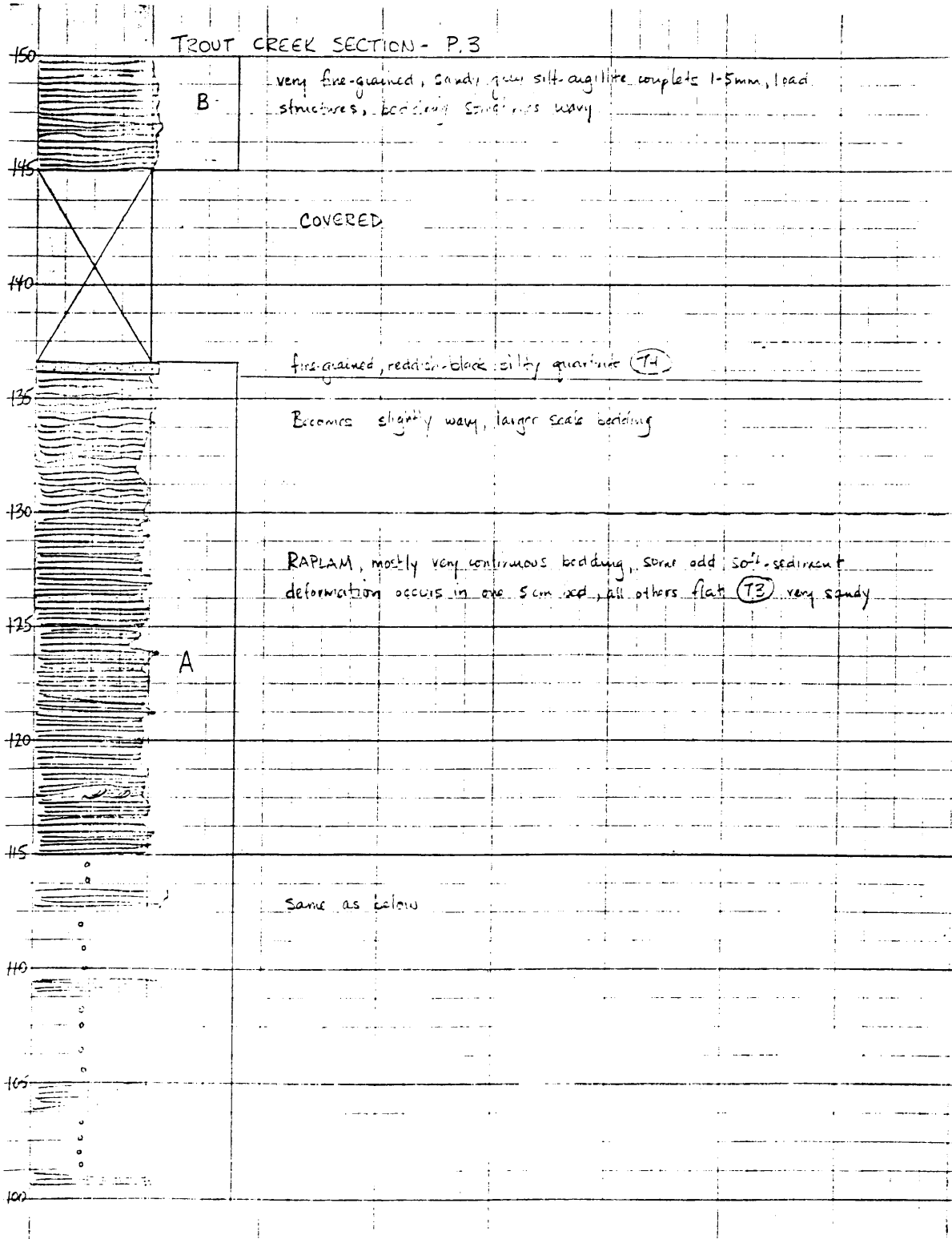


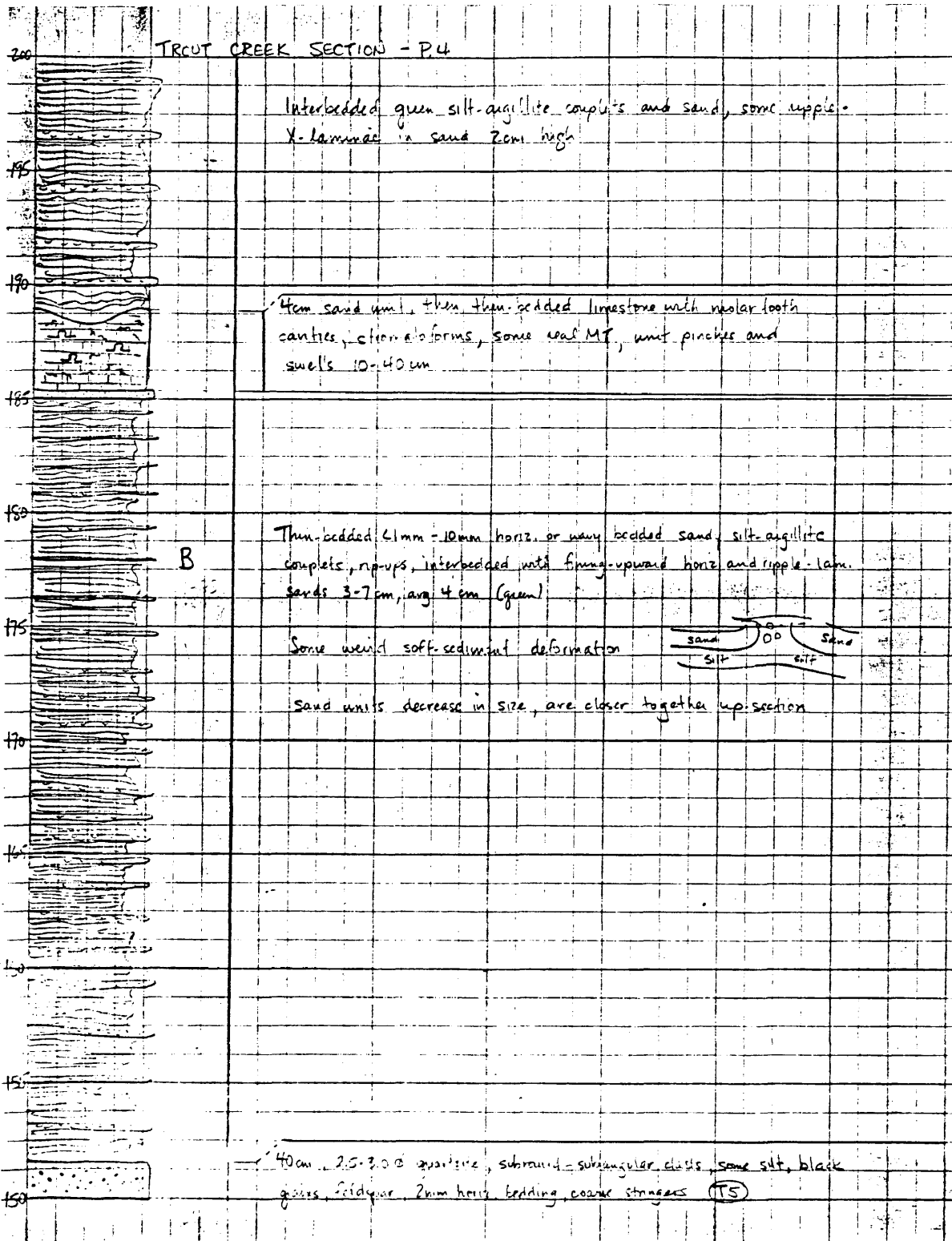
B

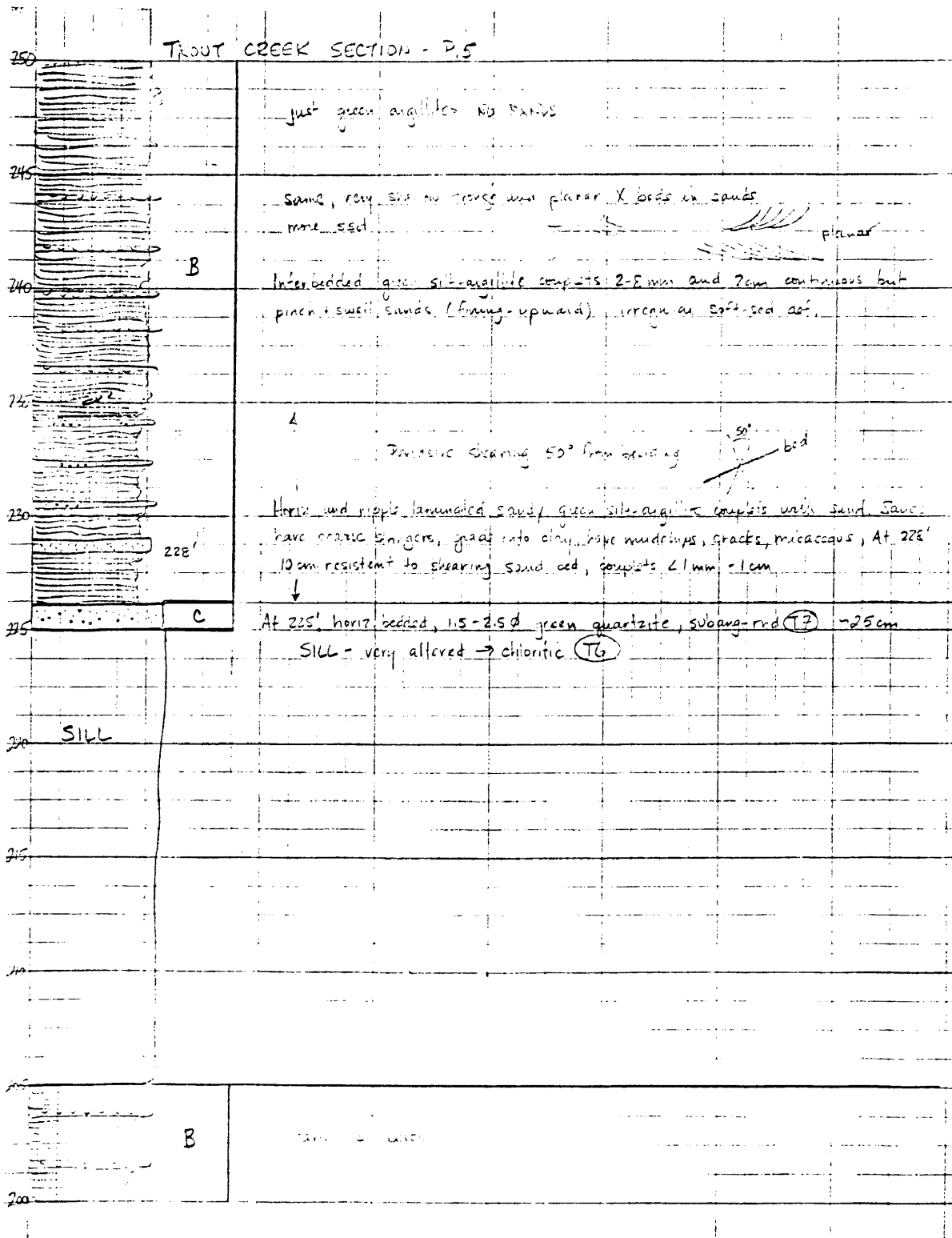
same

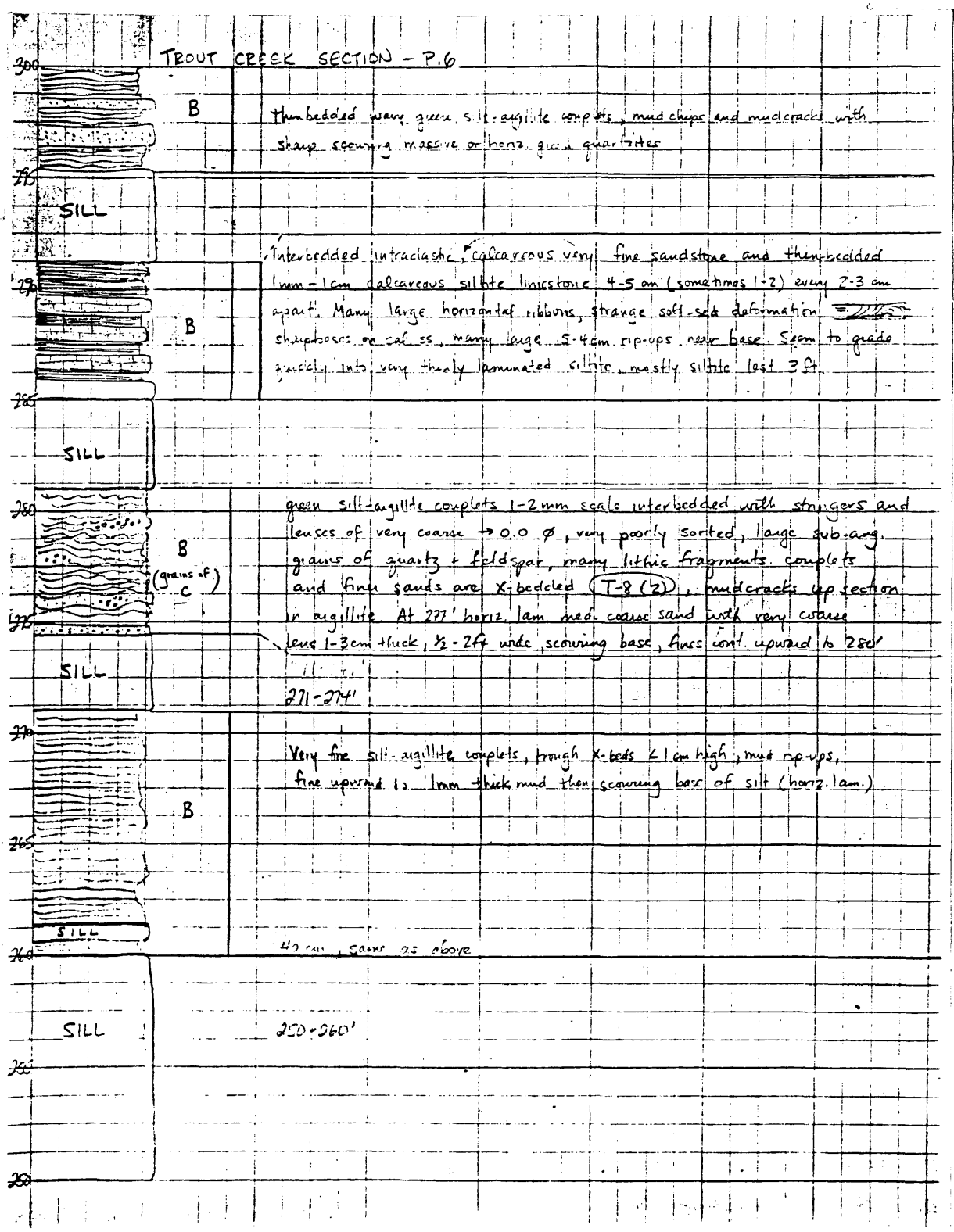


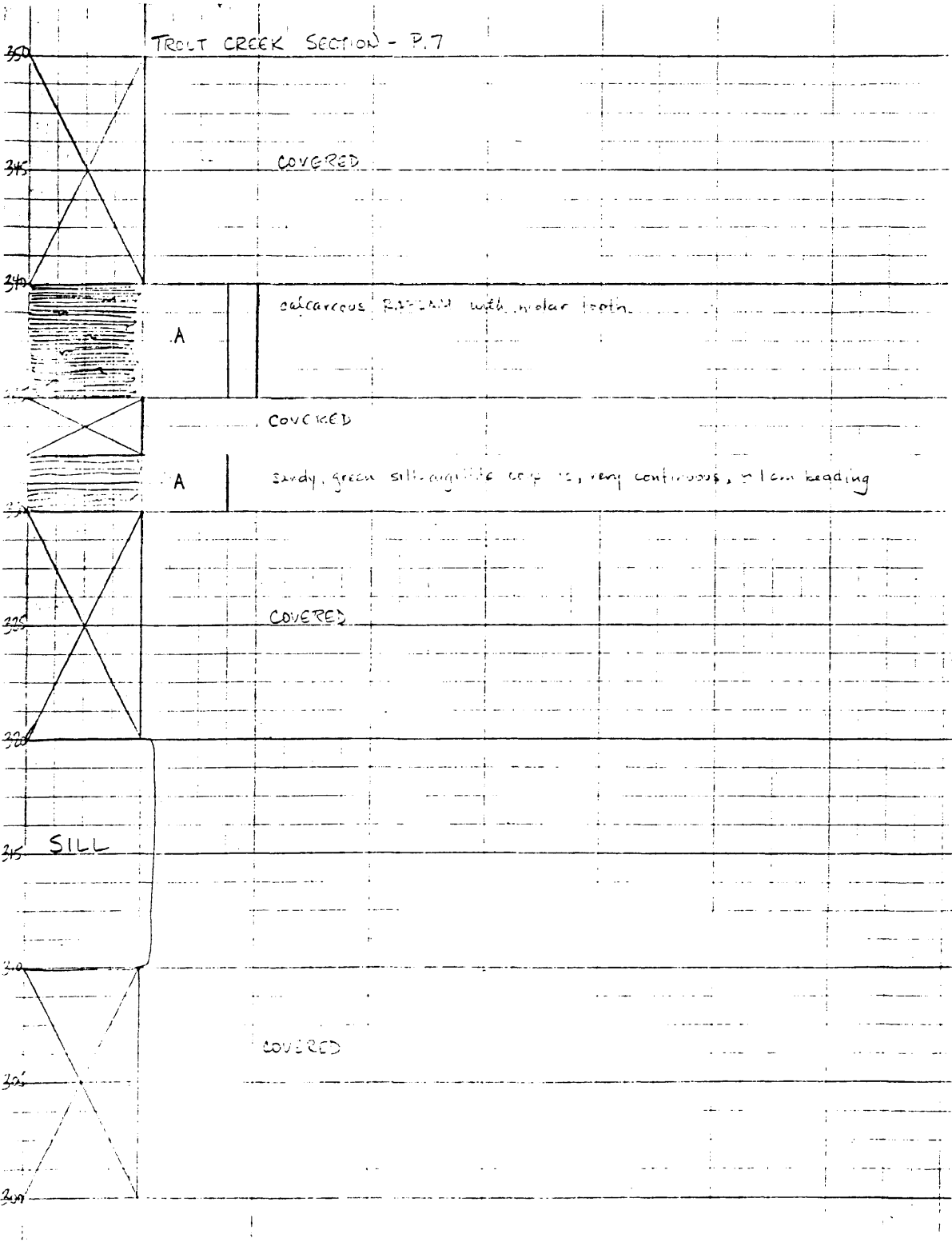


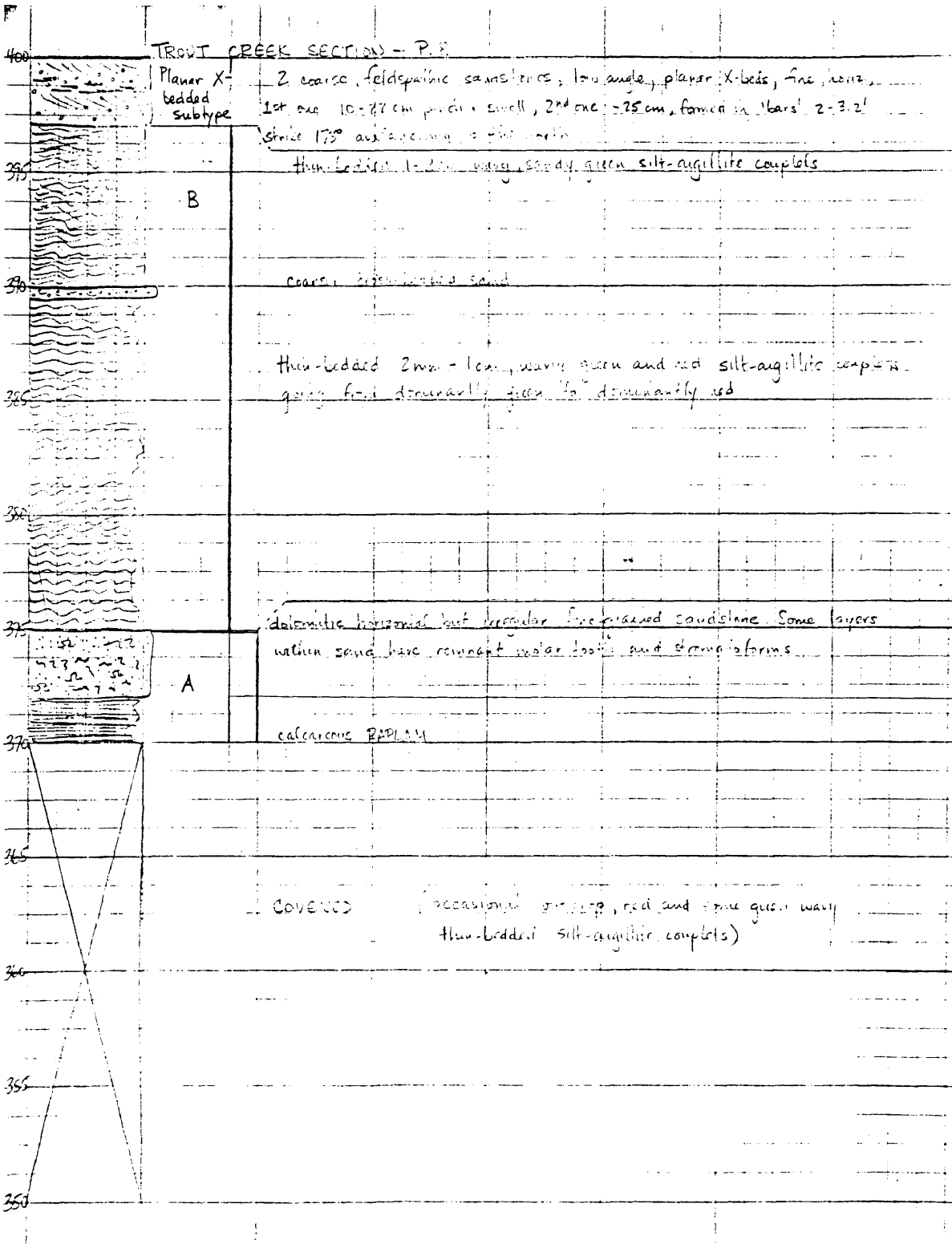




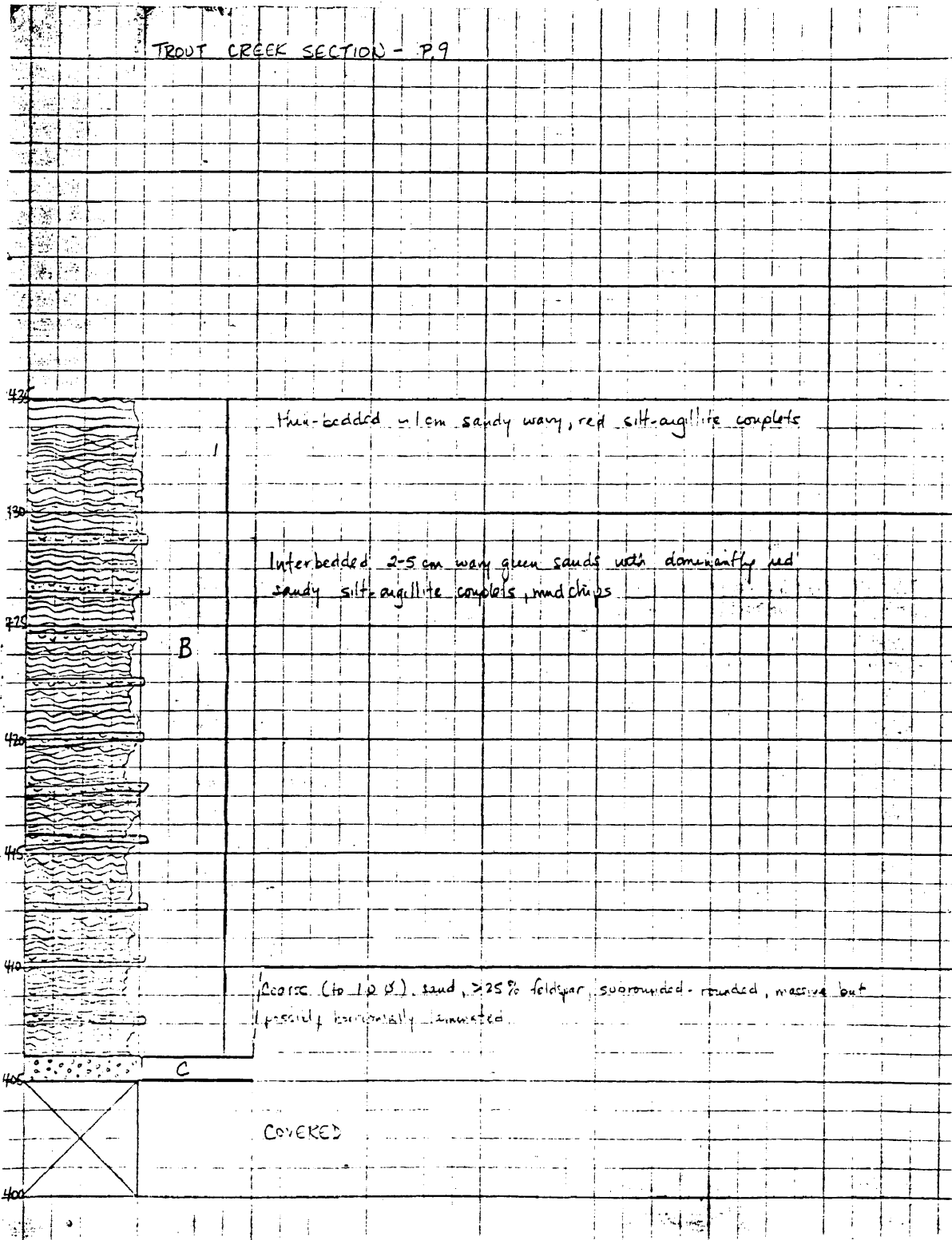


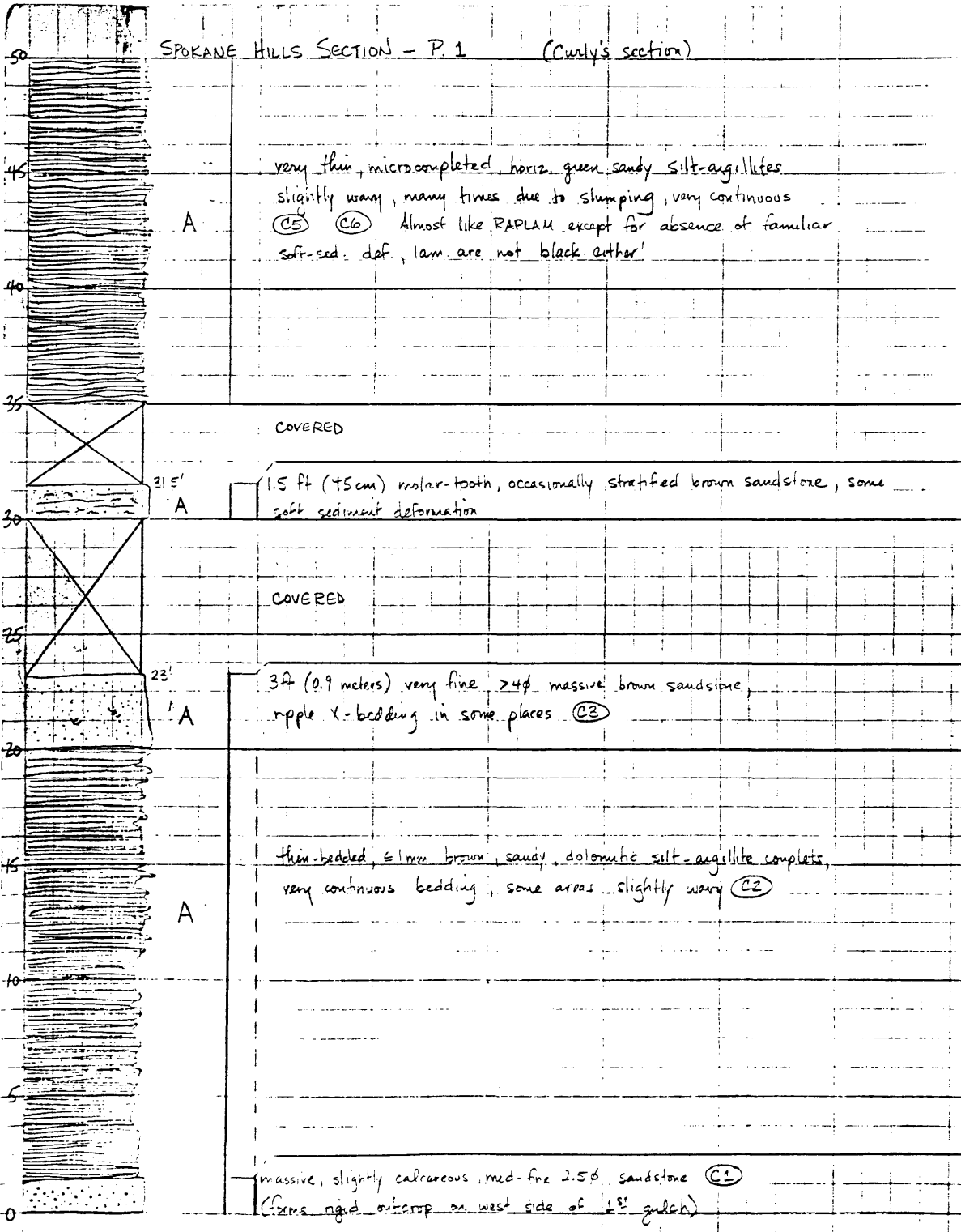


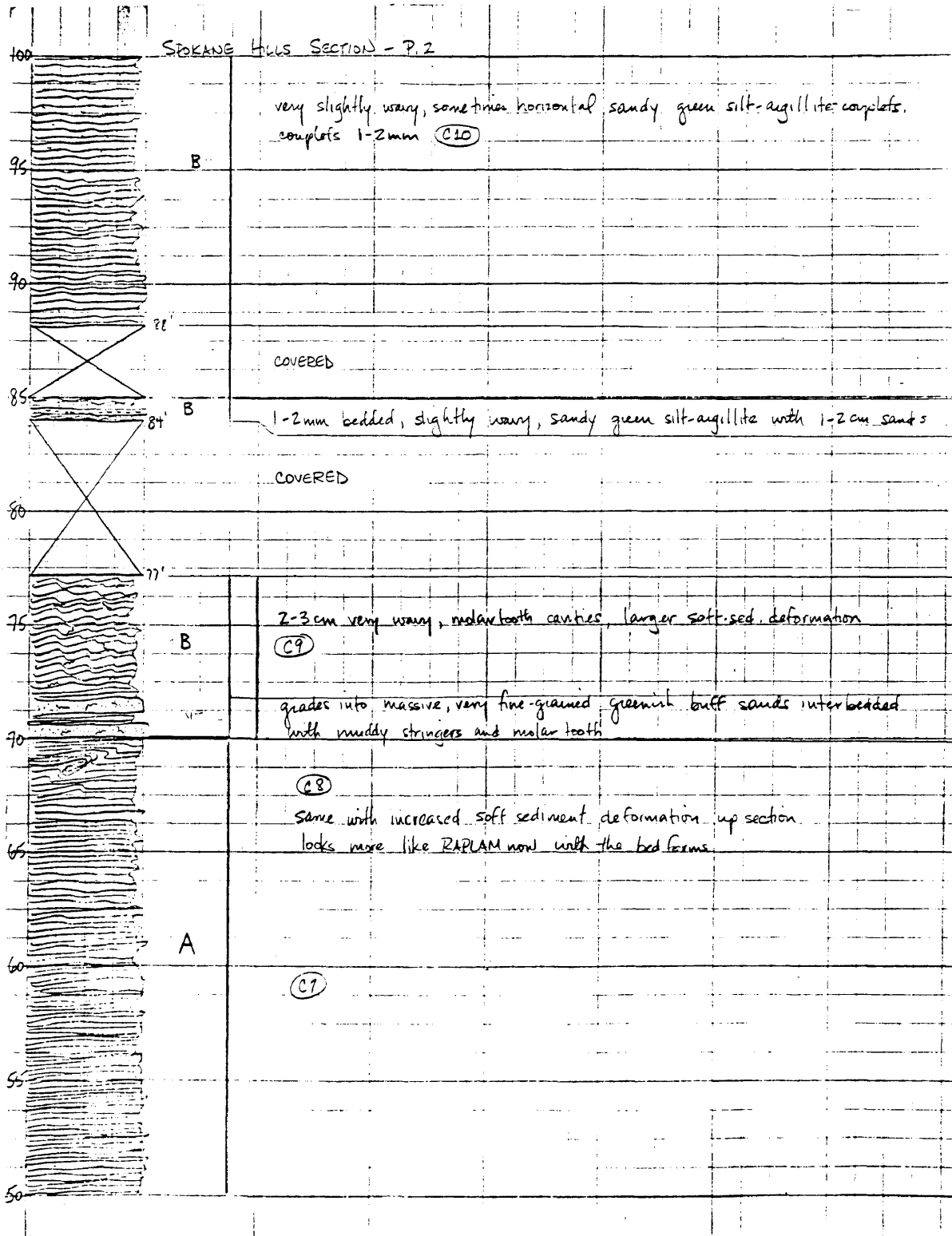


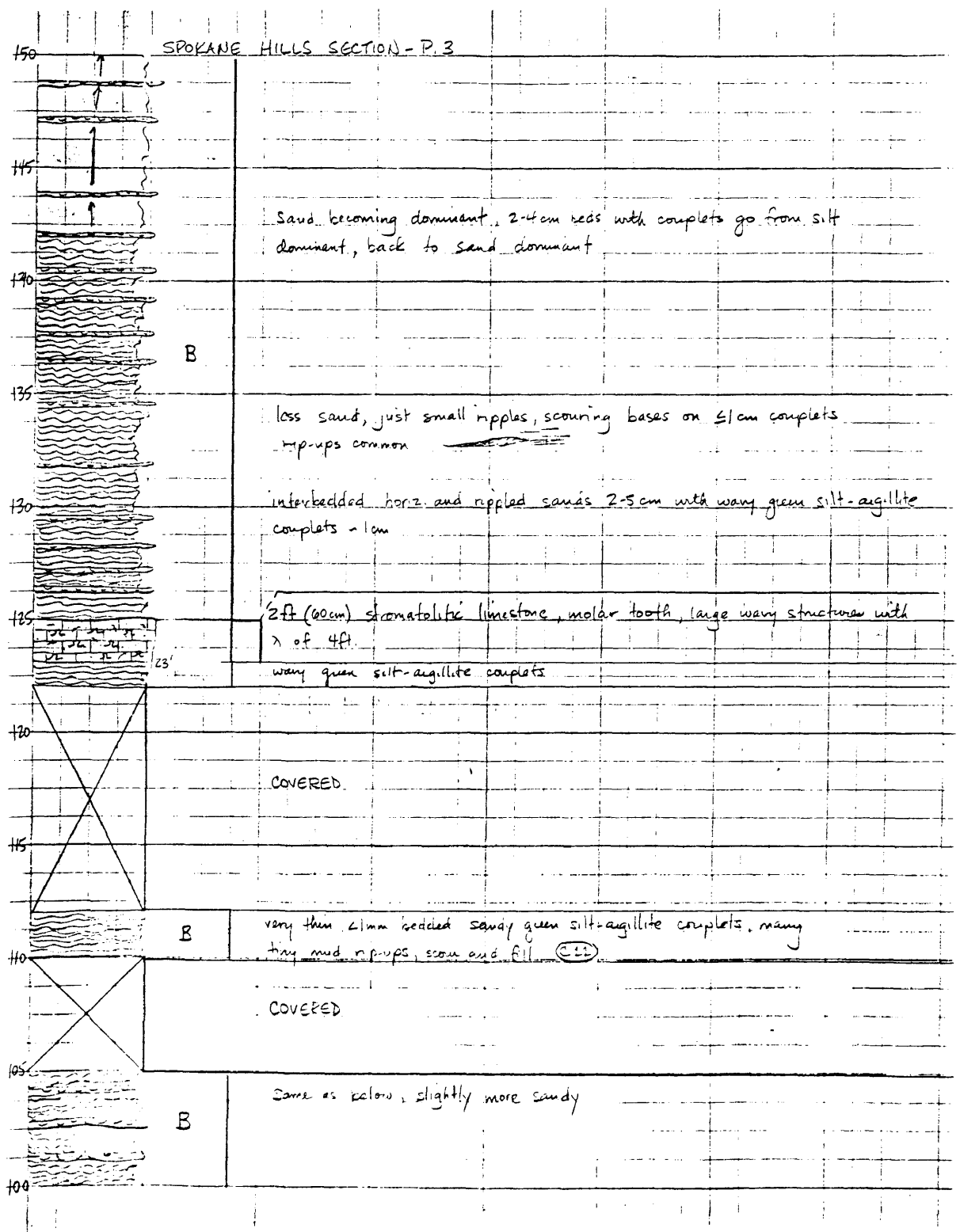


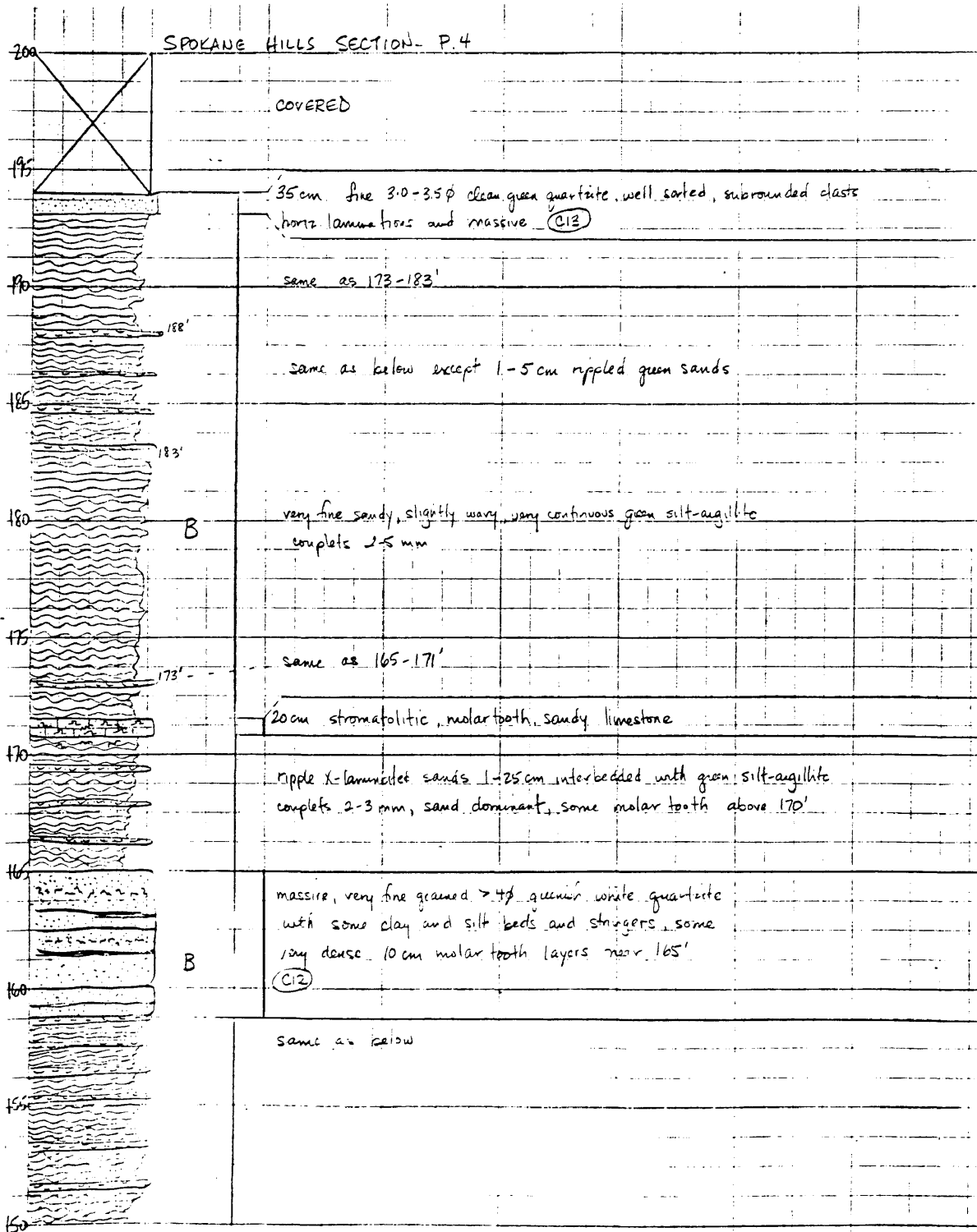
TROUT CREEK SECTION - P. 9

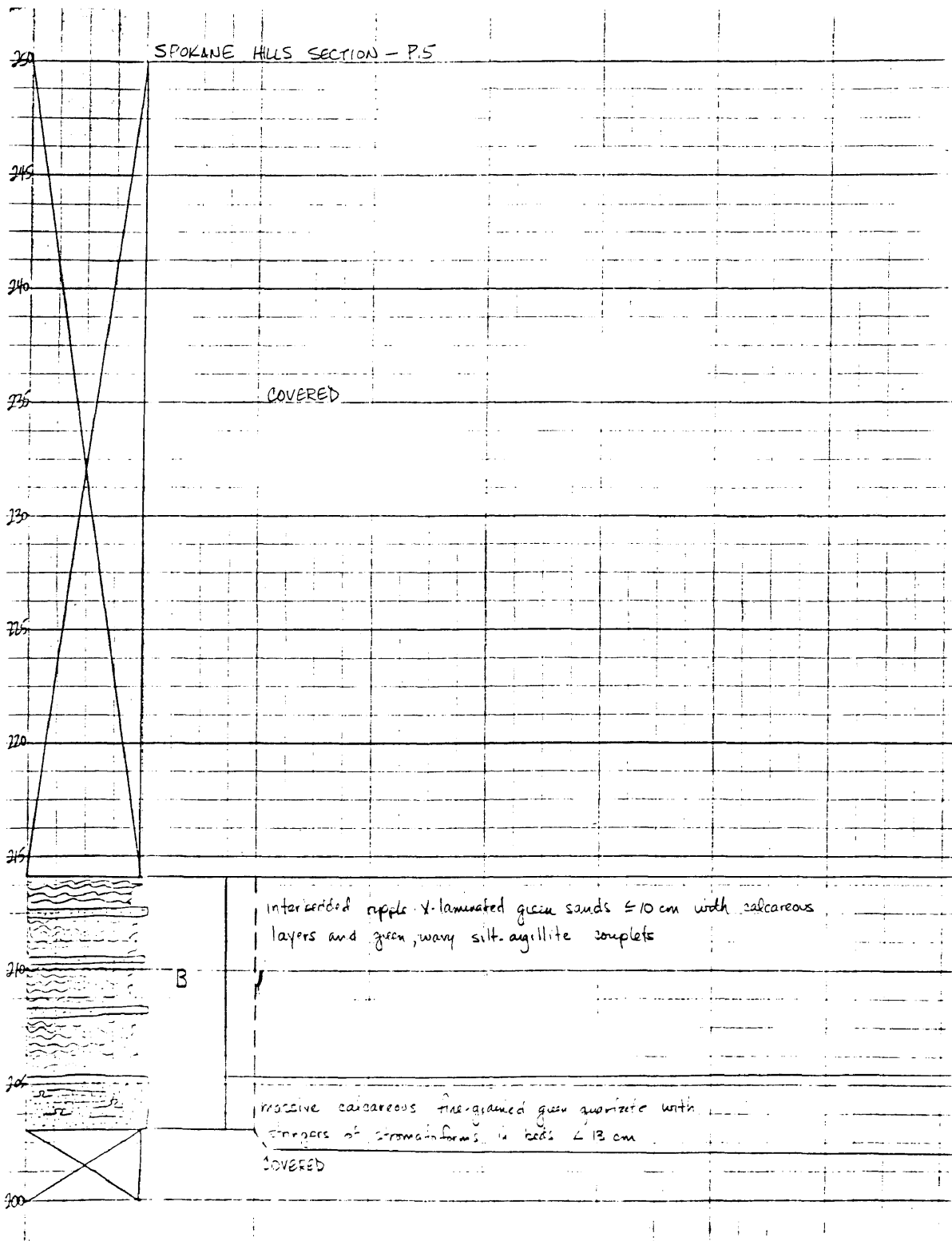


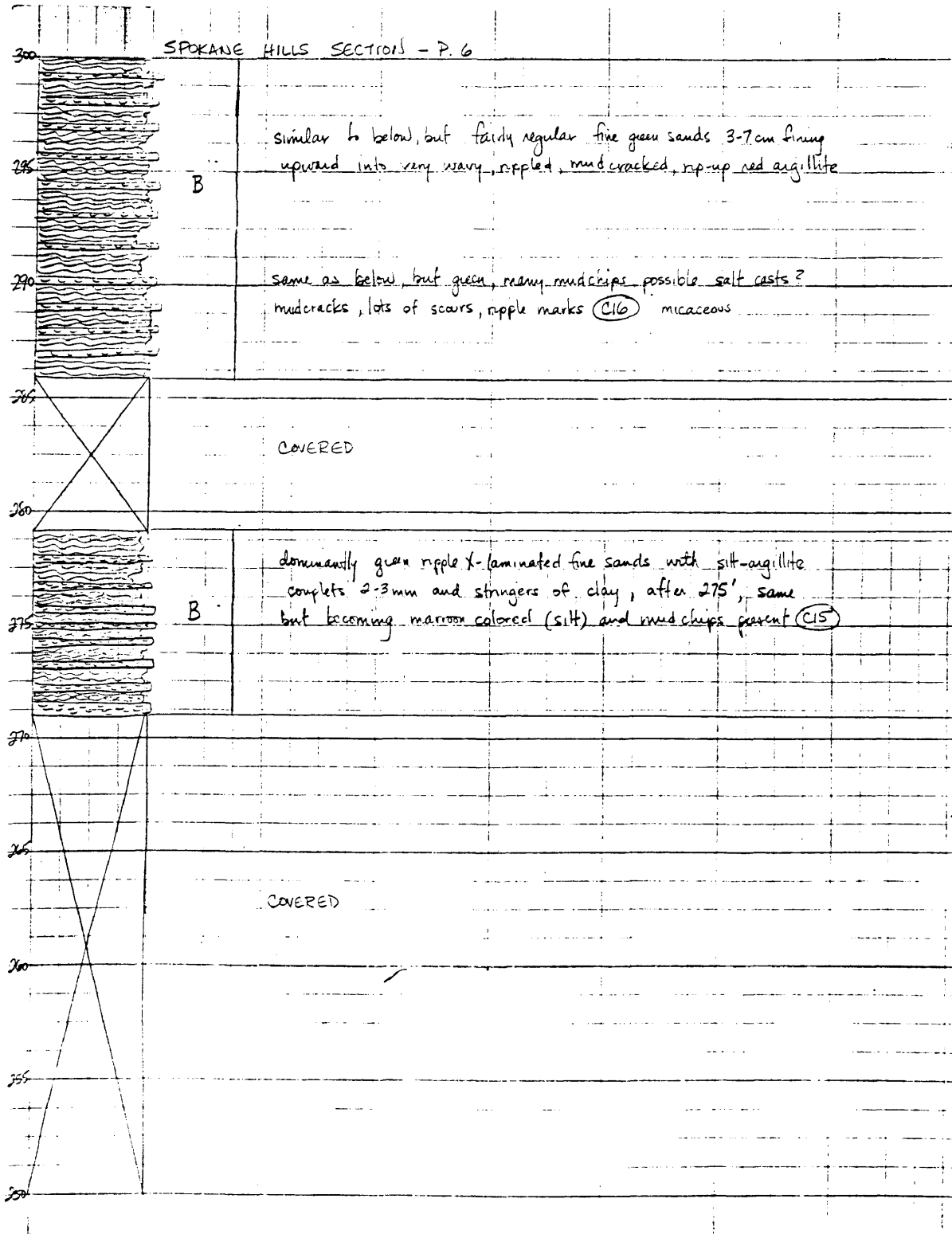


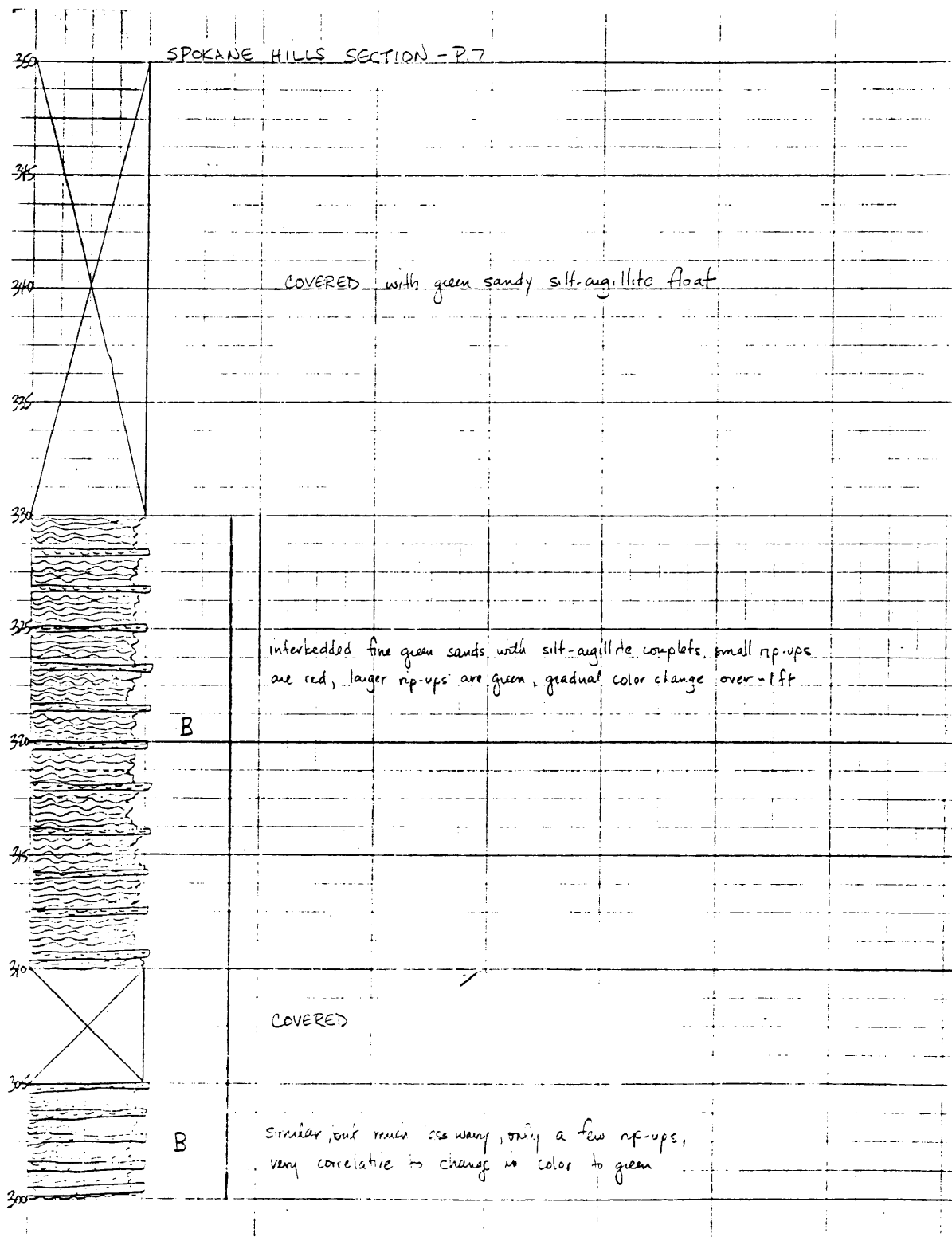


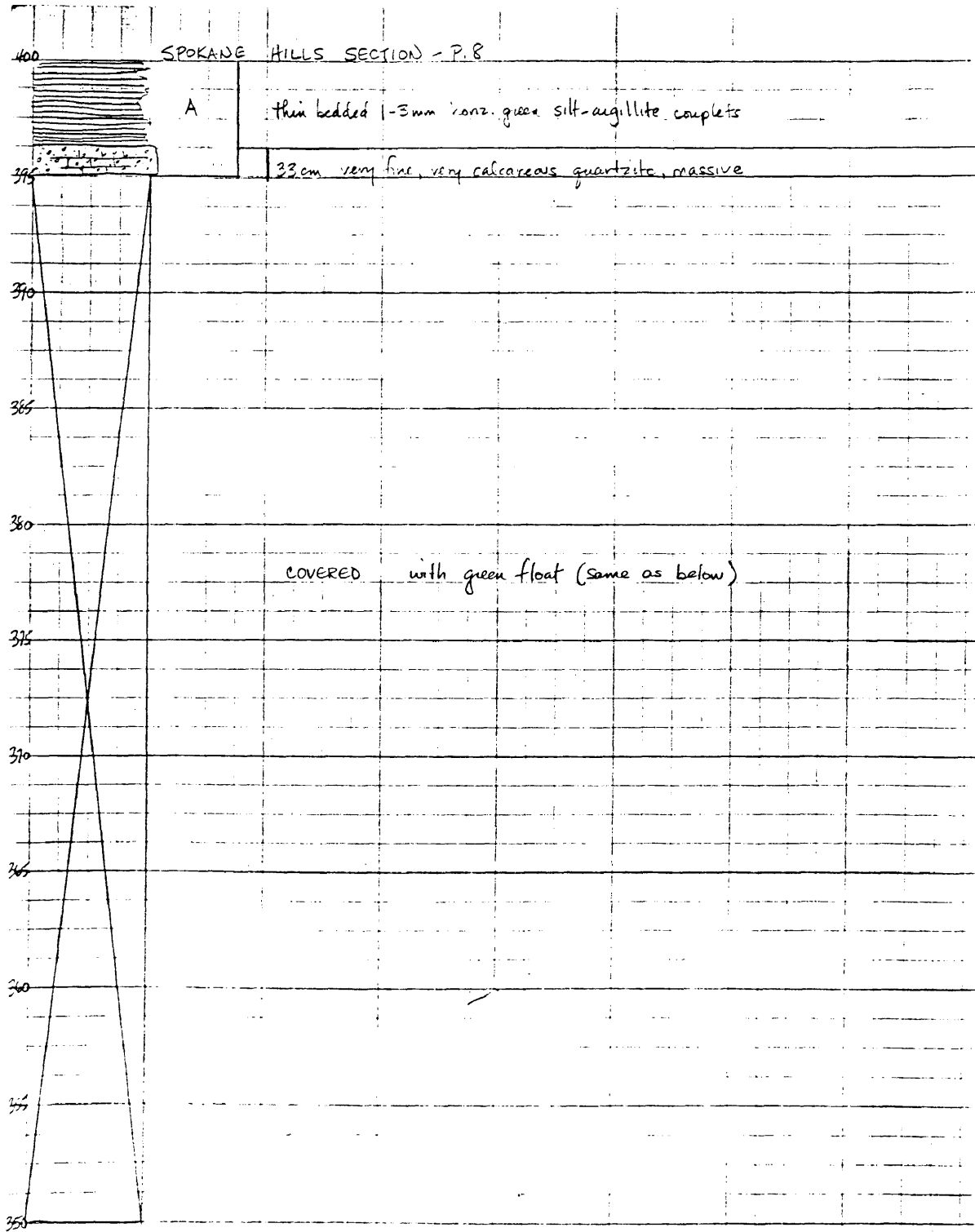


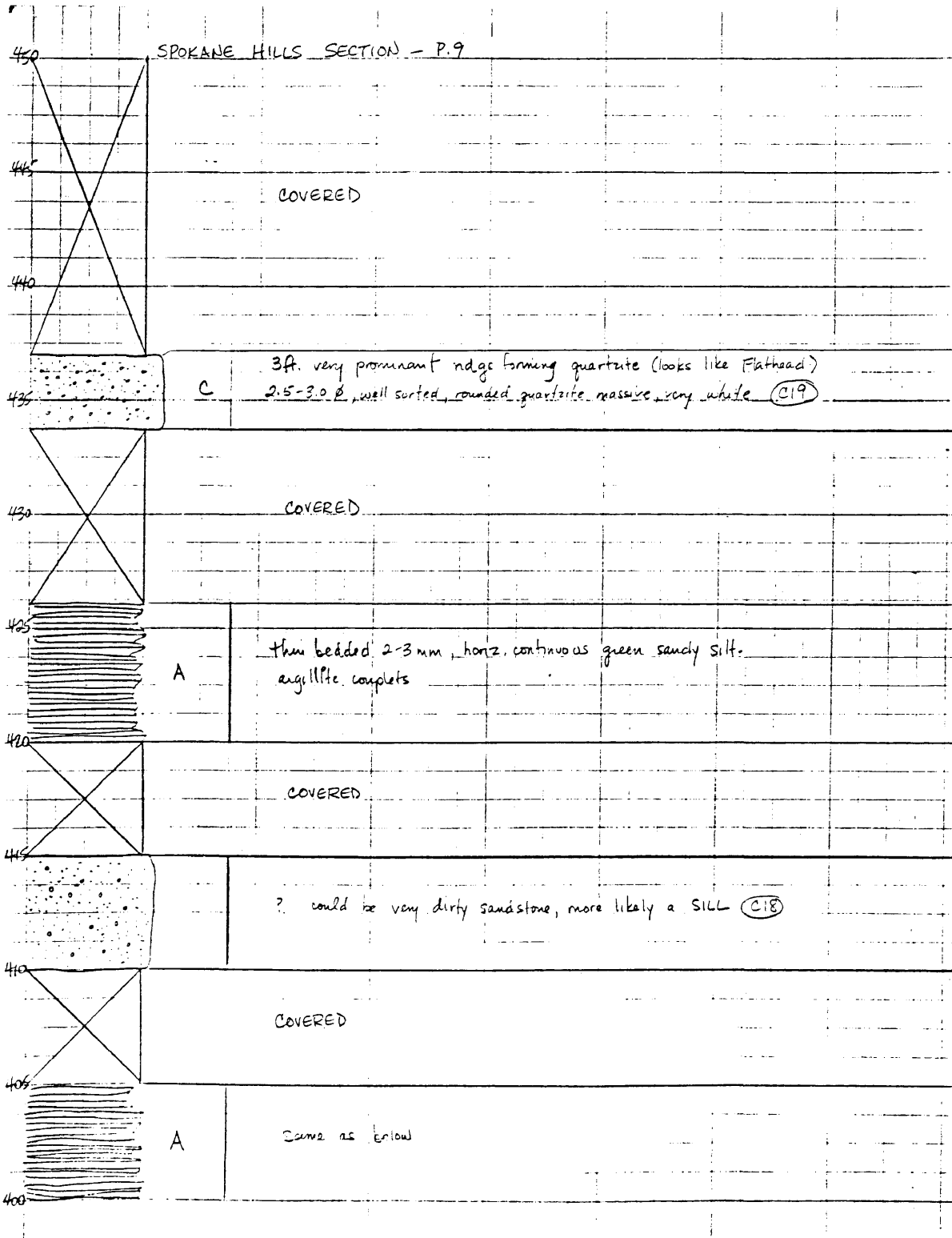


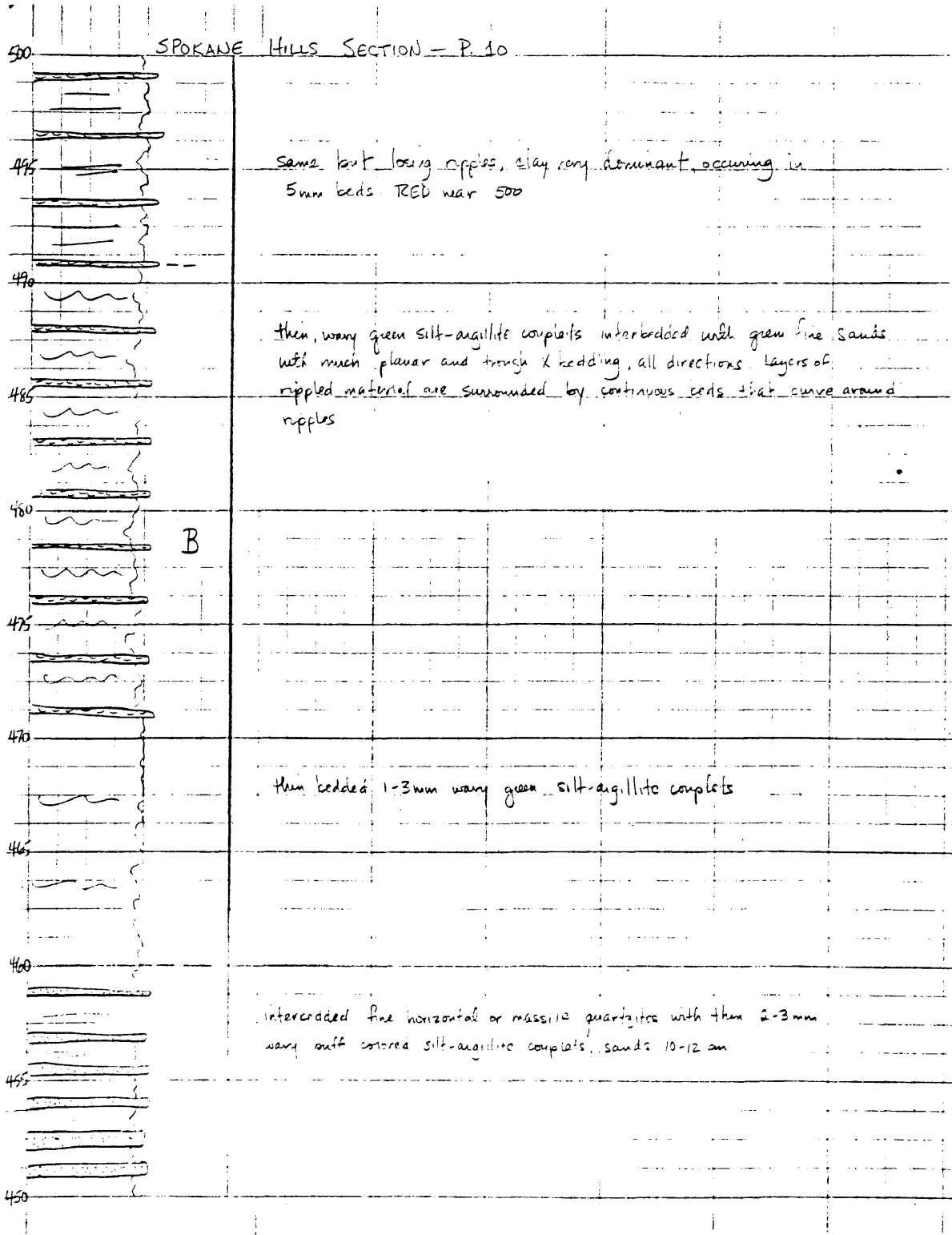


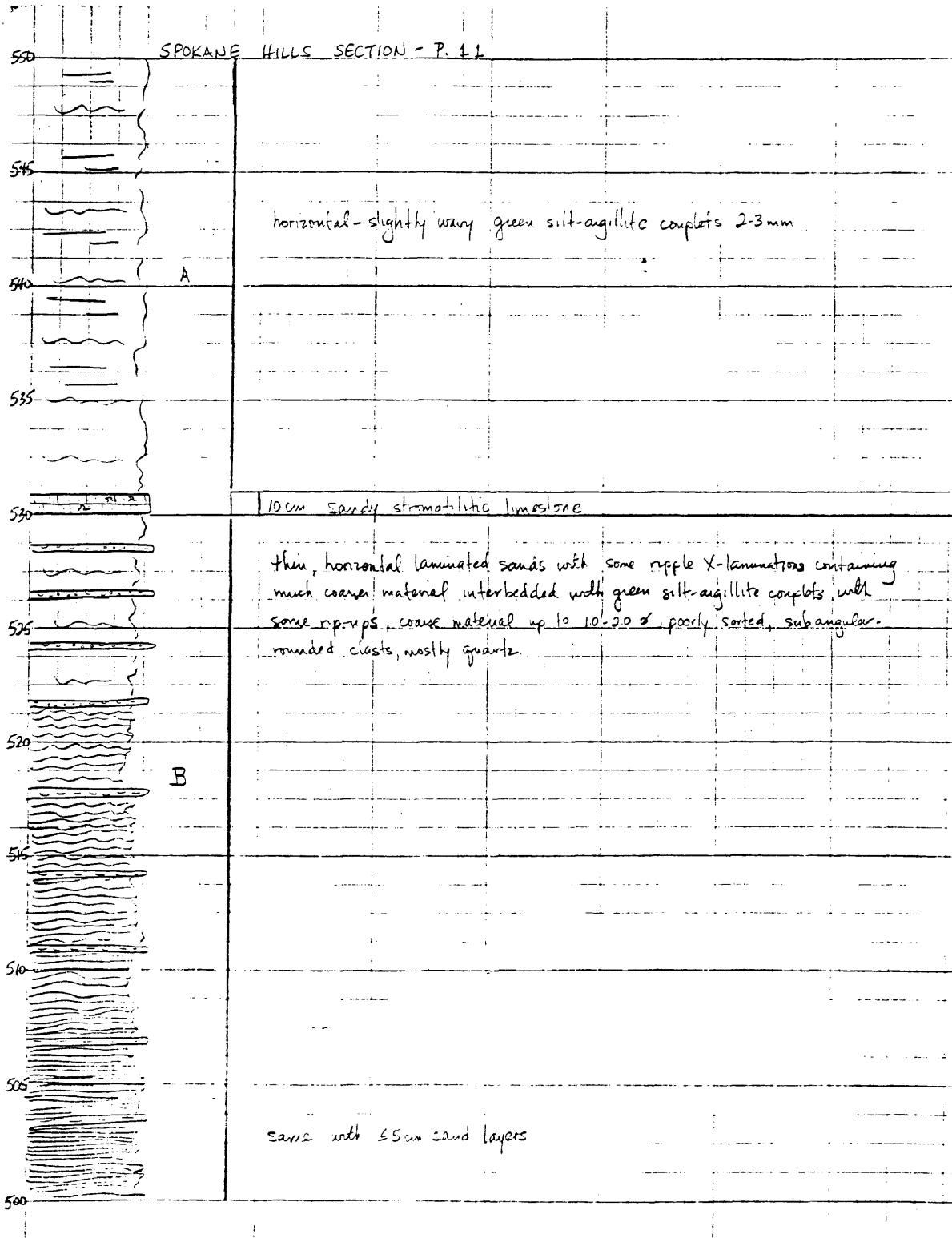


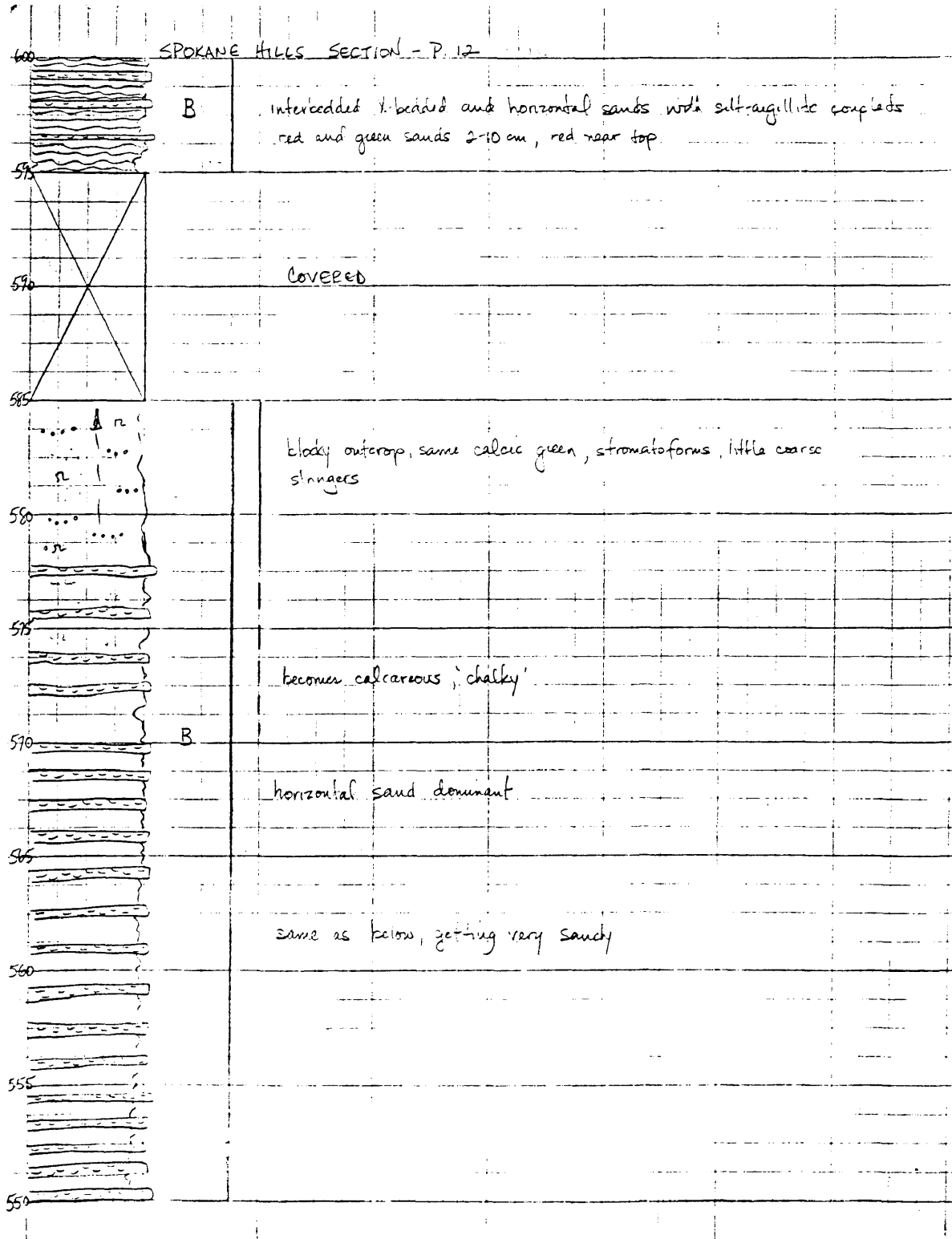


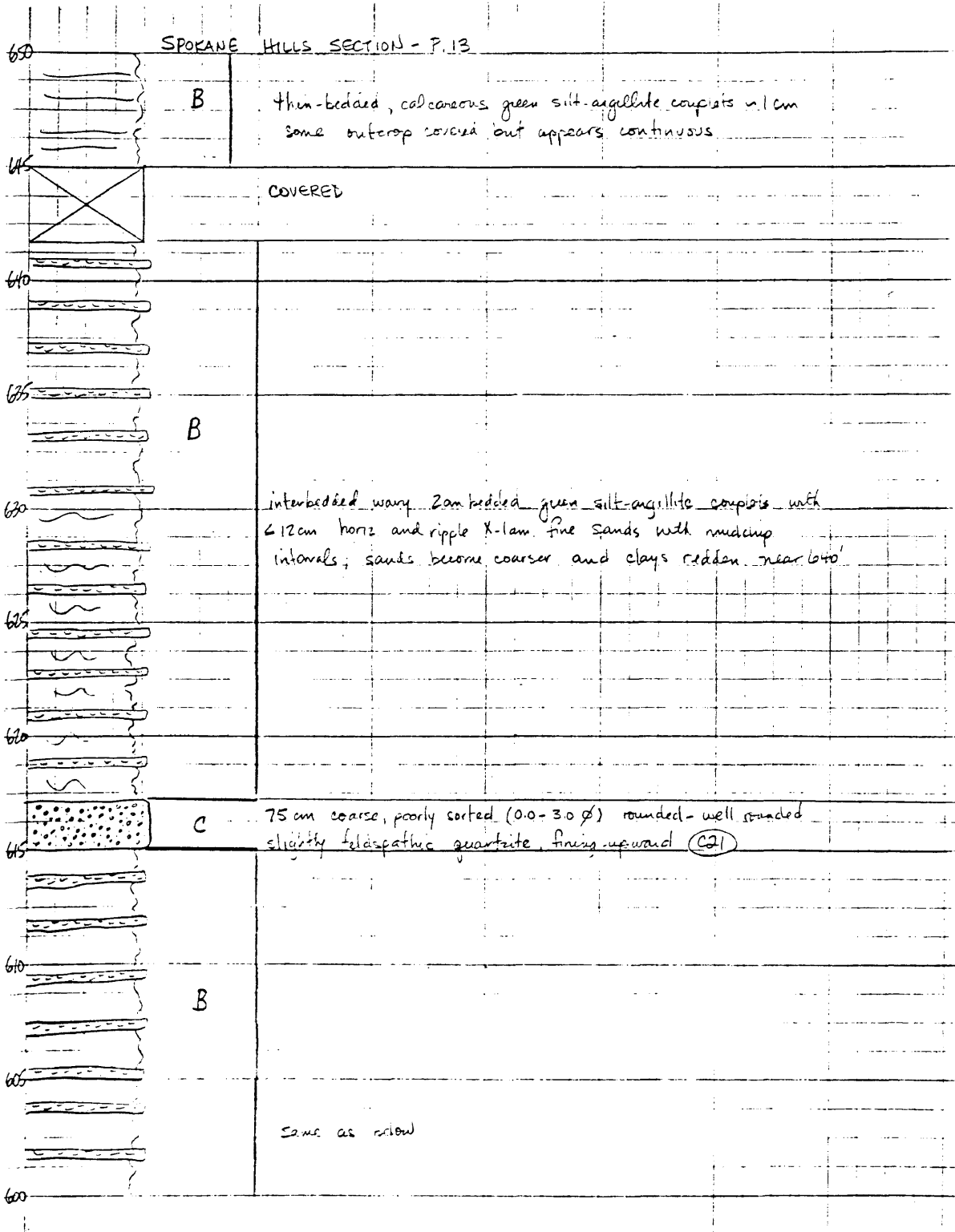


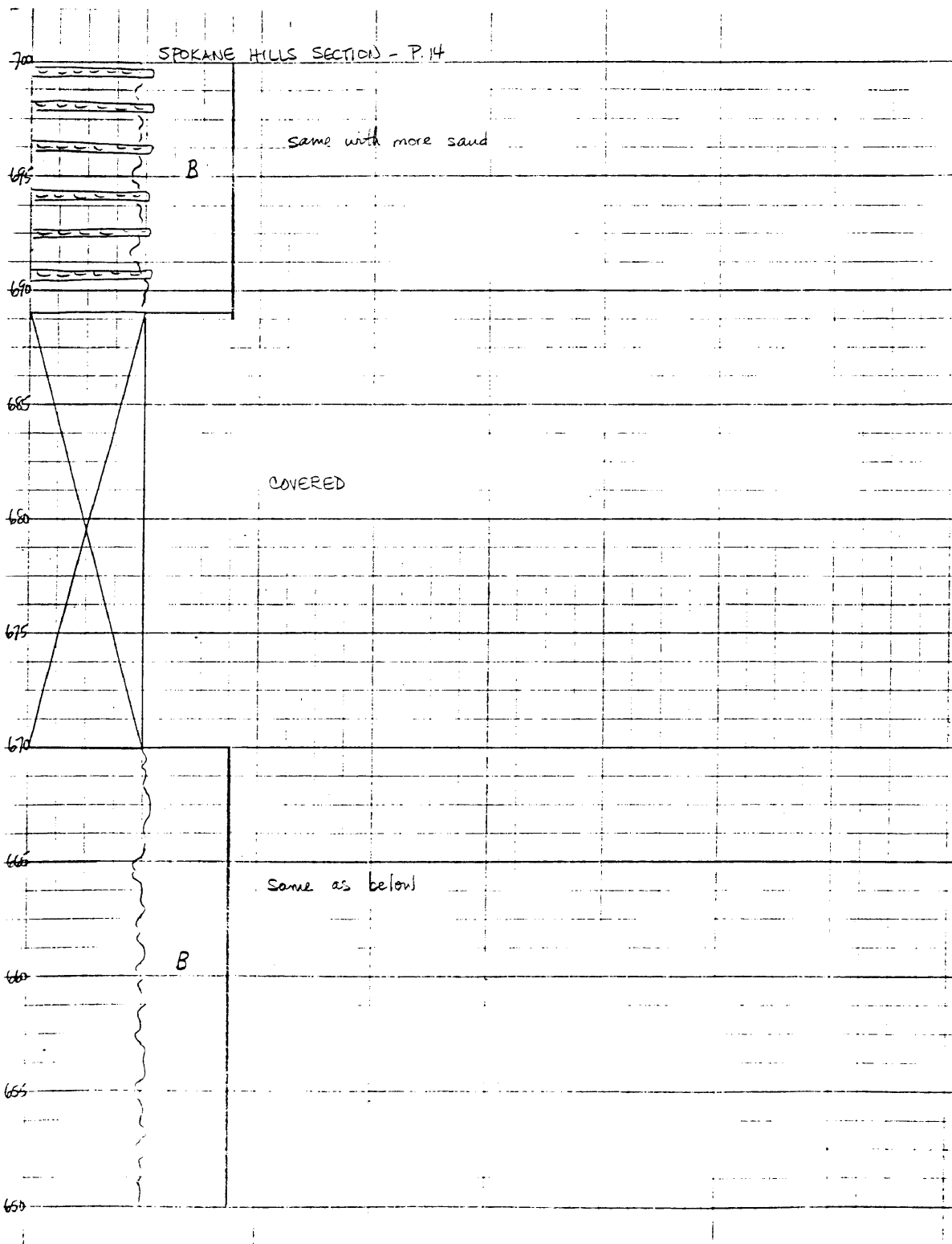


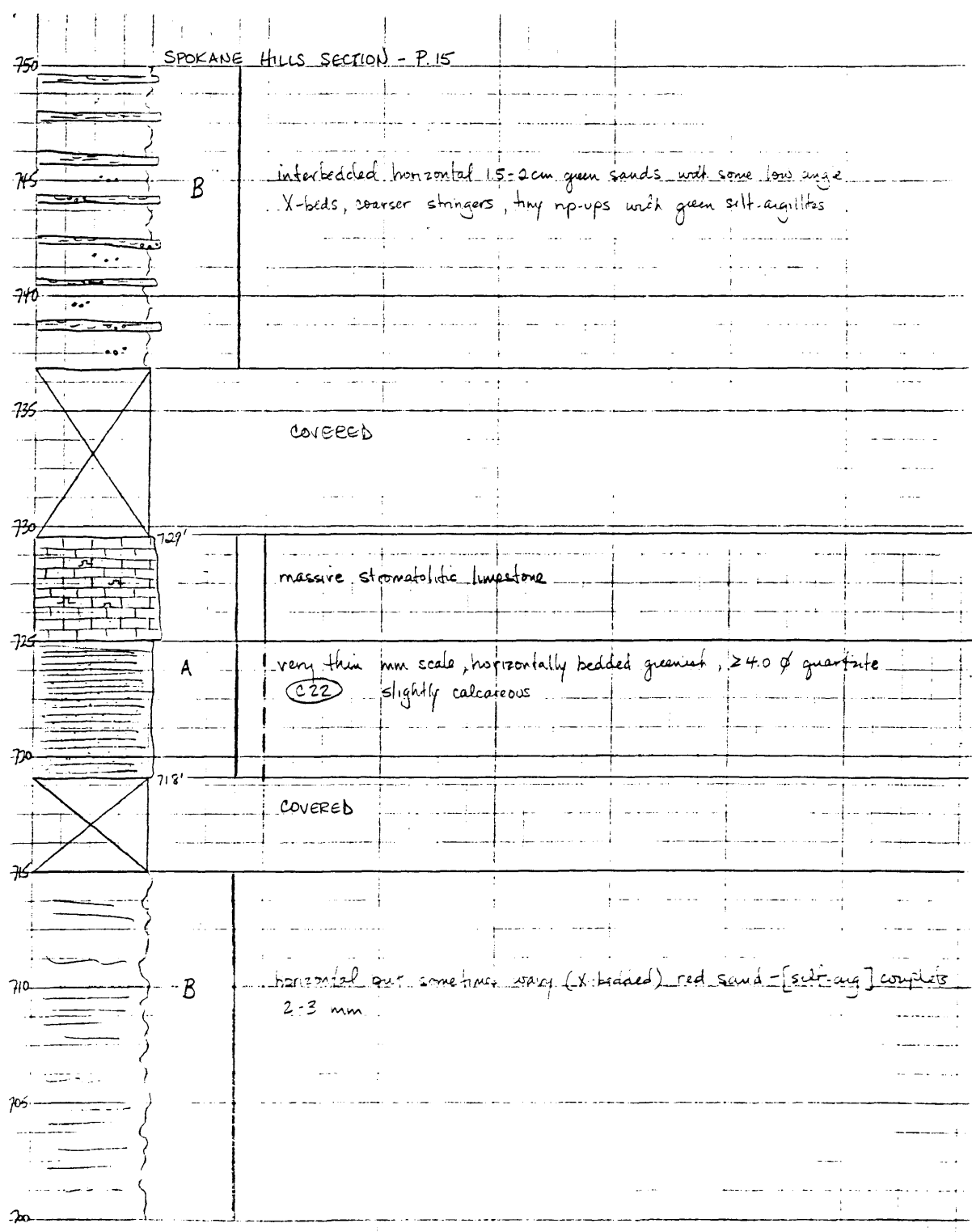


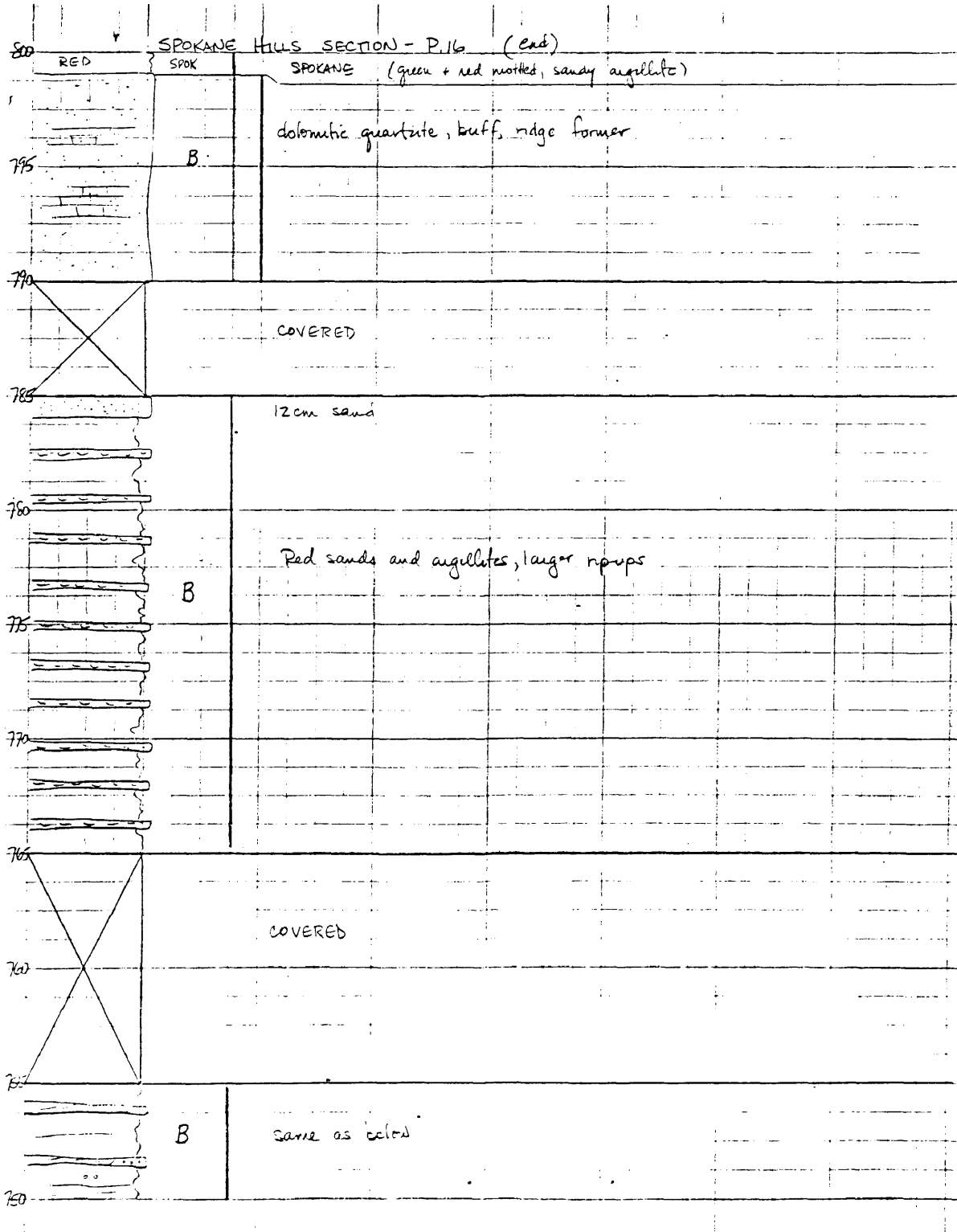












Appendix C
Gravity data

Lat.	Long.	Elev.	Obs. grav.	F.A.A.	S.B.A.
47.0027	-112.1063	1568.2	980336.12	19.20	-155.50
47.0053	-112.0412	1579.6	980341.38	-25.70	-146.90
47.0067	-112.0703	1584.8	980437.57	-27.90	-149.30
47.0083	-112.0650	1585.1	980437.49	-23.20	-149.60
47.0100	-112.0650	1599.4	980435.12	-25.40	-148.40
47.0148	-112.5475	1492.6	980349.54	8.30	-158.00
47.0200	-112.9443	1316.1	980384.99	-10.50	-157.50
47.0202	-112.9850	1298.1	980367.72	-33.40	-178.70
47.0388	-112.2392	1649.0	980332.56	38.00	-146.40
47.0460	-112.5453	1544.4	980351.31	23.70	-148.90
47.0463	-112.2635	1341.1	980373.58	-16.50	-156.60
47.0483	-112.4300	1542.1	980346.77	20.30	-152.10
47.0490	-112.9213	1338.0	980376.08	-15.30	-155.00
47.0517	-112.1300	1295.4	980400.37	-4.30	-149.30
47.0535	-112.7463	2422.8	980174.55	117.40	-153.50
47.0538	-112.8905	2458.4	980350.61	1.90	-151.30
47.0552	-112.6323	2359.8	980172.40	98.70	-156.30
47.0560	-112.7539	2547.8	980152.69	131.60	-152.40
47.0600	-112.5462	1574.6	980349.54	29.30	-146.70
47.0630	-112.7200	2425.6	980174.71	117.50	-153.70
47.0663	-112.9520	1356.3	980379.81	-7.50	-159.30
47.0710	-112.3252	2431.0	980164.91	108.70	-153.20
47.0725	-112.7765	2644.7	980134.89	144.50	-151.30
47.0742	-112.0610	2209.5	980228.03	103.10	-143.90
47.0768	-112.9363	1715.1	980317.63	29.90	-151.60
47.0775	-112.3700	1709.6	980325.07	45.70	-145.60
47.0780	-112.7583	2452.1	980171.20	120.80	-153.40
47.0783	-112.6220	1634.6	980349.56	38.20	-144.60
47.0812	-112.8532	2401.8	980171.87	104.70	-153.90
47.0817	-112.0650	1176.2	980434.07	-14.10	-145.70
47.0868	-112.5995	1692.2	980331.17	45.50	-143.70
47.0877	-112.5325	2034.2	980259.98	79.80	-147.70
47.0880	-112.6132	1703.2	980330.93	48.60	-141.80
47.0903	-112.5417	1634.9	980342.37	38.70	-144.10
47.0950	-112.3550	1654.2	980329.07	30.90	-154.50
47.0970	-112.7307	2513.0	980162.41	129.10	-151.90
47.0983	-112.6830	2238.1	980219.94	101.70	-148.60
47.1002	-112.8713	2443.2	980168.53	113.40	-159.60
47.1033	-112.7675	2548.4	980147.20	124.30	-150.70
47.1112	-112.0643	1254.6	980419.22	-4.50	-144.90
47.1127	-112.8470	2214.6	980223.58	96.80	-150.80
47.1133	-112.6980	2062.2	980253.29	79.40	-151.20
47.1147	-112.5272	2368.6	980189.72	110.30	-154.60
47.1147	-112.5277	2368.6	980189.28	109.80	-155.00
47.1150	-112.1683	1352.7	980392.37	-0.40	-151.70
47.1167	-112.7380	2868.4	980071.97	146.60	-174.20
47.1170	-112.8103	1812.3	980309.53	57.20	-145.40
47.1200	-112.8998	2460.7	980153.04	104.80	-171.80
47.1218	-112.5913	2419.2	980187.27	122.90	-147.70
47.1225	-112.5812	1765.9	980338.10	72.30	-125.30
47.1272	-112.6700	2263.4	980221.28	108.20	-144.80
47.1278	-112.4658	1673.0	980336.59	41.60	-145.40
47.1302	-112.8315	2432.6	980175.61	114.50	-157.50
47.1317	-112.7273	2554.2	980154.68	131.00	-154.60
47.1330	-112.6160	1355.0	980306.20	60.60	-140.80
47.1347	-112.1750	1414.5	980389.17	13.60	-144.60
47.1370	-112.5133	2360.9	980195.07	111.30	-152.70
47.1385	-112.4565	1698.9	980333.79	45.50	-144.40
47.1390	-112.6392	2124.7	980266.91	91.20	-145.20
47.1395	-112.5603	2289.9	980212.73	106.30	-149.30
47.1400	-112.3200	1371.3	980390.57	1.20	-152.10
47.1410	-112.9130	2355.1	980139.60	115.50	-170.20
47.1422	-112.7710	2345.7	980221.24	100.40	-150.70
47.1430	-112.5870	2277.1	980216.99	106.80	-147.80

47.1453	-112.8207	2490.5	980161.36	116.80	-151.70
47.1465	-112.6825	2058.6	980263.09	69.00	-142.30
47.1500	-112.0850	1242.1	980400.47	-9.40	-149.50
47.1550	-112.2133	1257.0	980410.17	-10.40	-151.00
47.1550	-112.6033	2381.4	980193.98	114.30	-151.50
47.1562	-112.8398	1752.6	980322.23	48.90	-147.00
47.1580	-112.8990	2564.5	980139.38	115.50	-171.30
47.1630	-112.5630	2434.1	980188.66	125.10	-147.10
47.1678	-112.9672	2545.3	980141.12	111.60	-173.20
47.1687	-112.4535	1920.2	980293.61	71.00	-143.70
47.1703	-112.5532	2441.8	980103.63	121.50	-151.50
47.1712	-112.5033	2478.6	980170.41	119.80	-157.30
47.1772	-112.7225	2293.1	980236.77	100.60	-145.70
47.1790	-112.9248	1524.0	980356.08	10.20	-150.20
47.1805	-112.7713	2298.5	980211.33	104.30	-152.20
47.1815	-112.6740	2428.0	980181.89	114.80	-156.70
47.1852	-112.8037	2141.2	980250.30	94.30	-145.10
47.1883	-112.5730	2608.5	980124.27	130.80	-157.70
47.1885	-112.5272	2150.6	980246.64	93.30	-147.20
47.1893	-112.8500	2033.6	980269.33	78.90	-148.60
47.1932	-112.5963	2637.1	980137.62	134.00	-150.90
47.1933	-112.6933	1174.7	980438.22	-16.50	-148.00
47.1902	-112.2722	1294.7	980417.88	-0.50	-145.40
47.2002	-112.7950	2524.3	980164.38	125.30	-157.00
47.2065	-112.7427	2514.3	980171.56	128.80	-152.40
47.2085	-112.6613	2115.9	980273.07	77.10	-148.30
47.2097	-112.7705	2616.4	980147.13	135.60	-157.00
47.2098	-112.9630	2137.5	980239.25	78.90	-160.10
47.2117	-112.5217	1595.0	980361.45	31.50	-145.70
47.2138	-112.6562	2195.1	980240.26	98.40	-147.10
47.2167	-112.1117	1205.8	980430.97	-16.30	-151.30
47.2187	-112.4760	1869.7	980300.66	63.20	-147.90
47.2200	-112.6967	2349.7	980211.74	110.90	-145.80
47.2207	-112.9048	2304.5	980202.94	94.20	-163.50
47.2222	-112.2267	1278.7	980424.01	-1.50	-144.40
47.2222	-112.8432	2331.5	980206.79	105.90	-154.70
47.2232	-112.3378	1663.6	980343.82	35.70	-147.90
47.2232	-112.6133	2551.1	980159.39	126.50	-158.80
47.2245	-112.7630	2545.3	980164.57	129.80	-154.80
47.2257	-112.0873	1216.9	980428.80	-15.90	-152.10
47.2267	-112.5650	2199.7	980229.74	88.10	-157.80
47.2270	-112.8200	2438.4	980131.34	113.30	-159.40
47.2280	-112.8815	2251.2	980213.94	93.00	-158.70
47.2308	-112.3250	1363.0	980407.98	7.90	-144.70
47.2310	-112.4790	1585.0	980365.48	33.30	-143.40
47.2350	-112.6433	2155.9	980241.59	85.70	-155.30
47.2388	-112.9227	2171.0	980229.30	77.70	-155.00
47.2423	-112.6530	2198.6	980256.56	85.50	-150.30
47.2457	-112.3512	1368.1	980406.91	6.90	-146.10
47.2465	-112.8113	2357.6	980204.69	110.00	-153.60
47.2467	-112.2250	1272.2	980426.77	-2.60	-145.10
47.2478	-112.7452	2599.9	980144.55	124.50	-156.20
47.2482	-112.7550	2449.0	980168.60	102.00	-171.90
47.2488	-112.9085	1918.1	980274.90	44.30	-170.10
47.2553	-112.2227	1284.7	980424.49	-2.00	-145.80
47.2638	-112.3823	1467.6	980378.03	7.10	-156.90
47.2650	-112.6467	1639.8	980352.06	35.10	-148.20
47.2667	-112.8717	2517.6	980174.27	127.10	-154.40
47.2667	-112.9333	2255.5	980219.84	91.60	-150.40
47.2667	-112.4343	1925.4	980298.88	37.90	-156.10
47.2700	-112.6750	2014.7	980275.49	72.80	-152.40
47.2717	-112.9383	2371.1	980180.31	30.40	-177.10
47.2733	-112.8983	2192.1	980261.08	82.60	-151.90
47.2733	-112.9450	2407.0	980130.66	98.80	-170.40
47.2750	-112.8250	2246.3	980226.98	95.40	-155.80
47.2755	-112.4817	1435.5	980337.55	5.70	-154.60

47.2766	-112.3805	1423.3	980394.49	13.70	-150.40
47.2783	-112.7250	2346.6	980209.68	108.70	-153.70
47.2805	-112.4060	1424.7	980385.48	2.60	-156.50
47.2833	-112.5517	2290.7	980203.63	36.80	-170.00
47.2850	-112.5133	1554.5	980368.27	22.30	-151.50
47.2883	-112.1583	1273.0	980423.72	-7.80	-150.80
47.2900	-112.1600	1266.8	980424.37	-11.60	-152.70
47.2900	-112.0150	2198.5	980236.43	88.70	-157.10
47.2927	-112.1667	1271.0	980423.74	-10.10	-152.40
47.2933	-112.7467	2180.8	980238.41	85.00	-158.90
47.2933	-112.7917	2445.7	980195.17	111.10	-157.90
47.2933	-112.9717	1960.4	980281.62	60.10	-159.10
47.2950	-112.6600	2170.8	980238.85	39.90	-159.50
47.3057	-112.8067	2610.6	980141.59	119.70	-172.20
47.3065	-112.4110	1409.7	980395.61	2.90	-154.60
47.3092	-112.2585	1341.3	980413.99	2.00	-150.00
47.3100	-112.8667	2615.1	980141.42	128.60	-172.00
47.3100	-112.9283	2576.4	980146.50	113.60	-174.50
47.3108	-112.6458	2610.6	980158.92	128.50	-163.50
47.3115	-112.1080	1239.9	980433.05	-12.30	-151.10
47.3133	-112.7500	2189.9	980237.67	65.00	-159.80
47.3133	-112.8300	2635.0	980142.74	127.60	-157.10
47.3138	-112.4752	1487.4	980377.65	0.30	-158.00
47.3150	-112.7117	1758.7	980331.76	46.10	-150.50
47.3150	-112.7600	2169.3	980238.33	79.40	-163.20
47.3168	-112.1055	1256.6	980429.34	-11.70	-152.20
47.3183	-112.9017	2413.1	980176.50	92.40	-177.40
47.3217	-112.7833	1892.8	980296.37	51.50	-160.10
47.3217	-112.8150	2334.5	980213.95	95.40	-165.60
47.3262	-112.4067	1425.5	980301.05	1.50	-157.60
47.3275	-112.3688	1388.7	980412.26	1.20	-154.00
47.3285	-112.2233	1290.1	980422.00	-3.40	-153.80
47.3313	-112.7297	1797.1	980320.21	44.90	-156.10
47.3317	-112.8767	2703.8	980119.97	124.40	-178.00
47.3330	-112.4652	1460.2	980353.27	3.80	-159.50
47.3333	-112.7717	2312.2	980215.93	39.30	-159.20
47.3333	-112.8333	2493.2	980161.81	101.00	-177.80
47.3343	-112.5800	1509.0	980357.41	2.90	-155.90
47.3350	-112.2183	1306.7	980420.77	-0.00	-152.30
47.3357	-112.7133	2136.9	980250.16	79.30	-159.60
47.3358	-112.3800	1385.9	980472.53	-8.10	-155.90
47.3367	-112.7700	2376.2	980196.29	99.10	-166.60
47.3417	-112.7867	1986.4	980284.26	66.40	-155.70
47.3417	-112.9100	2767.5	980096.82	120.00	-189.50
47.3433	-112.8033	2342.6	980208.19	100.00	-151.90
47.3457	-112.8917	2530.1	980154.42	104.00	-179.90
47.3455	-112.3350	1360.9	980409.46	-1.70	-153.90
47.3467	-112.6883	1836.4	980312.87	48.20	-157.10
47.3467	-112.8150	2356.4	980200.77	96.60	-166.90
47.3467	-112.9333	2681.7	980152.49	117.00	-170.80
47.3533	-112.4850	1413.4	980382.37	-3.30	-151.30
47.3592	-112.5217	1425.8	980386.51	-3.80	-163.40
47.3617	-112.8500	2491.1	980167.61	103.60	-174.90
47.3627	-112.2667	1341.8	980411.63	-6.70	-156.90
47.3633	-112.5417	1537.7	980366.29	7.00	-164.00
47.3642	-112.3500	1262.9	980437.29	-8.80	-149.00
47.3650	-112.9250	2484.1	980170.00	103.60	-174.20
47.3663	-112.7600	2418.5	980186.19	101.20	-169.20
47.3705	-112.4982	1377.7	980403.17	-5.60	-159.10
47.3722	-112.4477	1375.3	980413.48	-5.50	-159.40
47.3733	-112.6267	1570.7	980356.24	3.10	-163.20
47.3767	-112.8583	2478.9	980168.64	99.60	-177.50
47.3783	-112.2933	1360.6	980411.07	-3.10	-155.30
47.3783	-112.2950	1291.1	980415.42	-10.20	-154.60
47.3820	-112.3000	1352.1	980410.69	-0.20	-157.60
47.3822	-112.1233	1352.0	980409.92	-7.20	-153.50

47.3843	-112.4489	1359.7	980446.37	-8.60	-159.60
47.3883	-112.9217	1366.7	980185.74	85.30	-159.90
47.3900	-112.7750	2482.6	980172.09	102.90	-174.70
47.3913	-112.1992	1282.4	980424.41	-15.10	-158.60
47.3917	-112.5467	1677.3	980335.36	18.10	-159.40
47.3958	-112.6297	1539.9	980364.26	3.70	-158.50
47.3967	-112.8433	1777.3	980317.48	28.10	-159.90
47.3997	-112.3235	1297.2	980422.31	-13.40	-158.50
47.4017	-112.7967	2474.9	980171.50	98.90	-177.60
47.4017	-112.9433	2425.3	980174.90	87.00	-154.20
47.4050	-112.5950	1487.4	980374.12	-3.40	-159.70
47.4060	-112.3925	1289.3	980422.83	-15.80	-150.10
47.4067	-112.7550	1697.7	980336.94	24.10	-153.70
47.4100	-112.7083	1571.2	980366.14	16.00	-159.70
47.4110	-112.1315	1193.3	980445.60	-21.60	-155.70
47.4130	-112.5788	1487.3	980375.33	-2.70	-159.20
47.4133	-112.9200	2485.7	980167.97	97.50	-136.40
47.4168	-112.2502	1239.1	980435.80	-19.40	-158.90
47.4197	-112.2563	1236.8	980436.11	-20.00	-158.40
47.4200	-112.7867	1780.9	980322.40	34.00	-155.00
47.4217	-112.8500	1737.6	980323.42	21.40	-172.10
47.4223	-112.4640	1310.9	980415.87	-17.50	-164.20
47.4233	-112.3417	1275.3	980430.14	-14.30	-157.10
47.4233	-112.8950	1747.1	980320.59	21.50	-173.80
47.4250	-112.4750	1312.3	980414.17	-18.90	-155.60
47.4250	-112.5550	1357.3	980430.86	-19.30	-171.20
47.4250	-112.6333	1386.8	980395.36	-14.90	-170.10
47.4250	-112.8717	2241.8	980218.58	72.00	-178.70
47.4258	-112.8142	2377.1	980192.82	85.80	-179.30
47.4300	-112.6767	1525.5	980378.67	17.60	-159.90
47.4338	-112.1333	1175.0	980451.60	-24.60	-156.10
47.4367	-112.8033	1779.4	980324.61	34.30	-161.60
47.4388	-112.5500	1173.9	980459.34	-17.90	-149.30
47.4392	-112.4588	1397.3	980418.28	-19.50	-165.40
47.4400	-112.5233	1314.3	980414.73	-18.00	-155.50
47.4417	-112.3450	1291.1	980430.87	-11.20	-155.60
47.4427	-112.5253	1322.3	980413.17	-18.50	-166.50
47.4470	-112.8200	1723.3	980331.82	23.30	-169.50
47.4483	-112.8157	1744.4	980331.75	29.60	-155.40
47.4483	-112.9133	1712.1	980330.56	13.50	-172.90
47.4500	-112.9900	2472.2	980168.00	90.20	-186.20
47.4517	-112.4423	1282.6	980425.20	-19.60	-163.10
47.4517	-112.8917	2442.9	980168.66	81.70	-191.40
47.4518	-112.3592	1253.9	980435.85	-17.90	-158.20
47.4533	-112.6917	2460.5	980168.42	87.40	-198.00
47.4547	-112.6575	1454.9	980388.79	-3.10	-155.90
47.4550	-112.8551	2115.3	980251.45	63.50	-173.00
47.4583	-112.8383	1723.0	980337.97	28.30	-164.30
47.4583	-112.9983	2347.0	980201.53	84.40	-178.00
47.4633	-112.8733	1677.3	980351.11	24.70	-162.00
47.4683	-112.9083	2349.4	980191.82	74.50	-188.20
47.4693	-112.5930	1382.2	980409.93	-14.80	-159.40
47.4700	-112.2572	1239.6	980442.92	-10.30	-155.50
47.4717	-112.9250	1659.3	980334.49	7.00	-179.60
47.4717	-112.9283	1663.6	980336.60	9.40	-176.60
47.4733	-112.8583	1689.2	980346.67	25.80	-163.40
47.4750	-112.4167	1255.2	980436.87	-13.90	-159.40
47.4807	-112.1700	1317.6	980420.56	-16.20	-164.80
47.4898	-112.3910	1241.1	980443.31	-17.80	-156.70
47.4932	-112.3967	1243.6	980442.44	-14.10	-157.30
47.4950	-112.1850	1169.3	980456.96	-27.50	-163.70
47.4950	-112.8383	1622.3	980360.82	16.10	-155.30
47.4985	-112.2410	1173.1	980461.58	-21.20	-152.50
47.5000	-112.1350	1173.5	980462.87	-21.70	-152.00
47.5022	-112.1207	1159.7	980463.00	-24.30	-154.10
47.5033	-112.2533	1170.2	980460.95	-21.30	-152.90

47.5050	-112.4383	1161.9	980468.27	-12.50	-148.50
47.5050	-112.2567	1187.2	980461.77	-17.90	-150.80
47.5053	-112.9653	2502.1	980133.25	179.80	-170.10
47.5052	-112.2287	1166.8	980462.28	-23.10	-153.70
47.5067	-112.0133	1124.4	980475.08	-23.60	-149.40
47.5075	-112.7262	1760.2	980337.62	35.00	-161.30
47.5100	-112.3033	1194.8	980453.04	-19.10	-152.80
47.5117	-112.3600	1235.0	980449.52	-15.40	-153.60
47.5117	-112.3650	1224.1	980449.85	-18.40	-153.40
47.5133	-112.3600	1235.0	980450.37	-14.60	-152.80
47.5138	-112.5953	1433.8	980396.15	-7.70	-168.20
47.5212	-112.3603	1250.9	980451.42	-9.50	-149.50
47.5235	-112.5808	1408.2	980409.69	-11.80	-169.40
47.5238	-112.4573	1276.3	980437.13	-16.00	-153.90
47.5240	-112.9180	1963.9	980284.27	44.90	-175.40
47.5283	-112.4583	1273.1	980440.07	-14.50	-157.00
47.5315	-112.9552	2245.7	980241.97	37.00	-164.20
47.5368	-112.5992	1433.0	980398.74	-7.40	-157.70
47.5447	-112.9437	1959.8	980302.28	57.90	-161.30
47.5458	-112.4717	1263.5	980441.85	-15.40	-157.50
47.5483	-112.3633	1213.1	980458.29	-16.60	-152.60
47.5578	-112.4975	1283.7	980440.16	-14.80	-158.20
47.5587	-112.9205	1524.0	980377.71	-2.30	-172.70
47.5650	-112.3483	1253.6	980453.87	-10.00	-150.30
47.5663	-112.9397	1549.5	980316.13	35.80	-171.10
47.5667	-112.8733	2224.1	980241.38	76.70	-172.00
47.5683	-112.2352	1266.3	980447.78	-12.70	-154.40
47.5813	-112.0627	1103.7	980461.31	-19.50	-154.20
47.5817	-112.3315	1304.1	980445.64	-4.30	-150.20
47.5817	-112.5250	1334.1	980425.47	-14.10	-153.40
47.5818	-112.8533	1938.8	980297.06	43.80	-173.10
47.5865	-112.1553	1319.3	980437.70	-8.00	-155.00
47.5867	-112.9920	2885.3	980161.84	106.50	-182.70
47.5870	-112.9792	2388.7	980203.29	87.50	-179.70
47.5913	-112.5742	1368.9	980418.57	-12.10	-155.30
47.5928	-112.1565	1301.5	980441.73	-10.00	-155.60
47.5962	-112.2417	1353.9	980435.78	-0.10	-151.60
47.6000	-112.2412	1349.0	980439.29	0.40	-150.40
47.6003	-112.8515	1925.7	980383.60	43.70	-171.70
47.6013	-112.9417	2225.9	980236.69	71.40	-177.60
47.6023	-112.7607	1441.7	980407.76	-1.60	-152.90
47.6028	-112.9068	2123.8	980257.01	58.00	-179.40
47.6030	-112.9237	2123.8	980265.49	66.50	-171.10
47.6042	-112.6008	1322.5	980428.97	-17.30	-165.30
47.6100	-112.7400	1357.0	980422.57	-10.30	-153.20
47.6132	-112.9820	2567.9	980166.32	125.50	-181.80
47.6145	-112.7923	1441.7	980409.53	-0.90	-162.10
47.6160	-112.6605	1349.7	980428.48	-10.50	-161.50
47.6167	-112.6217	1332.3	980428.27	-16.00	-155.10
47.6177	-112.6950	1361.3	980426.43	-9.10	-161.40
47.6192	-112.8797	1463.0	980403.01	-1.30	-164.90
47.6208	-112.8506	1680.0	980358.94	21.40	-166.50
47.6217	-112.2783	1348.4	980445.67	5.70	-144.90
47.6227	-112.9885	2115.3	980276.34	72.90	-163.60
47.6238	-112.7373	1414.3	980415.04	-3.70	-161.90
47.6267	-112.2683	1342.3	980446.12	3.70	-146.30
47.6280	-112.9625	2451.9	980274.75	58.40	-172.20
47.6292	-112.5087	1374.0	980416.69	-16.80	-159.40
47.6302	-112.8507	1449.3	980415.50	-2.60	-164.70
47.6350	-112.6967	1352.4	980481.27	-21.20	-160.20
47.6355	-112.8842	1936.1	980397.16	3.00	-167.90
47.6357	-112.6468	1365.0	980423.16	-12.50	-165.40
47.6372	-112.6333	1368.1	980424.43	-13.20	-165.40
47.6392	-112.8480	1404.5	980434.19	10.00	-147.00
47.6458	-112.1380	1401.4	980420.37	3.10	-152.60
47.6503	-112.9563	1941.0	980312.01	52.30	-164.60

47.6515	-112.8523	1776.5	983345.29	34.60	-154.90
47.6552	-112.8272	2174.1	983277.31	53.30	-173.70
47.6625	-112.5817	1343.7	983429.51	-15.70	-156.00
47.6682	-112.8827	1494.4	983450.55	1.40	-155.70
47.6695	-112.6433	1476.5	983466.71	2.00	-153.10
47.6707	-112.6930	1168.3	983485.63	-14.30	-145.00
47.6763	-112.1237	1174.1	983487.43	-11.50	-142.90
47.6800	-112.2417	1398.4	983445.47	15.60	-149.70
47.6803	-112.3525	1297.6	983460.69	-9.10	-145.30
47.6815	-112.9873	2427.4	983211.39	99.00	-172.50
47.6823	-112.8080	2516.3	983189.71	151.60	-178.70
47.6842	-112.3292	1150.5	983494.67	-12.00	-146.70
47.6842	-112.7733	1479.5	983191.85	90.00	-182.30
47.6850	-112.8775	1747.4	983361.45	25.50	-164.40
47.6874	-112.2335	1392.3	983445.94	13.60	-142.10
47.6875	-112.9183	1651.4	983371.65	19.30	-155.40
47.6897	-112.8805	2476.5	983231.82	103.60	-173.10
47.6950	-112.1533	1150.5	983500.57	-7.10	-135.80
47.6967	-112.2175	1386.8	983449.93	15.00	-146.10
47.6980	-112.9872	2130.5	983276.85	71.40	-158.90
47.7003	-112.3875	1624.8	983380.40	15.50	-163.10
47.7072	-112.9335	1830.5	983337.97	38.90	-155.80
47.7080	-112.9727	1845.5	983339.46	45.10	-151.30
47.7130	-112.5917	1465.9	983424.77	-5.50	-152.90
47.7132	-112.7762	2432.3	983218.60	104.90	-157.20
47.7217	-112.5867	1492.5	983413.40	8.70	-153.10
47.7230	-112.8768	1741.3	983355.44	31.60	-153.20
47.7322	-112.8117	2545.6	983189.61	169.20	-175.60
47.7343	-112.3655	1250.4	983470.50	-9.80	-149.70
47.7392	-112.4997	1377.9	983438.77	-2.60	-156.80
47.7398	-112.8533	1635.2	983384.21	22.10	-150.80
47.7470	-112.7773	2509.5	983177.82	112.60	-173.10
47.7500	-112.2250	1220.7	983489.57	-1.50	-133.00
47.7510	-112.9852	1820.5	983351.81	45.90	-157.70
47.7552	-112.3366	1670.6	983379.51	25.90	-150.90
47.7600	-112.1958	1150.6	983517.86	4.40	-124.30
47.7640	-112.8432	1744.9	983364.26	33.80	-151.30
47.7667	-112.1992	1170.1	983501.75	-8.20	-137.10
47.7695	-112.5632	1448.7	983427.52	5.20	-156.80
47.7697	-112.9048	1675.1	983380.06	27.60	-159.80
47.7698	-112.5967	1491.3	983420.08	10.90	-155.90
47.7787	-112.2633	1223.8	983487.35	-4.40	-141.40
47.7710	-112.1148	1146.2	983516.50	1.40	-127.00
47.7732	-112.7768	2563.3	983192.10	113.40	-173.30
47.7750	-112.7767	2322.9	983248.05	95.00	-154.90
47.7775	-112.3478	1263.0	983474.91	-5.30	-146.70
47.7783	-112.9965	2134.5	983289.36	78.40	-150.40
47.7813	-112.2957	1252.1	983481.82	-2.20	-142.30
47.7840	-112.5633	1437.4	983432.87	5.70	-155.00
47.7860	-112.8055	2086.3	983311.34	74.40	-159.00
47.7883	-112.8647	2145.7	983287.80	78.90	-151.10
47.7895	-112.9395	1622.1	983395.88	22.90	-158.60
47.7908	-112.7697	2345.7	983249.49	102.40	-159.90
47.7913	-112.4967	1297.2	983469.69	-1.30	-146.40
47.7918	-112.2357	1230.9	983490.11	-1.40	-139.10
47.7960	-112.3965	1675.5	983377.80	24.00	-153.70
47.7967	-112.5470	1410.3	983440.55	3.90	-153.80
47.8042	-112.7847	2701.1	983153.49	124.50	-177.60
47.8055	-112.3130	2458.5	983216.02	112.00	-153.00
47.8065	-112.8575	1750.2	983372.89	49.20	-155.50
47.8080	-112.3390	1706.8	983378.07	31.90	-153.50
47.8100	-112.1800	1164.3	983500.02	-7.70	-133.00
47.8117	-112.1833	1163.4	983506.27	-7.70	-137.90
47.8117	-112.3512	1874.5	983344.17	44.40	-150.20
47.8133	-112.1750	1163.4	983506.43	-4.10	-138.30
47.8133	-112.1817	1164.3	983506.29	-7.50	-137.90

47.8197	-112.4695	1368.5	980458.53	3.90	-149.10
47.8202	-112.5053	1357.5	980458.14	7.90	-150.10
47.8202	-112.5402	1378.0	980457.56	1.30	-152.30
47.8212	-112.9145	1632.8	980394.88	23.90	-158.70
47.8252	-112.4228	1371.6	980459.67	8.50	-144.90
47.8270	-112.5623	1397.8	980446.99	3.70	-152.00
47.8292	-112.8117	2554.2	980208.32	118.70	-167.00
47.8317	-112.1992	1177.1	980506.41	-5.20	-136.90
47.8402	-112.5730	1405.4	980446.35	4.30	-152.90
47.8403	-112.5075	1409.7	980449.42	8.60	-149.00
47.8460	-112.5793	1410.1	980445.74	4.50	-153.10
47.8475	-112.7813	1747.7	980371.14	34.00	-161.40
47.8503	-112.8255	2499.3	980219.04	114.00	-165.60
47.8530	-112.9913	1760.6	980374.72	41.20	-165.80
47.8542	-112.7757	1734.0	980379.42	37.10	-166.90
47.8552	-112.4250	1133.2	980526.56	-1.80	-127.00
47.8552	-112.1553	1181.7	980511.44	-0.90	-133.20
47.8568	-112.3258	1270.7	980489.88	3.90	-138.20
47.8580	-112.5890	1437.4	980441.34	7.50	-153.20
47.8589	-112.9650	1745.7	980381.10	35.50	-165.50
47.8590	-112.2415	1206.0	980492.24	-13.00	-147.90
47.8592	-112.2412	1206.1	980506.88	1.50	-133.30
47.8638	-112.7573	1686.4	980392.62	35.10	-163.50
47.8663	-112.8850	1760.9	980369.79	37.80	-160.10
47.8678	-112.7125	1647.8	980407.48	25.30	-154.50
47.8678	-112.7322	1641.5	980401.14	29.50	-154.10
47.8698	-112.0910	1153.5	980521.33	-1.10	-130.10
47.8705	-112.6473	1512.4	980429.51	17.70	-151.40
47.8720	-112.6950	1575.8	980416.19	23.80	-152.40
47.8727	-112.5943	1450.5	980439.81	8.70	-153.50
47.8768	-112.2630	1222.0	980508.20	5.20	-130.40
47.8795	-112.5312	1482.8	980435.32	13.50	-152.20
47.8805	-112.9305	1737.0	980371.75	27.40	-166.90
47.8827	-112.6782	1519.4	980431.21	20.50	-149.40
47.8830	-112.8302	2371.3	980257.15	109.30	-165.90
47.8832	-112.6107	1450.9	980439.35	10.50	-152.80
47.8843	-112.3297	1259.7	980498.92	7.90	-133.00
47.8848	-112.6638	1504.1	980430.72	15.10	-153.10
47.8850	-112.5395	1426.3	980452.56	6.70	-150.50
47.8852	-112.4803	1360.0	980467.12	7.00	-145.10
47.8857	-112.7185	1550.6	980420.19	18.90	-154.60
47.8859	-112.4242	1317.0	980479.88	6.40	-140.90
47.8862	-112.5617	1423.7	980450.83	9.50	-149.80
47.8867	-112.6413	1488.9	980435.80	14.50	-152.00
47.8867	-112.7042	1554.4	980422.58	22.30	-151.50
47.8885	-112.6520	1495.9	980433.86	15.40	-151.90
47.8892	-112.3663	1272.6	980491.30	5.70	-137.30
47.8963	-112.7242	1569.1	980418.79	22.10	-153.40
47.8990	-112.2640	1227.4	980501.67	-0.50	-137.90
47.8992	-112.2633	1226.8	980511.44	4.90	-126.20
47.8997	-112.8847	2359.1	980255.89	102.80	-161.10
47.9017	-112.6443	1749.6	980388.85	47.40	-148.20
47.9033	-112.8408	2433.8	980238.57	108.20	-164.10
47.9068	-112.7260	1590.4	980415.70	24.70	-153.20
47.9134	-112.9750	1761.7	980320.05	41.40	-165.70
47.9135	-112.5784	1457.1	980442.67	3.90	-153.00
47.9172	-112.7417	1614.5	980413.48	29.00	-151.60
47.9175	-112.5940	1467.3	980442.36	10.30	-153.10
47.9190	-112.5043	1659.2	980371.15	62.00	-145.00
47.9205	-112.6555	1623.0	980409.77	27.60	-153.90
47.9215	-112.7594	1734.3	980385.76	37.90	-160.10
47.9218	-112.8835	2451.5	980235.94	110.30	-163.40
47.9235	-112.6443	1548.3	980424.05	19.30	-153.80
47.9250	-112.5483	2255.5	980257.04	69.70	-162.50
47.9257	-112.7653	1640.5	980409.43	29.70	-162.50
47.9262	-112.6205	1584.3	980414.50	-0.50	-172.90

47.9265	-112.8367	2314.8	980275.71	106.27	-152.60
47.9282	-112.8597	1408.2	980455.87	6.20	-151.30
47.9285	-112.4167	1259.6	980493.13	7.30	-136.90
47.9322	-112.5422	1537.7	980429.80	20.30	-151.70
47.9342	-112.7412	1693.4	980481.24	39.60	-149.80
47.9357	-112.8235	1993.1	980355.56	61.60	-151.30
47.9363	-112.9193	2464.6	980231.10	107.20	-158.50
47.9395	-112.6923	2405.7	980250.87	177.70	-161.40
47.9417	-112.8475	1148.5	980536.90	6.40	-122.50
47.9423	-112.1560	1164.9	980535.05	9.50	-120.70
47.9425	-112.2975	1208.2	980523.56	11.40	-123.60
47.9427	-112.3675	1204.6	980523.77	10.50	-124.20
47.9433	-112.2850	1203.8	980523.54	11.60	-123.50
47.9447	-112.3570	2271.3	980250.09	95.70	-158.60
47.9458	-112.3748	1777.5	980393.31	40.60	-152.30
47.9462	-112.6602	1627.6	980414.29	31.20	-150.80
47.9482	-112.6893	1912.6	980361.92	66.60	-147.30
47.9530	-112.4182	2384.4	980228.57	109.60	-158.30
47.9533	-112.1548	1162.4	980539.10	10.80	-119.10
47.9577	-112.8198	1734.0	980386.53	30.30	-158.70
47.9630	-112.9912	1771.8	980389.62	49.50	-148.70
47.9692	-112.8480	2356.1	980264.08	103.80	-159.80
47.9713	-112.6152	1459.1	980448.31	10.50	-152.40
47.9720	-112.3845	1207.0	980525.60	10.40	-124.60
47.9767	-112.3150	1211.0	980528.01	14.00	-121.30
47.9782	-112.8472	2704.1	980174.96	121.20	-181.30
47.9783	-112.3100	1210.4	980528.96	14.30	-121.00
47.9800	-112.3133	1210.4	980529.47	14.60	-120.60
47.9867	-112.2650	1191.3	980534.73	13.50	-119.60
47.9867	-112.2867	1201.2	980532.52	14.20	-120.00
47.9867	-112.3693	1211.3	980530.10	14.90	-120.40
47.9867	-112.3800	1219.2	980527.42	14.70	-121.00
47.9867	-112.3517	1230.2	980525.18	13.80	-123.60
47.9867	-112.3620	1234.7	980521.17	13.50	-124.50
47.9867	-112.3733	1245.1	980518.54	13.80	-126.30
47.9867	-112.3960	1253.9	980514.75	12.70	-127.50
47.9867	-112.3967	1255.9	980514.00	12.40	-127.80
47.9867	-112.4133	1264.9	980510.84	12.20	-129.10
47.9867	-112.4267	1274.1	980507.73	11.90	-130.50
47.9867	-112.4383	1278.6	980505.86	11.40	-131.40
47.9867	-112.4492	1286.3	980503.46	11.40	-132.30
47.9867	-112.4583	1292.7	980500.19	10.10	-134.30
47.9870	-112.4590	1292.6	980500.27	10.20	-134.40
47.9882	-112.9192	2359.1	980267.18	106.10	-157.80
47.9900	-112.4758	1306.4	980495.78	9.60	-136.30
47.9940	-112.5967	1418.5	980460.52	8.60	-150.00
47.9942	-112.4983	1327.4	980489.36	9.30	-139.00
47.9942	-112.5128	1339.6	980484.42	8.20	-141.50
47.9942	-112.5357	1360.6	980476.99	7.20	-144.80
47.9942	-112.5560	1378.9	980470.95	6.80	-147.40
47.9943	-112.5565	1378.9	980471.03	6.90	-147.20

Appendix D

Two-dimensional gravity modeling program

```

      DIMENSION XX(300),X(51),Z(51),GSUM(300),XA(51),ZA(51)
      DIMENSION POLY(51)
      TAN(X)=SIN(X)/COS(X)
      PI=3.1415927
      OPEN(UNIT=1,DEVICE='DSK',ACCESS='SEQUENT',FILE='GRAVO.DAT')
      TYPE 790
790  FORMAT(' ENTER NUMBER OF POLYGONS IN MODEL'/)
      ACCEPT 791,NPOL
791  FORMAT(I)
      TYPE 802
802  FORMAT(' ENTER NUMBER OF POINTS IN PROFILE'/)
      ACCEPT 803,KKK
803  FORMAT(I)
      TYPE 806
      806 FORMAT(' ENTER DISTANCE (IN M) INTERVAL BETWEEN PROFILE POINTS'/)
      ACCEPT 807,CO
      807 FORMAT(F)
C...ZERO THE POLY ARRAY
      DO 925 I=1,KKK
795  POLY(I)=0.
      GZE=6.67E-3
C...NOW LOOP THROUGH COMPUTATIONS FOR NPOL TIMES
      DO 650 NCD=1,NPOL
      TYPE 799,NCD
799  FORMAT(' POLYGON NUMBER ',I5)
      TYPE 800
      800 FORMAT(' ENTER NUMBER OF SIDES OF POLYGON'/)
      ACCEPT 801,N
      801 FORMAT(I)
      TYPE 804
      804 FORMAT(' ENTER THE DENSITY CONTRAST'/)
      ACCEPT 805,DENS
      805 FORMAT(F)
      TYPE 809
809  FORMAT(' READ IN COORD.(M) IN CLOCKWISE FASHION,ONE
      1X,Z PAIR PER LINE'/)
      DO 900 I=1,N
      ACCEPT 810, X(I),Z(I)
      810 FORMAT(2F)
      900 CONTINUE
      DO 20 I=1,N
      XA(I)=X(I)
      ZA(I)=Z(I)
      20 CONTINUE
      X(N+1)=X(1)
      Z(N+1)=Z(1)
      DIST=-CO
C...ZERO THE GRAVITY ARRAY
      DO 920 I=1,KKK
920  GSUM(I)=0.

      DO 600 K=1,KKK
      DIST=DIST+CO
      XX(K)=DIST
496  FORMAT(/)
      DO 500 I=1,N
      J=I+1
      A=X(I)
      B=X(J)
      C=Z(I)
      D=Z(J)
      GO TO 49
      50 GZ=0.0
      PHI=0.

```

```

      GO TO 499
C THE FOLLOWING LOGIC TESTS FOR SPECIAL CASES
49 IF(A) 71,51,71
51 IF(C)52,50,52
52 IF(B) 53,50,53
53 IF (C-D) 110,130,110
71 IF(P) 72,81,72
72 THETA1=ATAN(C/A)
   THETA2=ATAN(D/B)
   IF (THETA1-THETA2) 73,50,73
73 IF (A-B) 74,140,74
74 IF (C-D) 160,130,160
81 IF(C-D) 82,131,82
82 IF(D-B) 120,50,120
C COMPUTATION FOR CASE ONE
110 CALL APCHEC(A,B,C,D,PHI)
   CALL ATERM(A,B,C,D,PHI,AA)
   CALL ACHEK(B,D,T2)
   ALPHA=T2-PI/2.0
   TPHI=((D-C)/(B-A))
   BETA=TPHI*ALOG(COS(T2)*(TAN(T2)-TPHI))
490 GZ=AA*(ALPHA+BETA)*(-1.0)
   GO TO 499
C COMPUTATION FOR CASE TWO
120 CALL APCHEC(A,B,C,D,PHI)
   CALL ATERM(A,B,C,D,PHI,AA)
   CALL ACHEC(A,C,T1)
   ALPHA=T1-PI/2.0
   TPHI=((D-C)/(E-A))
   BETA=TPHI*ALOG(COS(T1)*(TAN(T1)-TPHI))
   GZ=AA*(ALPHA+BETA)
   GO TO 499
C COMPUTATION FOR CASE THREE
130 IF(A) 131,132,131
131 IF(B) 134,133,134
132 T1=PI/2.0
   CALL ACHEK(B,D,T2)
   GO TO 135
133 T2=PI/2.0
   CALL ACHEC(A,C,T1)
   GO TO 135
134 CALL ACHEC(A,C,T1)
   CALL ACHEK(B,D,T2)
135 GZ=C*(T2-T1)
   PHI=0.0
   GO TO 499
C COMPUTATION FOR CASE FOUR
140 CALL ACHEC(A,C,T1)
   CALL ACHEK(B,D,T2)
   GZ=A*ALOG(ABS((COS(T1))/(COS(T2))))
   PHI=0.0
   GO TO 499
C COMPUTATION FOR THE GENERAL CASE
160 CALL APCHEC(A,B,C,D,PHI)
   CALL ATERM(A,B,C,D,PHI,AA)
   CALL ACHEC(A,C,T1)
   CALL ACHEK(B,D,T2)
   ALPHA=T1-T2
   TPHI=((D-C)/(B-A))
   R1=COS(T1)*(TAN(T1)-TPHI)
   R2=COS(T2)*(TAN(T2)-TPHI)
   R=R1/R2
   BETA=TPHI*ALOG(R)
   GZ=AA*(ALPHA+BETA)
499 GSUM(K)=GZ*2.0*DENR*GLE+GSUM(K)
500 CONTINUE

```

```

      NN=N+1
      DO 10 I=1,NN
      X(I)=X(I)-CO
13 CONTINUE
600 CONTINUE
C FOR HORIZONTAL DISTANCE OUTPUT IN METERS, DROP THIS DO LOOP
      DO 12 K=1,KKK
      XX(K)=XX(K)/1000.0
12 CONTINUE
      TYPE 905
      DO 792 K=1,KKK
      TYPE 910,XX(K),GSUM(K)
      POLY(K) = POLY(K) + GSUM(K)
792 CONTINUE
650 CONTINUE
      IF(NPOL.LE.1)GO TO 607
      TYPE 904,NPOL
904 FORMAT('' COMBINED GRAVITY EFFECT OF ''I3, '' POLYGONS'')
      TYPE 905
905 FORMAT(' X (IN KM.) G (IN MGAL.)'')
      DO 607 K=1,KKK
      TYPE 910, XX(K),POLY(K)
910 FORMAT(F11.4,2X,F12.3)
      WRITE(10,905) XX(K),POLY(K)
906 FORMAT(F11.4,2X,F12.3)
607 CONTINUE
      STOP
      END
      SUBROUTINE ATERM (AX,BX,CX,DX,P2,AA)
      A1=BX+(DX*((BX-AX)/(CX-DX)))
      AA=A1*SIN(P2)*COS(P2)
      RETURN
      END
      SUBROUTINE A1CHEC (XA,XC,T1)
      PI=3.1415927
      IF (XC/XA) 2,4,4
2 T1=ATAN(XC/XA)+PI
      GO TO 11
4 T1=ATAN(XC/XA)
11 CONTINUE
      RETURN
      END
      SUBROUTINE A2CHEC (XB,XD,T2)
      PI=3.1415927
      IF (XD/XB) 5,6,6
5 T2=ATAN(XD/XB)+PI
      GO TO 11
6 T2=ATAN (XD/XB)
11 CONTINUE
      RETURN
      END
      SUBROUTINE A3CHEC (XA,XB,XC,XD,PHI)
      PI=3.1415927
      IF ((XD-XC)/(XB-XA)) 7,8,8
7 PHI=ATAN((XD-XC)/(XB-XA))+PI
      GO TO 11
8 PHI=ATAN((XD-XC)/(XB-XA))
11 CONTINUE
      RETURN
      END

```